Author:
Riley, Alex E

Title:
Routes to Ethylene Glycol with Homogeneous Ruthenium Catalysts

Routes to Ethylene Glycol with Homogeneous Ruthenium Catalysts

Alexander Riley

A degree submitted to the University of Bristol in accordance with the requirements for award of the degree of Doctor of Philosophy in the Faculty of Science

November 2019

Approx. 43000 words

Abstract

This thesis concerns the synthesis of ethylene glycol using homogeneous catalysts. Three different routes were studied each based around a different starting material, which could potentially be prepared from renewable sources.

Chapter 2 details attempts to synthesise ethylene glycol by the reductive hydroformylation of formaldehyde using both cobalt and rhodium catalysts. Despite extensive condition screening and modification to the catalyst systems, these efforts were largely unsuccessful.

Chapter 3 consists of the synthesis of a range of ruthenium complexes with tridentate phosphorus-based ligands and their application as catalysts for the hydrogenation of C2 oxalates to ethylene glycol. Focus was given to a family of air stable dimer complexes featuring tripodal, tridentate phosphine ligands which showed good performance for these hydrogenation reactions. Preliminary mechanistic studies and kinetic investigation were also conducted as well as brief, but successful tests performing these ester hydrogenations in flow.

Chapter 4 is based on finding a synthetic pathway from glycerol to ethylene glycol *via* a combination of stoichiometric organic reactions and homogeneous catalysis. The results were mixed with no clear route all the way from glycerol to ethylene glycol achieved.

Chapter 5 discusses several other reactions of interest using the ruthenium complexes first introduced in Chapter 3 as catalysts. Some success was achieved with the heterocoupling of methanol and ethanol to *iso*butanol while the hydrogenation of C3 diesters and amides proved more challenging. The transfer hydrogenation of an aldehyde using ammonium formate was tested which showed unexpected reactivity producing secondary amines as well as the desired alcohol.

Author's Declaration

I declare that the work in this dissertation was carried out in accordance with the requirements of the University's *Regulations and Code of Practice for Research Degree Programmes* and that it has not been submitted for any other academic award. Except where indicated by specific reference in the text, the work is the candidate's own work. Work done in collaboration with, or with the assistance of, others, is indicated as such. Any views expressed in the dissertation are those of the author.

SIGNED: ..... DATE:.....

Alexander Riley

University of Bristol

Acknowledgements

Firstly, I would like to thank my supervisor Duncan for giving me the chance to work on this project and for all his help over the last four years. I've thoroughly enjoyed my time in the Wass group, it has been a great team to be a part of. I would also like to thank my industrial sponsors BP and supervisor Glenn. The robust discussions with you were always a source of focus and promising ideas. Thanks also to Greg for the input during the last couple of years and for managing me on my visit up to Hull.

A special mention must go to Rich for all the day-to-day Chemistry advice even when you were busy, tired or just generally not in the mood. I hope all the Friday nights in the pub made up for it. Hope, you were always there to talk to and keep me sane in addition to your role as official fun organizer. Hugh, you've always been a brilliant mate, despite questionable taste in music and football teams. Ashley, I always thought that my time working alongside you caused a state of permanent annoyance, but now I realise that you were much more humble than I would understand. Thanks to Owen for showing me the ropes and Sam for basically being my only mate in Cardiff when we first moved over. Harry, despite a few odd aspects to your personality, I think you have a bright future in the group. I would like to wholeheartedly apologise to all the project students unfortunate enough to have been supervised by me; Aidan, Matt Sinclair, Amy and Maisarah, I hope the experience wasn't too traumatic. Best wishes go out to all the other members of the Wass group that I've had the pleasure of working with Anna, Patryk, Krishna, Katy, Matt Everett, Josephine, Taha and Andres. The Pringle group (Adam, Louise, Tim, Charli, Callum, Hubert, Ailis, Lexy, Dan, Sarah and Rachel) and the rest of Level 5 were always good for a pub trip or night out.

I would like to thank all the technical and support staff at both Bristol and Cardiff, especially those involved with NMR and mass spec facilities and crucially, Tony Rogers for constantly fixing our broken autoclaves.

Finally, I would like to thank my family and friends for all the support they have given me during me studies.

Glossary

DIBAL-H	Di*iso*butylaluminium hydride
DMC	Dimethyl carbonate
DMO	Dimethyl oxalate
DMM	Dimethyl malonate
DMSO	Dimethyl sulfoxide
EC	Ethylene carbonate
EG	Ethylene glycol
ESI	Electrospray ionisation
GC	Gas chromatography
GLC	Glycerol carbonate
GC-MS	Gas chromatography-mass spectrometry
LDA	Lithium di*iso*propylamide
MHP	Methyl 3-hydroxypropionate
MG	Methyl glycolate
NMR	Nuclear magnetic resonance
PDO	1,3-propanediol
TH	Transfer hydrogenation
THF	Tetrahydrofuran

Table of Contents

List of Figures

List of Schemes

List of Tables

Chapter 1 – Introduction

1.1 – The Need for Ethylene Glycol

Ethylene Glycol (EG) is a commodity chemical of vital importance built around two main uses, antifreeze and polyesters. When mixed with water, EG dramatically lowers the boiling point due to the alcohol groups of the glycol disrupting the hydrogen bonding in water, which subsequently prevents the crystallisation of the tetrahedral ice crystals. EG is much more viscous than water and has around half the specific heat capacity. The ratio of EG to water in a mixture therefore has a marked effect on the cooling and flow properties of the solution; for example, a 60% volume ratio of EG stops freezing down to -55 °C.[1] As well as traditional antifreeze applications, EG is also used as a coolant or heat transfer agent in motor vehicles, air conditioning systems, liquid-cooled computers and electronics, and in geothermal pumps.

The other major use of EG is in the production of polyesters for food packing, clothing fibres and fibreglass. The most common EG-based polymer is polyethylene terephthalate (PET). PET is the fourth most widely produced polymer in the world after polyethylene (PE), polypropylene (PP) and polyvinyl chloride (PVC) (Figure 1.1).

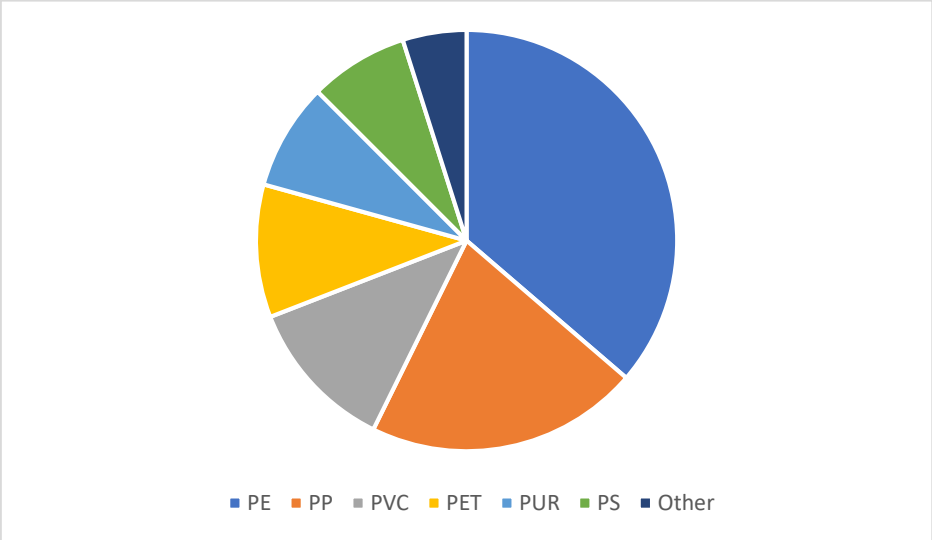

Figure 1.1. The percentage share of polymer production by type from 2002-2014 across the USA, Europe, China and India. Data from Geyer et al. (PUR – polyurethane, PS- polystyrene)[2]

It was estimated that over 50 million tonnes of PET were produced in 2016. The majority of PET, around 60%, is used for polyester fibres while 30% is used for plastic bottles.[3] PET is a popular material as it is very lightweight, impact resistant and provides a good air and moisture barrier. Depending on its preparation PET can be amorphous or semi-crystalline. Fast cooling below its glass transition temperature (T_g) gives an amorphous, transparent product used for packaging, while slower cooling gives a more crystalline structure useful for fibres.

PET is prepared from co-polymerisation with dimethyl terephthalate or terephthalic acid (Scheme 1.1). In the former case, a two-step double transesterification occurs at high temperatures with a base catalyst. The first step is performed at 150-200 °C with the second at 270-280 °C.[4] The methanol by-product is distilled off to thermodynamically pull the reaction equilibrium to the product side. Excess EG is also removed by high temperature distillation at reduced pressure. With terephthalic acid the reaction is performed under a pressure of 2 to 5.5 bar at 220-260 °C. Water is the by-product rather than methanol and this is also removed by distillation.

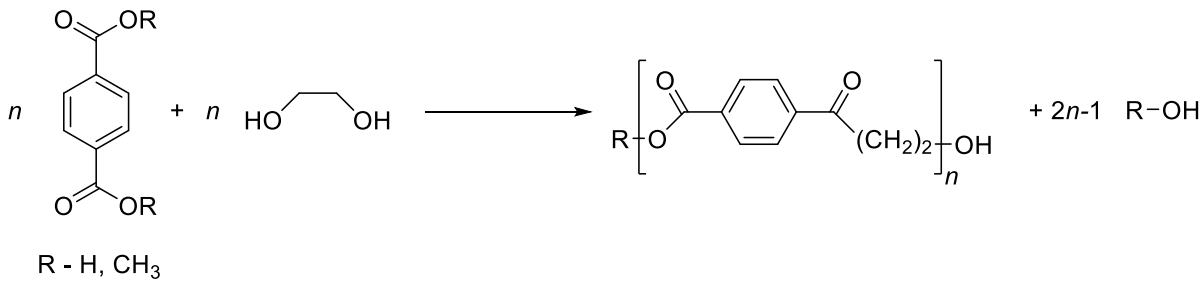

Scheme 1.1. General Synthesis of PET

PET has become ubiquitous across the modern world largely due to its application in plastic bottles. These products have fallen under heavy scrutiny in recent years for their environmental impact. Namely, the volume of plastic waste building up in landfill and in the world's oceans and for the consumption of fossil fuel-based products used in their manufacture. As well as limiting the total amount of bottles and other packaging produced there are demands for thorough recycling of these items. PET is one of the most widely recycled plastics largely since so much of it is used as one form,

i.e. plastic bottles and the resulting recycled product has a range of uses. There are three main types of PET recycling; firstly, chemical recycling to the starting monomers, secondly, chemical recycling by transesterification to make a different polyol or finally, mechanical recycling where the original polymer is reshaped and reused. Chemical recycling has not been widely adopted by either method as large scale plants are needed to make the operation cost effective. Mechanical recycling however is much more popular. The bottles go through an intensive multi-step process where they are crushed, washed and dried with any traces of caps or labels removed giving a product known as PET flake (Figure 1.2).

Figure 1.2. Crushed PET bottles in bales sorted by colour, PET flake

This flake can then be used to make clothing and carpet fibres, sheeting, or more bottles. Reported collection and recycling rates can vary severely across the globe. Despite some calls for a total ban on single use plastic bottles, PET is a material with a wide range of uses and strong recycling potential which will surely still be in large scale demand for years to come. More pressing concerns are increasing the amount and efficiency of collection and recycling. If PET is still being used on a scale anywhere near that of current production a reliable source of EG will be required well into the future.

Another use of EG is as a desiccant, particularly in natural gas pipelines. At high pressure, methane gas can condense alongside water forming a clathrate cage structure where the methane is essentially trapped within ice (Figure 1.3). These clathrate cages can cause pipe blockages and are a potential fire and explosion hazard. Furthermore, as the cages thaw, they can release methane, which has a global warming potential over 100 years around 30 times that of carbon dioxide, into the atmosphere.[5] The

crude gas streams are passed against a flow of EG which removes the water. The EG water mixture is then separated with the EG reused.

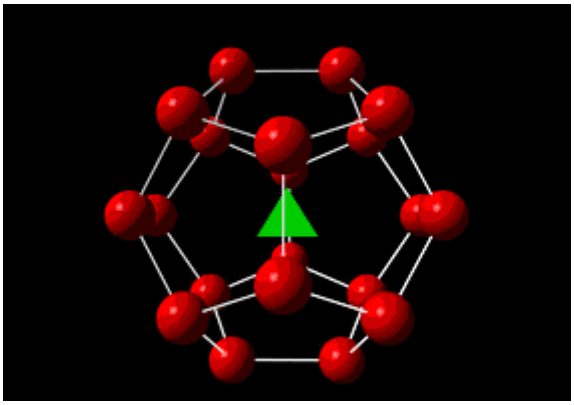

Figure 1.3. Methane hydrate clathrate cage (methane - green, water – red)

More esoteric applications of EG include in varnishes, paints, dyes and inks, as a preservative instead of the more toxic and carcinogenic formaldehyde and as an organic protecting group. EG reacts with carbonyl compounds to give an acetal which is stable to basic conditions and many oxidising and reducing agents, although it is easily removed with acid.

1.2 – Current Synthesis of Ethylene Glycol

EG was first synthesised by Charles-Adolphe Wurtz in 1856; 1,2-diiodoethane was reacted with silver acetate to give the corresponding diacetate. This was hydrolysed with KOH to yield EG.[6] Most commercial EG production is currently performed by the hydrolysis of ethylene oxide (Scheme 1.2).

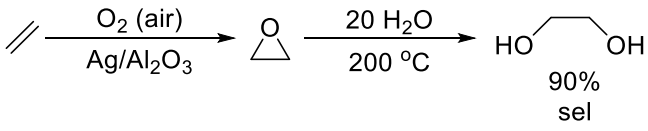

Scheme 1.2. Synthesis of EG by hydrolysis of ethylene oxide

Ethylene oxide is prepared by reacting ethylene with oxygen or air in the presence of a silver metal catalyst. The silver is deposited on a support in concentrations of up to 20% with the best system using aluminium oxide.[7] Common support systems such as silica, magnesium oxide and silicon carbide are unsuitable as they catalyse further oxidation of ethylene oxide or isomerisation to acetaldehyde. The

ethylene oxide is heated with water at approximately 200 °C with no catalyst required. Di-, tri- and tetra-ethylene glycols are also produced as the ethylene oxide reacts faster with a glycol than with water. Using an excess of water (20 equivalents) limits these by-products to around 10% yield with 90% converted to the desired monoethylene glycol.[8] The water is removed and glycol products separated by a series of distillations under reduced pressure. This approach to EG has a couple of key drawbacks; the low selectivity giving approximately 10% unwanted by-products and the high energy demands due to the high temperature and intensive distillation steps. To address these issues Shell developed the OMEGA (Only MEG Advanced) process which converts the ethylene oxide into ethylene carbonate (EC) (Scheme 1.3)

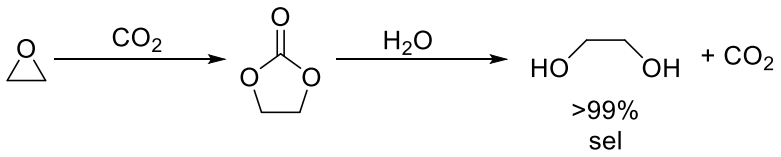

Scheme 1.3. Synthesis of EG via OMEGA process

The EC can be obtained in high yields from ethylene oxide and much less water, only one equivalent, is required for the hydrolysis step. The procedure has a reported selectivity of 99.5% for monoethylene glycol (MEG) and uses less heat than the ethylene oxide hydrolysis route.[9] The exact nature of the process is not published, but similar systems have been investigated using ammonium and phosphonium salts as catalysts.[1] The first OMEGA plant opened under licence in South Korea in 2008. The following year Shell opened a custom plant on Jurong Island, Singapore which produces 750,000 tonnes of MEG per year. Despite clear improvements in selectivity and reaction conditions, the OMEGA process shares one crucial disadvantage with the ethylene oxide route in that they both use ethylene as the starting material.

1.3 – Problems with Fossil Fuels

Ethylene used for industrial processes can be derived from several routes all using petrochemical feedstocks. The most popular is steam cracking where hydrocarbons and steam are heated to over 750 °C which breaks down the larger hydrocarbon molecules into smaller ones and can cause the formation of small alkenes.[10] Naptha and oils are common starting materials with the ethylene isolated by distillation from other products such as propylene and isomers of butene. Recently other methods have been adopted including oxidative coupling of methanol over metal oxides on alumina,[11] Fisher-Tropsch synthesis[12] and methanol to olefins chemistry with an acidic zeolite catalyst.[13] Ethylene is also produced biologically through a three-step reaction, each catalysed by a different enzyme, from the amino acid methionine.[14] This occurs in almost all plant species where the ethylene produced plays an important role in seed germination, fruit ripening and the shedding of leaves. These routes have their own associated problems and as such are performed on a much smaller scale dwarfed by that of steam cracking.

The wealth of scientific data reported over the last few decades highlighting the issues in relying upon fossil fuel derived feedstocks means that alternatives must be sought. Perhaps the most widely used argument against petrochemicals is centred on their impact on the environment and their role in global warming. The combustion of fossil fuels produces H_2O and crucially CO_2, which is largely released into the atmosphere. The Keeling curve (Figure 1.4) measured at the Mauna Loa Observatory in Hawaii shows how atmospheric CO_2 concentrations have increased from less than 320 ppm in 1958 when the measurements began to a current level of approximately 410 ppm.

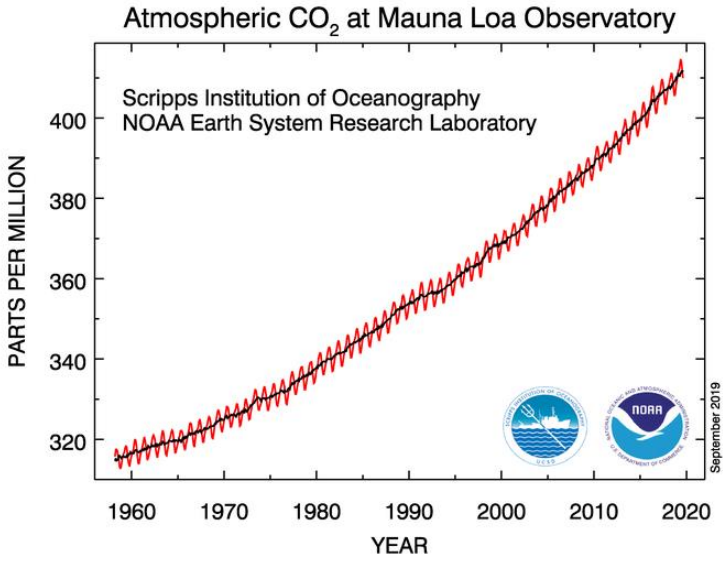

Figure 1.4. Atmospheric CO_2 over time from Mauna Loa Observatory[15]

The global temperature has been measured since approximately 1850, firstly with thermometers and since 1950 with weather balloons and satellites. The data from the NASA Goddard Institute for Space Studies (Figure 1.5) shows that since 1960 there has been a total increase in global temperature of around 1 °C in the annual mean temperature which is concurrent with the rising CO_2 concentrations.

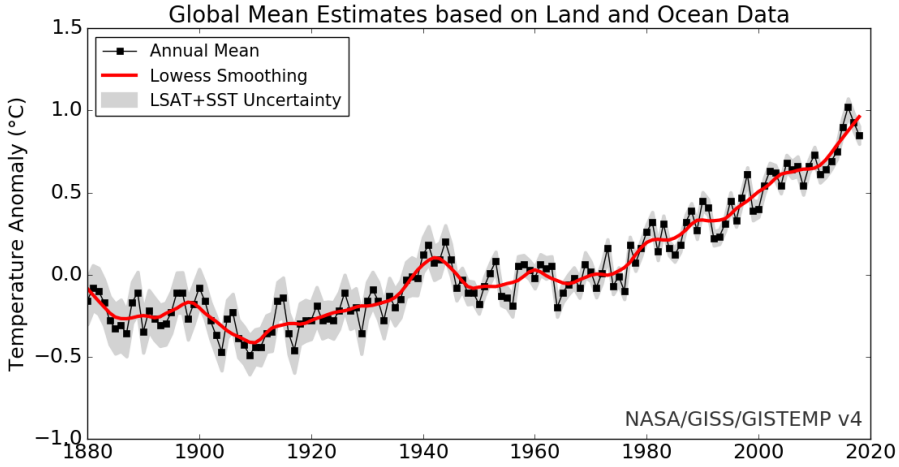

Figure 1.5. Global temperature data from NASA GISS [16]

Even small increases in the global temperature have been linked to a melting of the polar ice caps causing rising sea levels as well as to drought, loss of arable land and desertification across the globe. With these issues surrounding the use of petrochemicals as building blocks for synthesis there has

been a strong drive to investigate alternative, more environmentally friendly and renewable resources for preparing commodity chemicals.

1.4 – C1 Routes to Ethylene Glycol

1.4.1 – Syngas to EG

The direct transformation of syngas has been investigated for EG synthesis. This is a reaction with 100% atom economy using starting materials which can be obtained from renewable sources (Scheme 1.4)

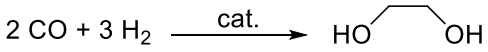

Scheme 1.4. Direct synthesis of EG from syngas

While syngas is traditionally made from coal gasification, alternative routes to its production include gasification of biomass by partial oxidation[17] or converting CO_2 to CO. The first reported synthesis of EG from syngas was conducted by DuPont in 1948 with $Co_2(CO)_8$ as a catalyst. This gave a low yield of EG and required very high gas pressure of 304 MPa (3040 bar).[18] UCC then utilised rhodium-carbonyl species as catalysts which showed low activity and stability at first, but could be improved by using large alkylphosphine or amine ligands. The best system gave EG selectivity of 67% with a space time yield of 259 g/(L.hr) at 230 °C, 490 bar 1:1 H_2:CO. This still represented a poor conversion and selectivity; glycerol, methanol and propylene glycol were all present as side products.[19] Further improvements were made by using ruthenium imidazolium catalyst systems. First pioneered by Murata in 1987 using $Ru_3(CO)_{12}$ with a substituted benzimidazolium bromide and triethylamine base these systems allowed milder conditions (100 bar, 150 °C), but still gave low selectivities (>70%) and the imidazolium was prone to decomposition. Similar ruthenium-benzimidazole catalysts had been used for syngas chemistry under harsh conditions and it was believed that the imidazole would interact with the glycolaldehyde produced to catalyse the hydrogenation to EG.[20] The harsh reaction

conditions needed and poor control have precluded wider research and expansion of the direct synthesis of EG from syngas, and subsequently more indirect pathways have been studied.

1.4.2 – CO Coupling

One possible indirect route to EG is *via* the coupling of CO to oxalates. First performed using a palladium/copper catalyst an alkyl nitrite is reacted with CO giving the corresponding oxalate and nitrous oxide (Scheme 1.5).[21]

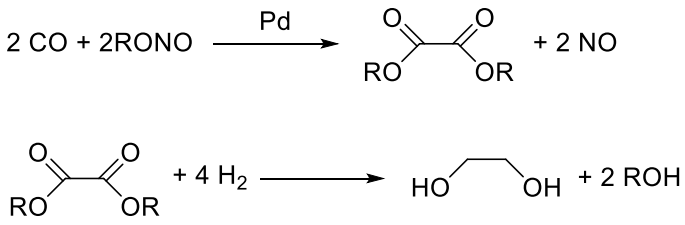

Scheme 1.5. Indirect EG synthesis by CO coupling via oxalate

The initial systems suffered from poor oxalate yields and low selectivities, as well as corrosion of the reaction vessels. Adaptions including using alkali metals salts gave some improvement, but slow catalyst turnover and the need for forcing reaction conditions persisted.[22] A large body of work was then performed testing palladium on alumina as the catalyst for a gaseous reaction with a series of additives. Bimetallic Pd-Fe and Pd-Ga systems showed some promise with conversions of 33% and 35% respectively and selectivity values of 95 and 85%. By far the best system tested used a nanocarbon-fibre support and gave 85% conversion to dimethyl oxalate with 100% selectivity.[23,24] Once the oxalate has been isolated it must then be hydrogenated to ethylene glycol. This reaction will be discussed in more detail below (Section 1.5).

CO coupling was then re-investigated by Beller who published a system using piperidine to form an oxamide with a palladium catalyst in 2016 (Scheme 1.7).[25] The active species was formed *in situ* with the best ligands being either xantphos or tri-*ortho*-tolyl phosphine. This oxamide species could then be hydrogenated back to piperidine and ethylene glycol using a homogeneous ruthenium catalyst.

Many ruthenium complexes showed some activity, but the best system used Ru-MACHO-BH featuring a tridentate PNP ligand.

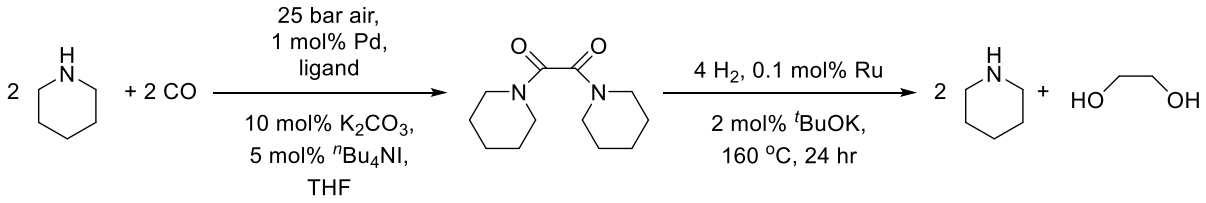

Scheme 1.6. Indirect CO coupling to EG via oxamide

While the above approach demonstrated promise, these CO coupling approaches also have significant disadvantages; the need for a substantial quantity of an expensive palladium catalyst and harsh reaction conditions. High temperatures and pressures are required to generate the oxalate compounds which then still need to be hydrogenated to EG, often with a completely different catalyst. Other methods to produce EG have been investigated using formaldehyde as the starting material.

1.4.3 – Routes to Formaldehyde

Formaldehyde is the simplest aldehyde and occurs naturally as a gas. It is commonly available in an aqueous formalin solution where it is present up to 37% wt with around 10% methanol used as a stabiliser. In higher concentrations formaldehyde polymerises to *para*formaldehyde or can condense to the cyclic compound trioxane (Figure 1.6).

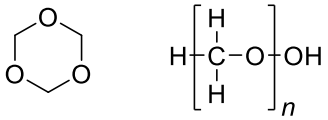

Figure 1.6. Trioxane and paraformaldehyde

Formaldehyde is prepared industrially from methanol through three methods; firstly the BASF process, a partial oxidation and dehydrogenation of methanol in air with silver crystals and steam at 680-720 °C, secondly a similar reaction with metallic silver crystals, or gauze and steam at 600-650 °C, and finally the Formox process, oxidation of methanol with a catalyst system of iron, molybdenum

and/or vanadium oxides at 250-400 °C.[26] The silver processes differ in that the BASF process specifies the use of a crystalline catalyst of specific particle sizes, operates at a higher temperature, and delivers a higher formaldehyde yield of 98% compared to between 77 and 87% for the more generic silver system. When a silver catalyst is used, both oxidation and dehydrogenation reactions occur simultaneously (Scheme 1.7).

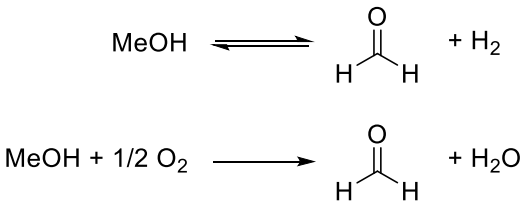

Scheme 1.7. Silver catalysed reactions producing formaldehyde

The Formox process is essentially a two-step redox reaction (Scheme 1.8). The catalyst metal reacts with air to form an oxidised catalyst which then reacts with methanol to give formaldehyde, water and the reduced form of the catalyst.

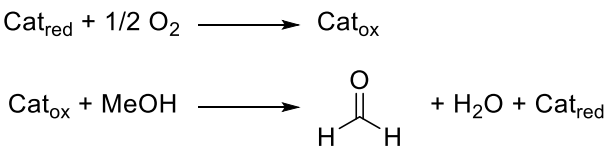

Scheme 1.8. Formox process

The methanol used for formaldehyde synthesis is usually prepared from syngas. There are two reactions that form methanol, the hydrogenation of carbon monoxide and carbon dioxide. These are linked by the water gas shift (WGS) reaction which also occurs under the same conditions (Scheme 1.9).

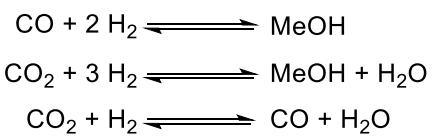

Scheme 1.9 Hydrogenations of CO and CO_2 and WGS reaction

The industrial scale systems use mixed copper, zinc oxide, aluminium oxide or chromium oxide catalysts with a range of promoters and other additives. These allow high conversion to methanol at low pressure (<100 bar).[27] While the majority of synthesis gas is currently derived from petrochemical feedstocks, mostly natural gas, it can also be produced from the gasification of biomass. Alternative methanol synthesis is a lively area of current research with the catalytic hydrogenation of carbon dioxide receiving much attention; the idea of a methanol economy was suggested over 10 years ago by Olah, Goeppert and Prakash as an alternative to fossil fuels.[28] Hydrogen produced by biomass gasification or electrolysis of water could be reacted with recycled waste CO_2 to produce methanol. This methanol could then be used as a fuel source replacing those derived from oil and gas. It can be burned directly in vehicle engines or used as a hydrogen carrier with the hydrogen released at another site and used for electrochemical energy generation. This would dramatically lower fossil fuel consumption and, depending on the H_2 and CO_2 sources, would lower net CO_2 emissions or even be carbon neutral. Achieving this goal hinges on the successful catalytic hydrogenation of CO_2 to methanol. Several heterogenous systems have been reported for this transformation; copper with zinc oxide[29] or zirconia,[30] palladium with zinc oxide[31] or indium oxide species with an oxygen deficient surface.[32] Homogeneous carbon dioxide hydrogenation has often utilised an indirect approach reacting the CO_2 with an amine in the presence of base and a ruthenium catalyst to form the relevant formamide[33,34] or, as published by Milstein a 5-membered oxazolidone,[35] which is then hydrogenated to methanol regenerating the amine (Scheme 1.10)

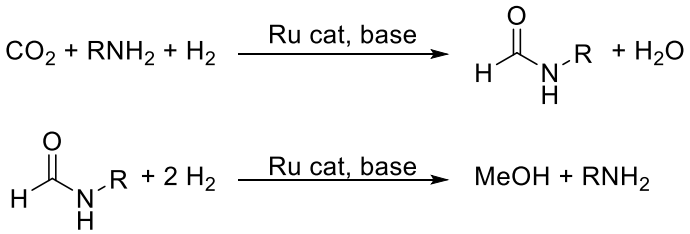

Scheme 1.10. General scheme for indirect CO_2 hydrogenation via amide

This indirect approach was adopted due to the high thermodynamic stability of carbon dioxide so its direct hydrogenation requires harsh reaction conditions that would degrade many homogenous catalysts. In 2011, Huff and Sanford published a 3 stage cascade synthesis of methanol from CO_2 and H_2 using three separate catalysts, two ruthenium complexes and scandium triflate.[36] Recently Beller has published a cobalt catalyst using the tridentate phosphine ligand tripod which can directly hydrogenate CO_2 to methanol using the triflimide super Brønsted acid $HNTf_2$, or its conjugate base as a ligand, at 100 °C with 20 bar CO_2 and 70 bar H_2.(Scheme 1.11)[37]

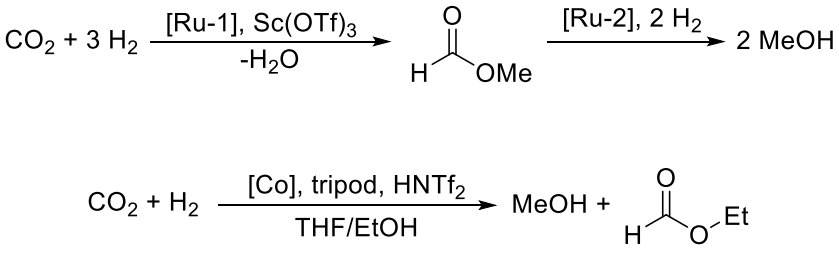

Scheme 1.11. Huff and Sanford and Beller direct CO_2 hydrogenation

With methanol being the precursor to formaldehyde, a catalytic hydrogenation of CO_2 offers a much more sustainable route to formaldehyde than the petrochemical one currently in use. A more benign source of formaldehyde then opens the door for non fossil fuel based ethylene glycol synthesis. There are three key formaldehyde routes to EG; carbonylation, hydroformylation, and condensation. The most widely studied of these is carbonylation.

1.4.4 - Carbonylation of Formaldehyde

The carbonylation of formaldehyde was first developed by DuPont and involved reacting formaldehyde with CO in the presence of water with an acid catalyst to produce glycolic acid (GA) (Scheme 1.12).

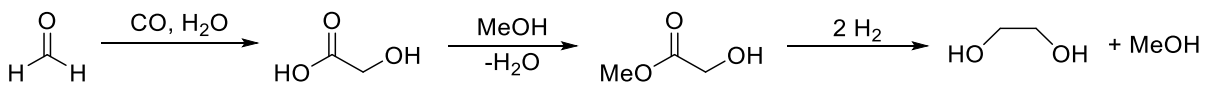

Scheme 1.12. Carbonylation of formaldehyde

GA was then esterified with methanol to methyl glycolate which was hydrogenated to EG using cupric chromate.[38] This process could give substantial (90%) yields of EG, but featured serious drawbacks including high pressure, (900 bar CO for the carbonylation step), and the use of vast quantities of strong acids, HCl and H_2SO_4, which corroded the apparatus and raised pollution concerns. To relieve these issues, a process using a metal catalyst, $[Cu(CO)_3]^+$ or $[Ag(CO)_3]^+$, with H_2SO_4 or BF_3 gave quantitative yields at room temperature with 1 bar CO.[39] The suggested mechanism (Scheme 1.13) showed a protonation of the formaldehyde then the carbonylation giving a cationic product that reacts with water to give GA or an alcohol to form the corresponding glycolate ester. Unfortunately this reaction required both high metal loadings and high H_2SO_4 concentration.

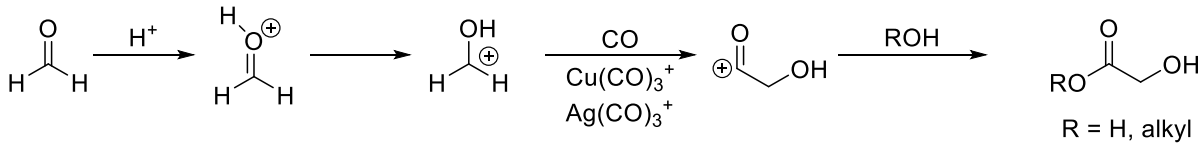

Scheme 1.13. Acid/Metal carbonyl catalysed carbonylation of formaldehyde

In recent decades, heterogeneous catalysts based around ion exchange resins and heteropolyacids were investigated. [40,41] The best performance reported was 85% MG yield over 2 hours at 135 °, 241 bar CO in 1,4-dioxane with an Amberlyst 15 catalyst.

Anhydrous systems for formaldehyde carbonylation were then developed (Scheme 1.14). Initial promise was shown by a Keggin heteropolyacid which operated under mild conditions.[42] This was then superseded by a ZSM-5 zeolite systems which gave an excellent selectivity of 99.6%.[43] A mechanism was suggested with the formaldehyde and CO reacting with the solid acid to give a polymer or 1,4-dioxan-2,5-dione either of which can be esterified to MG with methanol.

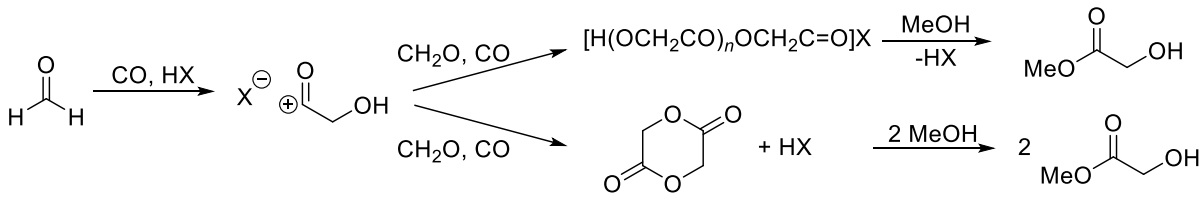

Scheme 1.14. Carbonylation of formaldehyde using an acid catalyst under anhydrous conditions

1.4.5 – Hydroformylation of Formaldehyde

An alternative formaldehyde-based pathway is the hydroformylation of formaldehyde. First discovered by Otto Roelen in 1938 hydroformylation traditionally involves the reaction of an olefin with an equivalent of hydrogen and carbon monoxide to give an aldehyde. Various hydroformylation reactions are carried out on large scales worldwide with around 10 million tonnes of products made annually.[44] Initial hydroformylation catalysis was based around the $[HCo(CO)_4]$ complex. This was then superseded by more active rhodium complexes first reported in 1968 by Geoffrey Wilkinson.[45] These catalysts gave both superior reaction rates and selectivities compared to their cobalt predecessors.[46] By 1995 around 80% of all hydroformylation processes used a rhodium catalyst.[47] Platinum, palladium, ruthenium and iridium have also been investigated as potential catalysts, but only at an academic level.[48] One potential advantage of a cobalt catalyst is that it can potentially perform both the hydroformylation and a subsequent aldehyde to alcohol hydrogenation if required. Rhodium is a poor hydrogenation catalyst and must be supplemented by a ruthenium complex[20] or, in some cases, an N-heterocyclic carbene for formose-type chemistry.[49] A general scheme for the adapted hydroformylation of formaldehyde is shown below (Scheme 1.15).

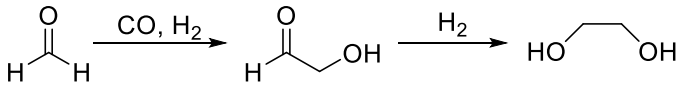

Scheme 1.15. General scheme for hydroformylation of formaldehyde with hydrogenation to EG

The initial hydroformylation produces glycolaldehyde which must subsequently be hydrogenated to EG. Early work by Monsanto examined rhodium carbonyl complexes as catalysts, but these gave poor yields and slow rates. These systems were then improved by incorporating donor solvents specifically

small disubstituted amides e.g. DMF and DMA[50] or benzonitrile.[51] These solvents were particularly useful for improving the selectivity for glycolaldehyde over methanol, formed from a hydrogenation of the formaldehyde. Catalytic activity was then enhanced by the use of phosphine-amide ligands with the rhodium carbonyl species (Figure 1.7).[52] Chan *et al* reported that the use of phosphine ligands improved catalysts stability, but that an excess could reduce activity.[53] The mechanism was deemed to follow that of the more well-known olefin hydrogenation route which proceeds *via* a dissociative mechanism that generates a free site at the metal centre. The loss of activity with excess phosphine was due to the more strongly coordinating phosphine competing with the formaldehyde substrate for this vacant site.

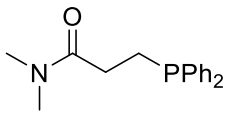

Figure 1.7. Example of phosphine-amide ligand

The use of tetra-*n*-butyl ammonium halides as an additive was published by Machionna and Longoni in 1987.[54] These halide salts resulted in the formation of a number of anionic rhodium carbonyl halide complexes which were found to activate the formaldehyde substrate. In later work a dual catalyst system of two of these species, $[Rh(CO)_2Cl_2]^-$ and $[Rh_5(CO)_{14}Cl]^{2-}$ gave an excellent selectivity of 95% for glycolaldehyde.[55]

1.4.6 – Condensation of Formaldehyde

The final, and least well studied, formaldehyde route to EG is the condensation of formaldehyde. Sanderson et al. has reported the reaction of formaldehyde with 1,3-dioxolane and a free radical initiator, di-*tert*-butylperoxide (Scheme 1.16). This forms the corresponding hydroxymethyl dioxolane which can be hydrogenated to EG with a selectivity of 45%. [56]

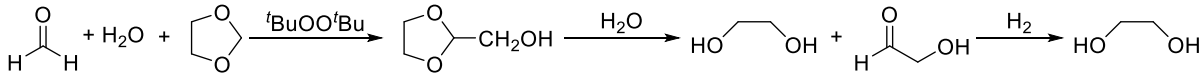

Scheme 1.16. Condensation of formaldehyde with 1,3-dioxolane and free radical initiator

1.5 – Ester Hydrogenation to EG

1.5.1 - Introduction

Many of the synthetic procedures discussed above (Sections 1.4.3-1.4.5) involve the formation of the methyl glycolate ester either directly or by the esterification of glycolic acid. An ester hydrogenation catalyst is therefore required to convert these compounds to EG. Traditional ester hydrogenation reactions have used stoichiometric amounts of inorganic hydride reagents such as $LiAlH_4$ or boron hydrides. In addition to their low atom economies, these reactions also produce significant quantities of inorganic waste products and have inherent safety concerns as many of these reagents are pyrophoric or cause strong effervescence. The catalytic hydrogenation of esters presents a much more efficient route to the desired alcohols with no waste. Heterogenous systems for the ester hydrogenation, largely based around copper chromium catalysts have been studied since the 1930s, but these systems require high temperatures (200-300 °C) and hydrogen pressures (200-300 bar).[57]

In an attempt to perform these hydrogenation reactions under mild conditions, homogeneous catalysts were investigated. Pioneering work by Grey and Pez studied dimeric ruthenium hydride complexes. The most effective species, $[(Ph_3P)(Ph_2P)RuH_2^-K^+diglyme]_2$, faciliatated the hydrogenation of methyl acetate to produce a mixture of methanol, ethanol and ethyl acetate (Scheme 1.17).[58]

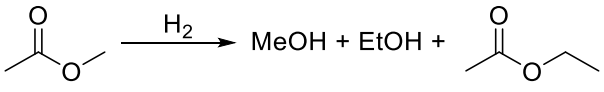

Scheme 1.17. Hydrogenation of methyl acetate

Bianchi and Matteoli then expanded the range of ruthenium complexes to ruthenium carbonyl hydrides with trialkylphosphine ligands. These were capable of hydrogenating dicarboxylic acid esters including succinates and adipates under forcing conditions of 200 °C and 130 bar H_2.[59] Matteoli later

used a similar complex $[Ru(CO)_2(CH_3COO)_2(PBu_3)_2]$ to hydrogenate dimethyl oxalate to methyl glycolate at 180 °C, 130 bar H_2. When the reaction was left for a long period of time, 144 h, a small quantity of EG (7%) was produced by the hydrogenation of this MG (Scheme 1.18).[60]

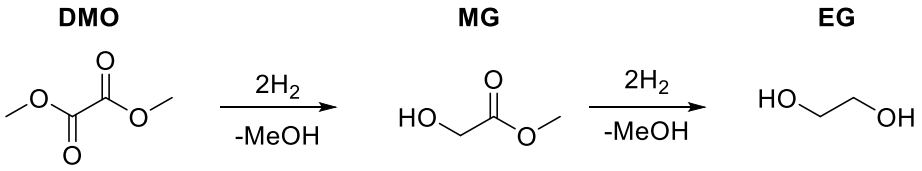

Scheme 1.18. Hydrogenation of DMO to EG via MG

1.5.2 – Tripodal Ester Hydrogenation Catalysts

The hydrogenation of DMO to EG through MG was examined in seminal work published by Elsevier and Teunissen.[61] The catalyst system comprised a $Ru(acac)_3$ precursor with the tridentate ligand tripod (**L1**) and a zinc metal additive (Figure 1.8). The role of the zinc was to remove the acac ligands from the ruthenium and reduce the Ru from the +3 oxidation state to +2.

The Tripod ligand has featured heavily in coordination chemistry over the past few decades with 1200 publications citing the ligand at time of writing. It was first synthesised in 1962 and has been used for a range of catalytic applications.[62] The majority of these uses have come in hydrogenation and hydroformylation reactions where the stable κ^3 complexes can retain their coordination due to the chelate effect. This rigid complex structure keeps the ruthenium centre solubilised and in the desired oxidation state(s), maintains catalytic activity and limits deactivation.

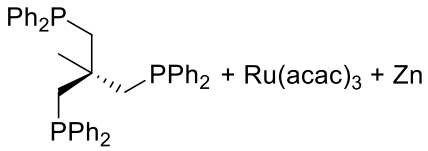

Figure 1.8. Elsevier and Teunissen catalytic components

This *in situ* system gave full conversion of DMO with a 95% EG yield at 100 °C, 70 bar H_2 and 0.74 mol% Ru, much milder conditions than the monodentate phosphine complexes. A range of phosphine

ligands were tested including the pincer-type triphos ligand, PPh_3 and PCy_3. It was observed that a tridentate phosphine with a facial coordination arrangement was crucial for efficient catalysis. This Ru/Tripod system has since been used to hydrogenate a range of esters including dimethyl phthalate, dimethyl palmitate and benzyl benzoate.[63] NEt_3 and HBF_4 were also discovered to be effective additives as an alternative to zinc metal. Frediani *et al.* tested this catalyst for the hydrogenation of fumaric and succinic acids to 1,4-butanediol via the corresponding diesters (Scheme 1.19). Although successful, these reactions gave moderate yields 33% for succinic acid and 56% with fumaric acid over long reaction times 72-96 hours with 80 bar H_2 at 120 °C.[64]

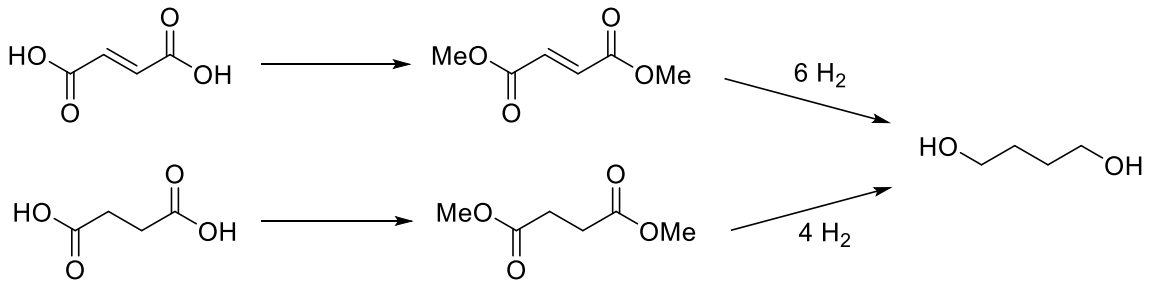

Scheme 1.19. Hydrogenation of fumaric (top) and succinic (bottom) acids to 1,4-butanediol

Klankermayer and Leitner published a pre-formed monomeric Ru-Tripod complex for the conversion of levulinic acid to 2-methylTHF *via* γ-valerolactone and 1,4-pentanediol (Scheme 1.20).[65] The latter step required an ionic liquid and/or an acidic component for the reduction of the cyclic lactone.

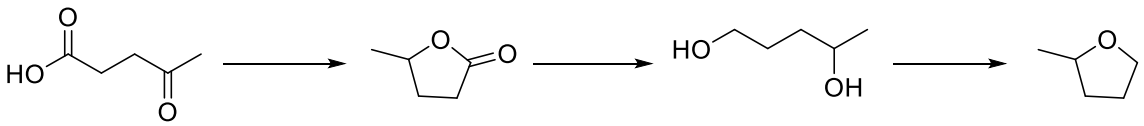

Scheme 1.20. Conversion of levulinic acid to 2-methylTHF

A 97% yield of 2-MTHF was obtained with full conversion of the levulinic acid. The *in situ* $Ru(acac)_3$/Tripod system with the acidic additive also performed well giving a 95% yield of 2-MTHF.[66] The reaction is of interest as levulinic acid can be obtained from cellulosic biomass e.g. tree bark and grasses, while the 2-MTHF produced has been earmarked as a useful solvent and potential fuel.

The tripodal tridentate facial scaffold has been adapted into other ligand types. A sulfur analogue TriSulf^{nBu} was reported by Hanton and co-workers at Sasol in 2006 that selectively hydrogenated DMO to MG (Figure 1.9).[67] Although a low catalyst loading was used (0.1 mol%) the reaction required over 60 hours to reach high conversion with full turnover achieved at 136 hours. Again, a high H_2 pressure of 80 bar was needed for the reaction.

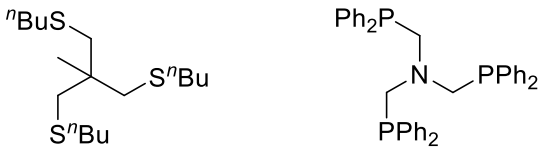

Figure 1.9. TriSulf^{nBu} and NTripod ligands

In 2011 Hanton and Miller reported a tripod variant with an apical nitrogen atom rather than the C-Me moiety (Figure 1.9).[68] It was used in the same *in situ* system as Tripod (**L1**) and was successful in the hydrogenation of DMO to EG. Kinetic experiments measuring hydrogen uptake were performed showing that not only was the rate slower for the N-Tripod variant, but that the mechanism appeared to be different. The Tripod system showed an apparent zero order dependence on substrate whereas with N-Tripod there was a first order relationship with the association of one molecule of DMO determined as part of the rate determining step. Furthermore, a degree of catalyst degradation occurred over the course of the reaction with the N-centred analogue. As a recurring theme with the *in situ* systems this catalyst also required a long reaction time of 66 hours to reached maximum conversion of 100%, and the resultant product consisted of 53.5% EG and 46.5% MG. The N-Tripod catalyst was later applied to the levulinic acid to 2-MTHF multi-step hydrogenation.[69] [(N-Tripod)Ru(PPh_3)H_2] was the most active complex giving almost quantitative conversion to 1,4-pentanediol then 87% 2-MTHF when an acidic $HNTf_2$ additive was used. Dissociation of the triphenylphosphine ligand was deemed crucial to reactivity as it generated a vacant site which is then available for substrate coordination. Using an acid with a non-coordinating conjugate base was also vital as other acids tested e.g. *p*-TsOH competed with the substrate in binding to the ruthenium centre.

1.5.3 – Pincer Complexes for Ester Hydrogenation

Ester hydrogenation catalysis has not solely been limited to ruthenium complexes with tripodal ligands. In 2006, Milstein published the hydrogenation of non-activated esters including benzoates, ethyl butyrate and ethyl acetate using pyridinyl pincer PNN and PNP complexes (Figure 1.10).[70]

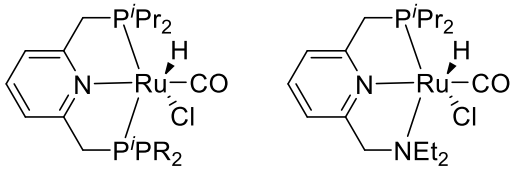

Figure 1.10. Ru-PNP and PNN catalysts published by Milstein

For some of the substrates, methyl benzoate, ethyl butyrate and dimethyl terephthalate, full conversion to the two alcohols was achieved at 115 °C with 5.3 bar H_2 without the need for any additives or co-catalysts. The reaction proceeds *via* an aromatisation/dearomatisation mechanism (Scheme 1.21). Quenching the non-aromatic intermediate provides the driving force for the addition of H_2 to the metal centre. The resulting hydride can then be inserted in the bound carbonyl substrate to perform the hydrogenation. These pincer catalysts were then superseded by a CNN ligand featuring an *N*-heterocyclic carbene moiety which were capable of giving near quantitative hydrogenation of a range of esters (pentyl pentanoate, ethyl butyrate, ethyl benzoate) over 2 hours with a catalytic quantity (1 mol%) of KO^{t}Bu base (Figure 1.11).

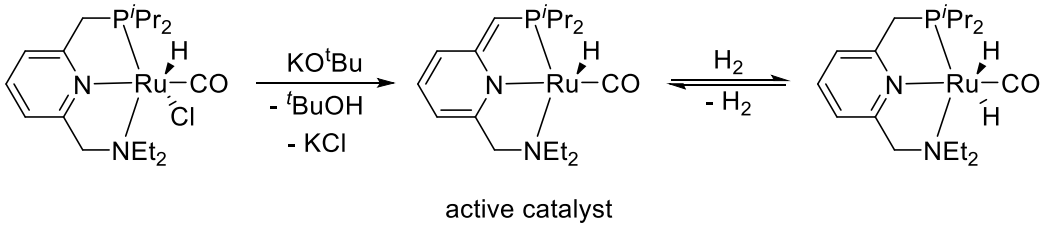

Scheme 1.21. Aromatisation/Dearomatisation of Milstein ester hydrogenation catalyst

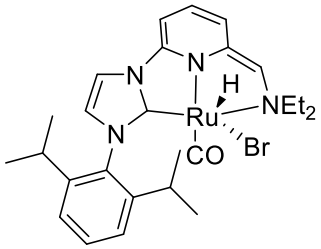

Figure 1.11. Ru pincer complex with CNN NHC ligand

Ester hydrogenation with pincer complexes was then further developed with the Ru-MACHO catalyst. First prepared by the Takasago Corporation, Ru-MACHO (Figure 1.12), which features a tridentate PNP ligand with an alkyl backbone, has been used to hydrogenate a range of esters including various benzoates, methyl laurate and dimethyl adipate to the corresponding alcohols in high yields (≥90%).[71] These reactions were conducted using 10 mol% (relative to substrate) NaOMe for catalyst activation with 0.1 mol% catalyst loading at 50 bar H_2 and 100 °C. Crucially, this catalyst is not deactivated by MeOH , unlike some other ester hydrogenation complexes, allowing the hydrogenation of a wider range of methyl esters.

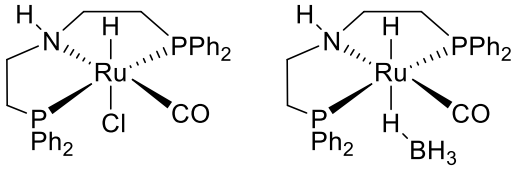

Figure 1.12. Ru-MACHO and Ru-MACHO-BH

This catalyst was examined for the hydrogenation of diethyl oxalate to ethyl glycolate and EG by Beller *et al*.[72] Both Ru-MACHO and Ru-MACHO-BH, where the axial chloride has been replaced by a BH_4 hydride moiety, gave a high yield , 92 and 96% respectively, of EG with a 10:1 ratio of NaOEt:catalyst and 100 °C, 60 bar H_2. Interestingly, changing the substituents on the phosphines from phenyl to *iso*-propyl completely stopped the second ester hydrogenation reaction giving only the ethyl glycolate intermediate. The hydrogenation of DMO to EG was also successful giving 84% yield with the Ru-MACHO-BH catalyst within an hour.

The Gusev group then produced a range of ruthenium catalysts featuring a similar structure to the MACHO ligand scaffold. A PNN complex with a pyridine in place of one of the diphenylphosphines on was particularly effective (Figure 1.11). This Ru-MACHO analogue gave quantitative hydrogenation of ethyl acetate and a 96% conversion of methyl benzoate at a low catalyst loading of 0.005 mol% with 1 mol% ethoxide base. These results correspond to TONs of 20000 and 18600 respectively, the highest of any reported ruthenium ester hydrogenation catalyst.[73] This same group has also prepared a range of SNS ligands with the resulting ruthenium complexes being effective catalysts for ester hydrogenation (Figure 1.13).[74] An air-stable, ethyl-substituted derivative was the most competent catalyst giving high conversions for a range of aromatic and aliphatic esters and diesters. The complexes also present an easier synthetic route that avoids the use of air sensitive and pyrophoric phosphines.

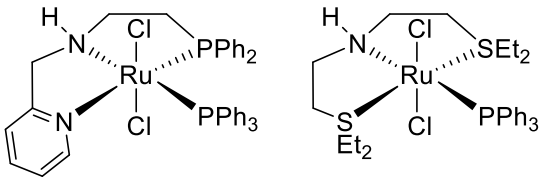

Figure 1.13. Gusev PNN and SNS ruthenium catalysts

Noyori-type catalysts featuring a diphosphine, diamine structure have also been used for ester hydrogenation (Figure 1.14). Initially developed for transfer hydrogenation reactions their scope has been expanded to other reactions. A ruthenium complex with a *bis*-chelate bidentate PN ligand and a similar bridged and phenyl variant were effective for the hydrogenation of methyl benzoate under reasonably mild conditions of 0.05 mol%, 5 mol% NaOMe, 50 bar H_2 and 100 °C.[75]

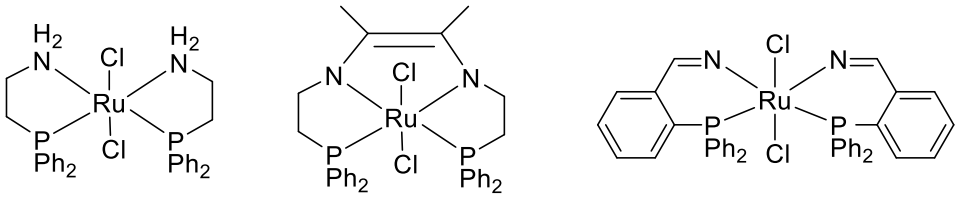

Figure 1.14. Noyori-type catalysts used for ester hydrogenation

Kuriyama *et al.* then used the bis-PN ligand complex for the hydrogenation of chiral esters to their corresponding alcohols (Figure 1.13). After this was successful, a related catalyst with a bidentate PP ligand and chiral NN ligand was prepared which gave high alcohol yields and a Δee ($ee_{subsrate} - ee_{product}$) value of <1 up to 6.[76] Clarke *et al.* formed this same complex *in situ* as well as a range of other PP,NN bis-chelate bidentate and PNP and PNO tridentate complexes all from the same ruthenium precursor, [$RuCl_2Py_2$(NDB)] (Figure 1.15). The best catalyst, shown below, was highly successful for the hydrogenation of a range of aromatic esters in quantitative yields at low temperatures of 50 or 100 °C.[77]

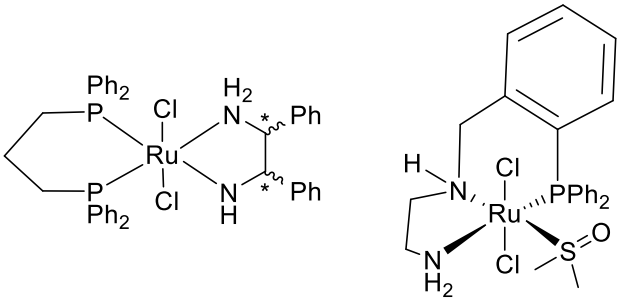

Figure 1.15. Chiral Kuriyama catalyst and best performing in situ Clarke complex

1.5.4 – Ester Hydrogenation with First Row Transition Metals

With ruthenium having a high cost and low natural abundance, other cheaper metals have been sought after to prepare effective catalysts. Iron sits above ruthenium in group 8, is inexpensive, and is the fourth most abundant element in the Earth's crust. In 2014 Milstein *et al*. presented an iron-PNP complex that was capable of hydrogenating a variety of esters with a -CF_3 activating group under mild conditions (10-25 bar H_2, 40 °C).[78] Guan *et al*. then reported an iron catalyst with a similar structure to Ru-MACHO-BH, that could hydrogenate a range of non-activated aromatic and long chain aliphatic esters in high yields (≥85%) under mild conditions albeit at a high 3 mol% loading.[79]

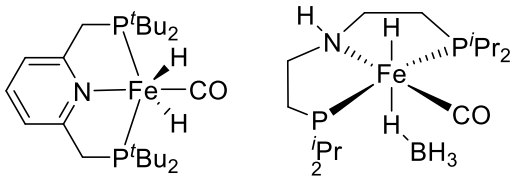

Figure 1.16. Milstein and Guan Fe-PNP ester hydrogenation catalysts

Although cobalt has received less attention than iron in this field, an *in situ* tripod/$Co(BF_4)_2.6H_2O$ catalyst for ester hydrogenation was published in 2015 by de Bruin and Elsevier.[80] Under relatively forcing conditions of 100 °C, 80 bar H_2, the complex was able to hydrogenate aromatic and aliphatic esters in near quantitative yields after 22 hours. While the majority of experiments proceeded at 5 or 10 mol% loading, some substrates were successfully converted at 0.25 and 0.1 mol%.

In recent years manganese has emerged a popular candidate for replacing ruthenium, due to its low cost, high abundance and low toxicity. The first reported manganese catalysed ester hydrogenation was from the Beller group in 2016.[81] This featured a variant on the MACHO ligand with ethyl substituents on the phosphines, as bulkier groups gave no activity (Figure 1.17). The ancillary ligands also had to be altered to support manganese in the +1 oxidation state, no catalysts based on Mn(II) have been reported at time of writing. This Mn catalyst was able to hydrogenate a range of largely aromatic esters, although dimethyl adipate was also hydrogenated successfully, in yields of 75-98% under mild conditions (100 °C, 30 bar H_2). As with the other first row transition metal catalyst, high loadings, 3 mol%, and long reaction times were required (24 h). Clarke then developed a chiral PNN pincer ligand featuring a ferrocenyl moiety that was able to enantioselectively hydrogenate a range of esters with high ee values up to 97% at 50 °C. [82] The first active manganese complex without a pincer ligand was published by Beller and Pidko *et al*. which featured the PN bidentate ligand discussed above.[83] This gave good conversion at a low catalyst loading of 0.2 mol%, however a large quantity, 75 mol%, of KO^{t}Bu base was required as well as a higher H_2 pressure, 50 bar. The Milstein group have also published a manganese catalyst based on the pyridinyl-PNP ligand. This gave high conversions for

the hydrogenation reactions studied, but long reaction times of 21-60 hours and the highly reactive base potassium hydride was required as an additive.[84]

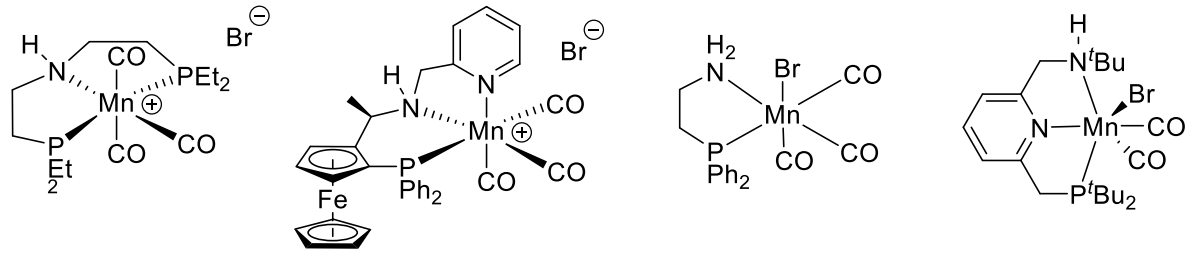

Figure 1.17. Manganese ester hydrogenation catalysts

1.6 – Glycerol to EG

A final route to EG, which is of growing interest, uses glycerol as the starting material. Glycerol is the main by-product formed during the production of biodiesel reaching up to 10 wt% of the total process with production expected to achieve 10 billion litres in 2020.[85] Long chain fatty acids undergo a transesterification with methanol to produce fatty acid methyl esters (FAME) which make up the biodiesel and glycerol. While glycerol itself has a few minor applications as a food additive and in pharmaceuticals and cosmetics, it has great potential to be transformed into a range of other chemicals with high value uses. Glycerol can undergo a number of chemical reactions, but the one most of interest here is hydrogenolysis. Glycerol reacts with hydrogen via three main pathways to give three major products; 1,2-PDO, 1,3-PDO and EG (Scheme 1.22).[86] These can react further to give a wider range of products including methanol, ethanol and 1-and 2-propanols.

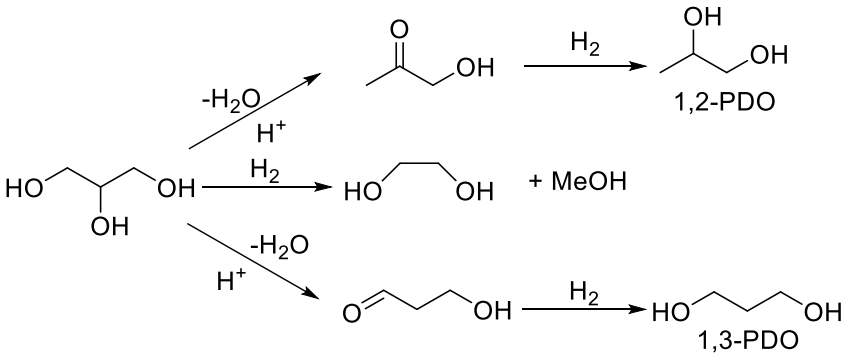

Scheme 1.22. Major reaction pathways from glycerol

EG is formed by a dehydrogenation-dehydration-hydrogenation mechanism (Scheme 1.23)[87]. The glycerol is dehydrogenated to form glyceraldehyde which can then be directly decarbonylated by the catalyst to EG or can undergo a retro-Claisen degradation also forming EG. The former reaction is performed by noble metal catalysts (ruthenium and palladium) while the latter is preferred by first row transition metal complexes (copper and nickel).[88] The glyceraldehyde can also undergo a retro-aldol condensation to give 2-hydroxyacetaldehyde and formaldehyde. Hydrogenation of the 2-hydroxyacetaldehyde gives EG while the formaldehyde is hydrogenated to methanol.

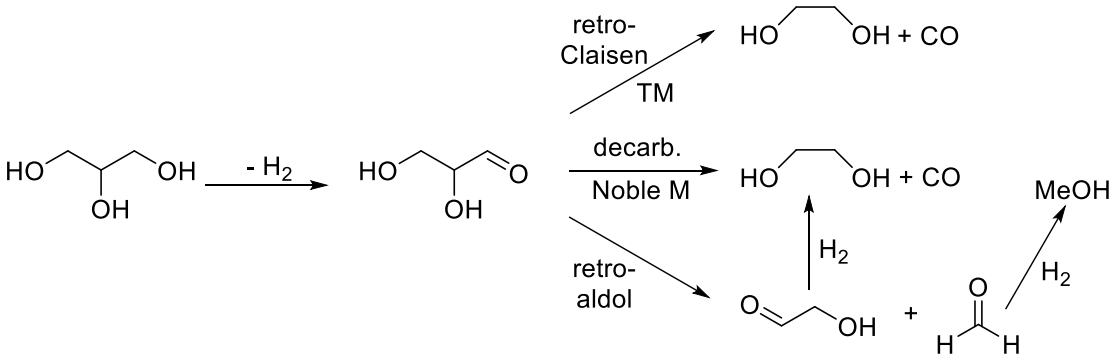

Scheme 1.23. Mechanism of EG formation from glycerol

The first homogeneous hydrogenolysis of glycerol was published by Che at Celanese, using a Rhodium/tungstate system in an aprotic basic solvent e.g. DMF or DMA.[89] This gave a mixture of 1,2- and 1,3-propanediols at very high pressures of 1:2 CO/H_2 syngas (>300 bar). Braca *et al*. then published the use of an anionic rhodium carbonyl complex, $[Rh(CO)_3I_3]^-$ which gave up to 90% selectivity for 1-propanol.[90] Shell also developed a palladium catalyst with a phosphine additive such as 1,2-bis(1,5-cyclooctylenephosphino)ethane or 1,2-bis(sec-butylphosphino)ethane that was used in a water/sulpholane mixture which again gave good selectivities to PDOs and propanols.[91] A range of homogeneous catalysts were tested at lower pressure with copper chromite giving the best conversion. At 5 wt%, 200 °C, 14 bar H_2, 47% 1,3-PDO was formed with 85% selectivity from a total conversion of 55% using glycerol with 20% water. This rose to 50% 1,3-PDO with 69% conversion when neat glycerol was used. These systems all produce either propanediols or propanols as the major

products, with EG as only a minor component. The best conversions and selectivities for EG have been obtained using heterogeneous systems.

The most studied heterogenous catalysts for glycerol hydrogenolysis to EG are based around copper, nickel and ruthenium. All these metals have been tested with a range of supports and reaction conditions. Copper received the largest amount of attention. The first published system used a Cu-ZnO catalyst prepared by co-precipitation.[92] It was found that the mechanism was bimetallic to a degree; dehydration to acetols and glycidols occurred on the acidic zinc oxide surface and the copper sites catalysed the hydrogenation reaction. Recent work using a copper catalyst in flow with a fixed reactor bed has given improved results over the older batch systems. The most effective system so far uses copper with silica and titania co-catalysts and supports which give 100% glycerol conversion and 35% EG selectivity in a fixed bed system at 280 °C, 1 bar H_2 pressure.[93]

The nickel catalysts require higher temperatures and pressures than their copper counterparts. RANEY-Ni gave the best performance (70% conversion, 40% selectivity) at 200 °C and 80 bar.[94] Despite many co-catalysts and supports being tested, this remained the best system until 2016 when Seretis and Tsiakaras presented a new catalyst featuring 65% Ni on silica modified alumina. This system gave 90% conversion of crude bio-glycerol from biodiesel production with over 40% selectivity to EG.[95]

Initial testing with ruthenium species showed that the best support materials were carbon-based rather than silica or alumina;[96] 2.4 wt% ruthenium on activated carbon gave a conversion of 58% with 29% selectivity at 220°C, 52 bar.[97] The EG yield was then improved by a Ru-Fe catalyst on carbon nanotubes which, at 200 °C, and 40 bar gave 86% conversion with 23.5% EG selectivity.[98]

1.7 – Project Aims

The chief aim of the project is to find a route to ethylene glycol that is not dependent on a C2 petrochemical feedstock. The reported work in this area highlights three major areas of interest. The first of these is the hydroformylation of formaldehyde. The published work discussed in Section 1.4.4 highlights that both the homogenous and heterogeneous systems reported to date feature forcing reaction conditions such as high temperatures and gas pressures. Catalyst modification and testing may allow for the creation of a catalyst that is active for this reaction under milder conditions. Ligand design, solvent effects, co-catalysts and additives have all been investigated to an extent in the literature and provide a starting point for experimental work. Ideally the system will be able to perform both the hydroformylation to GA and the subsequent hydrogenation to EG which may lend itself to a corresponding cobalt complex. Catalysts for the hydroformylation only will also be tested.

A second avenue for investigation is ester hydrogenation. The hydrogenation of glycolate esters to EG is of interest as these substrates can be prepared from non-fossil fuel sources in their own right or feature as part of another synthetic route to EG, such as the carbonylation of formaldehyde (Section 1.4.4) which produces glycolic acid and glycolate esters as intermediates. Oxalate compounds have also featured extensively as substrates for hydrogenation to EG. Complexes featuring tripod ligands have achieved catalysis for this reaction, although often using high hydrogen pressures. The nature of the ligands themselves offers significant scope for catalyst development. Much of the work published thus far has focussed exclusively on catalyst complexes formed *in situ*. The synthesis of pre-formed, defined catalysts could offer a route to improved catalyst performance. Other catalyst types including pincer complexes, Noyori type catalysts and species built around first-row transition metals, a growing field in recent years, have also been studied.

A third and final approach is to use glycerol as a starting point. As discussed above (Section 1.6) existing homogenous systems give mainly propanediols or propanols as a result of the hydrogenolysis of glycerol whilst heterogenous catalysts can produce more EG, but under harsh reaction conditions. By

using alternative reactivity to the hydrogenolysis route, perhaps using multi-step or indirect pathways, a more practical synthesis of EG from glycerol could be obtained, ideally using a homogeneous catalyst.

1.8 – References

1. S. Rebsdat and D. Mayer, *Ethylene Glycol in Ullman's Encyclopedia of Industrial Chemistry*, 2000.

2. R. Geyer, J. R. Jambeck, and K. L. Law, *Sci. Adv.*, 2017, **3**.

3. J. Li-Na, *Applied Mechanics and Materials*, 2013, vol. 312, pp. 406–410.

4. E. Gubbels, T. Heitz, M. Yamamoto, V. Chilekar, S. Zarbakhsh, M. Gepraegs, H. Köpnick, M. Schmidt, W. Brügging, J. Rüter, and W. Kaminsky, *Ullmann's Encyclopedia of Industrial Chemistry*, Wiley-VCH Verlag GmbH & Co. KGaA, Weinheim, Germany, 2018, pp. 1–30.

5. T. F. Stocker, D. Qin, G. K. Plattner, M. M. B. Tignor, S. K. Allen, J. Boschung, A. Nauels, Y. Xia, V. Bex, and P. M. Midgley, *Climate change 2013 the physical science basis: Working Group I contribution to the fifth assessment report of the intergovernmental panel on climate change*, Cambridge University Press, 2013, vol. 9781107057999.

6. A. Wurtz, *C. R. Hebd. Seances Acad. Sci.*, 1856, 199.

7. S. A. Miller, *Ethylene and its industrial derivatives*, Benn, 1969.

8. J. H. Miller and T. E. Corrigan, 1967, **46**, 176–178.

9. OMEGA Process Shell, 2012, https://www.shell.com/business-customers/chemicals/factsheets-speeches-and-articles/factsheets/omega.html. Accessed 01-11-2019

10. P. Magnussen, *Chemie Ing. Tech.*, 1981, **53**, 116–116.

11. G. E. Keller and M. M. Bhasin, *J. Catal.*, 1982, **73**, 9–19.

12. I. Amghizar, L. A. Vandewalle, K. M. Van Geem, and G. B. Marin, *Engineering*, 2017, **3**, 171–178.

13. J. Q. Chen, A. Bozzano, B. Glover, T. Fuglerud, and S. Kvisle, *Catalysis Today*, 2005, vol. 106, pp. 103–107.

14. S. F. Yang and N. E. Hoffman, *Annu. Rev. Plant Physiol.*, 1984, **35**, 155–189.

15. NOAA, *J. Geophys. Res.*, 2014, **101**, 4115.

16. N. J. L. Lenssen, G. A. Schmidt, J. E. Hansen, M. J. Menne, A. Persin, R. Ruedy, and D. Zyss, *J. Geophys. Res. Atmos.*, 2019, **124**, 6307–6326. *GISS Surface Temperature Analysis (GISTEMP), version 4*. NASA Goddard Institute for Space Studies. Dataset accessed 20-10-2019 https://data.giss.nasa.gov/gistemp/.

17. University of Minnesota Office for Technology Comericialization, *Syngas Production Using a Biomass Gasification Process*, 2008.

18. W. Gresham, 1953, US2636046A.

19. R. L. Pruett and W. E. Walker, 1976, US3957857.

20. K. Murata, A. Matsuda, T. Masuda, Y. Kiso, and K. Saeki, *J. Mol. Catal.*, 1987, **42**, 389–393.

21. D. M. Fenton and P. J. Steinwand, *J. Org. Chem.*, 1974, **39**, 701–704.

22. S. I. Uchiumi, K. Ataka, and T. Matsuzaki, *J. Organomet. Chem.*, 1999, 576, 279–289.

23. J. Xuanzhen, 1991, CN1055492.

24. X. Gao, Y. Zhao, S. Wang, Y. Yin, B. Wang, and X. Ma, *Chem. Eng. Sci.*, 2011, **66**, 3513–3522.

25. K. Dong, S. Elangovan, R. Sang, A. Spannenberg, R. Jackstell, K. Junge, Y. Li, and M. Beller, *Nat. Commun.*, 2016, **7**.

26. G. Reuss, W. Disteldorf, A. O. Gamer, and A. Hilt, *Ullmann's Encyclopedia of Industrial Chemistry*, Wiley-VCH Verlag GmbH & Co. KGaA, Weinheim, Germany, 2000.

27. J. Ott, V. Gronemann, F. Pontzen, E. Fiedler, G. Grossmann, D. B. Kersebohm, G. Weiss, and C. Witte, *Ullmann's Encyclopedia of Industrial Chemistry*, Wiley-VCH Verlag GmbH & Co. KGaA, Weinheim, Germany, 2012.

28. G. A. Olah, A. Goeppert, and G. K. S. Prakash, *Beyond Oil and Gas: The Methanol Economy: Second Edition*, Wiley-VCH, 2009.

29. W. Ding, Y. Liu, F. Wang, S. Zhou, A. Chen, Y. Yang, and W. Fang, *RSC Adv.*, 2014, **4**, 30677–30682.

30. P. Gao, F. Li, F. Xiao, N. Zhao, N. Sun, W. Wei, L. Zhong, and Y. Sun, *Catal. Sci. Technol.*, 2012, **2**, 1447–1454.

31. H. Bahruji, M. Bowker, G. Hutchings, N. Dimitratos, P. Wells, E. Gibson, W. Jones, C. Brookes, D. Morgan, and G. Lalev, *J. Catal.*, 2016, **343**, 133–146.

32. O. Martin, A. J. Martín, C. Mondelli, S. Mitchell, T. F. Segawa, R. Hauert, C. Drouilly, D. Curulla-Ferré, and J. Pérez-Ramírez, *Angew. Chem. Int. Ed.*, 2016, **55**, 6261–6265.

33. N. M. Rezayee, C. A. Huff, and M. S. Sanford, *J. Am. Chem. Soc.*, 2015, **137**, 1028–1031.

34. M. Everett and D. F. Wass, *Chem. Commun.*, 2017, **53**, 9502–9504.

35. J. R. Khusnutdinova, J. A. Garg, and D. Milstein, *ACS Catal.*, 2015, **5**, 2416–2422.

36. C. A. Huff and M. S. Sanford, *J. Am. Chem. Soc.*, 2011, **133**, 18122–18125.

37. J. Schneidewind, R. Adam, W. Baumann, R. Jackstell, and M. Beller, *Angew. Chem. Int. Ed.*, 2017, **56**, 1890–1893.

38. A. T. Larson, 1939, US2153064A.

39. Q. Xu and Y. Souma, *Top. Catal.*, 1998, **6**, 17–26.

40. Hendriksen and D.E., *Prepr. Pap. - Am. Chem. Soc., Div. Fuel Chem.; (United States)*, 1983, **28:2**.

41. S. Y. Lee, J. C. Kim, J. S. Lee, and Y. G. Kim, *Ind. Eng. Chem. Res.*, 1993, **32**, 253–259.

42. Y. Sun, H. Wang, J. Shen, H. Liu, and Z. Liu, *Catal. Commun.*, 2009, **10**, 678–681.

43. S. A. I. Barri and D. Chadwick, *Catal. Letters*, 2011, **141**, 749–753.

44. S. Naqvi, *Oxo Alcohols. Process Economics Program Report 21E*, Menlo Park, CA, 2010.

45. D. Evans, J. A. Osborn, and G. Wilkinson, *J. Chem. Soc. A Inorganic, Phys. Theor.*, 1968, 3133.

46. H. Song, R. Jin, M. Kang, and J. Chen, *Chinese J. Catal.*, 2013, **34**, 1035–1050.

47. M. Beller, B. Cornils, C. D. Frohning, and C. W. Kohlpaintner, *J. Mol. Catal. A Chem.*, 1995, **104**, 17–85.

48. R. Franke, D. Selent, and A. Börner, *Chem. Rev.*, 2012, **112**, 5675–5732.

49. R. H. Grubbs and P. E. Romero, 2010, US20100305368A1.

50. A. Spencer, *J. Organomet. Chem.*, 1980, **194**, 113–123.

51. R. W. Goetz, 1983, US4405821A.

52. S. E. Jacobson and C. F. Chueh, 1985, US4496781A.

53. A. S. C. Chan, W. E. Carroll, and D. E. Willis, *J. Mol. Catal.*, 1983, **19**, 377–391.

54. M. Marchionna and G. Longoni, *J. Chem. Soc. Chem. Commun.*, 1987, 1097–1098.

55. M. Marchionna and G. Longoni, *Organometallics*, 1987, **6**, 606–610.

56. J. R. Sanderson, E. L. Yeakey, J. J. Lin, R. Duranleau, and E. T. Marquis, *J. Org. Chem.*, 1987, **52**, 3243–3246.

57. H. Adkins, *Organic Reactions*, John Wiley & Sons, Inc., 8th edn., 1954, pp. 1–27.

58. R. A. Grey, G. P. Pez, A. Wallo, and J. Corsi, *J. Chem. Soc. Chem. Commun.*, 1980, 783–784.

59. M. Bianchi, G. Menchi, F. Francalanci, F. Piacenti, U. Matteoli, P. Frediani, and C. Botteghi, *J. Organomet. Chem.*, 1980, **188**, 109–119.

60. U. Matteoli, G. Menchi, M. Bianchi, and F. Piacenti, *J. Organomet. Chem.*, 1986, **299**, 233–238.

61. H. T. Teunissen and C. J. Elsevier, *Chem. Commun.*, 1997, **0**, 667–668.

62. W. Hewertson and H. R. Watson, *J. Chem. Soc.*, 1962, **0**, 1490.

63. H. T. Teunissen and C. J. Elsevier, *Chem. Commun.*, 1998, 1367–1368.

64. L. Rosi, M. Frediani, and P. Frediani, *J. Organomet. Chem.*, 2010, **695**, 1314–1322.

65. F. M. A. Geilen, B. Engendahl, A. Harwardt, W. Marquardt, J. Klankermayer, and W. Leitner, *Angew. Chem. Int. Ed.*, 2010, **49**, 5510–5514.

66. F. M. A. Geilen, B. Engendahl, M. Hölscher, J. Klankermayer, and W. Leitner, *J. Am. Chem. Soc.*, 2011, **133**, 14349–14358.

67. B. Boardman, M. J. Hanton, H. Van Rensburg, and R. P. Tooze, *Chem. Commun.*, 2006, 2289–2291.

68. M. J. Hanton, S. Tin, B. J. Boardman, and P. Miller, *J. Mol. Catal. A Chem.*, 2011, **346**, 70–78.

69. A. Phanopoulos, A. J. P. White, N. J. Long, and P. W. Miller, *ACS Catal.*, 2015, **5**, 2500–2512.

70. J. Zhang, G. Leitus, Y. Ben-David, and D. Milstein, *Angew. Chem. Int. Ed.*, 2006, **45**, 1113–1115.

71. W. Kuriyama, T. Matsumoto, O. Ogata, Y. Ino, K. Aoki, S. Tanaka, K. Ishida, T. Kobayashi, N. Sayo, and T. Saito, *Org. Process Res. Dev.*, 2012, **16**, 166–171.

72. C. Ziebart, R. Jackstell, and M. Beller, *ChemCatChem*, 2013, **5**, 3228–3231.

73. D. Spasyuk and D. G. Gusev, *Organometallics*, 2012, **31**, 5239–5242.

74. D. Spasyuk, S. Smith, and D. G. Gusev, *Angew. Chem. Int. Ed.*, 2013, **52**, 2538–2542.

75. L. A. Saudan, C. M. Saudan, C. Debieux, and P. Wyss, *Angew. Chem. Int. Ed.*, 2007, **46**, 7473–7476.

76. W. Kuriyama, Y. Ino, O. Ogata, N. Sayo, and T. Saito, *Adv. Synth. Catal.*, 2010, **352**, 92–96.

77. I. Carpenter, S. C. Eckelmann, M. T. Kuntz, J. A. Fuentes, M. B. France, and M. L. Clarke, *Dalton Trans.*, 2012, **41**, 10136–10140.

78. T. Zell, Y. Ben-David, and D. Milstein, *Angew. Chem. Int. Ed.*, 2014, **53**, 4685–4689.

79. S. Chakraborty, H. Dai, P. Bhattacharya, N. T. Fairweather, M. S. Gibson, J. A. Krause, and H. Guan, *J. Am. Chem. Soc.*, 2014, **136**, 7869–7872.

80. T. J. Korstanje, J. I. Van Der Vlugt, C. J. Elsevier, and B. De Bruin, *Science*, 2015, **350**, 298–302.

81. S. Elangovan, M. Garbe, H. Jiao, A. Spannenberg, K. Junge, and M. Beller, *Angew. Chem. Int. Ed.*, 2016, **55**, 15364–15368.

82. M. B. Widegren, G. J. Harkness, A. M. Z. Slawin, D. B. Cordes, and M. L. Clarke, *Angew. Chem. Int. Ed.*, 2017, **56**, 5825–5828.

83. R. van Putten, E. A. Uslamin, M. Garbe, C. Liu, A. Gonzalez-de-Castro, M. Lutz, K. Junge, E. J. M. Hensen, M. Beller, L. Lefort, and E. A. Pidko, *Angew. Chem. Int. Ed.*, 2017, **56**, 7531–7534.

84. N. A. Espinosa-Jalapa, A. Nerush, L. J. W. Shimon, G. Leitus, L. Avram, Y. Ben-David, and D. Milstein, *Chem. Eur. J.*, 2017, **23**, 5934–5938.

85. F. Yang, M. a Hanna, and R. Sun, *Biotechnol. Biofuels*, 2012, **5**, 13.

86. Y. Wang, J. Zhou, and X. Guo, *RSC Adv.*, 2015, 5, 74611–74628.

87. S. Wang, K. Yin, Y. Zhang, and H. Liu, *ACS Catal.*, 2013, **3**, 2112–2121.

88. S. Kandasamy, S. P. Samudrala, and S. Bhattacharya, *Catal. Sci. Technol.*, 2019, 9, 567–577.

89. T. M. Che, 1987, US4642394A.

90. G. Braca, A. M. Raspolli Galletti, and G. Sbrana, *J. Organomet. Chem.*, 1991, **417**, 41–49.

91. E. Drent and W. W. Jager, 2000, US6080898A.

92. S. Wang and H. Liu, *Catal. Letters*, 2007, **117**, 62–67.

93. Y. Feng, H. Yin, A. Wang, L. Shen, L. Yu, and T. Jiang, *Chem. Eng. J.*, 2011, **168**, 403–412.

94. T. Jiang, M. X. Ren, S. S. Chen, Q. Huai, W. Y. Ying, and F. H. Cao, *Adv. Mater. Res.*, 2014, **906**, 103–111.

95. A. Seretis and P. Tsiakaras, *Renew. Energy*, 2016, **97**, 373–379.

96. E. P. Maris and R. J. Davis, *J. Catal.*, 2007, **249**, 328–337.

97. R. Mane, S. Patil, M. Shirai, S. Rayalu, and C. Rode, *Appl. Catal. B Environ.*, 2017, **204**, 134–146.

98. B. Li, J. Wang, Y. Yuan, H. Ariga, S. Takakusagi, and K. Asakura, *ACS Catal.*, 2011, **1**, 1521–1528.

Chapter 2 – Hydroformylation of Formaldehyde

2.1 – Introduction

As discussed in the introductory chapter (Section 1.4), the reductive hydroformylation of formaldehyde presents a route to EG synthesis without the need for raw materials derived from petrochemical sources. The traditional hydroformylation reaction uses an olefin substrate which is converted to an aldehyde. This can then be converted to an alcohol by an additional hydrogenation step, either by a separate catalysts or, in the case of cobalt catalysts, the same hydroformylation-active species. Most of the focus around this reaction concerns rhodium complexes, around 80% of all commercial hydroformylation reactions being catalysed by this metal;[1] however, rhodium is traditionally a poor metal for hydrogenation catalysis meaning that the reaction only proceeds to the aldehyde, in this case glycolaldehyde (Section 1.4). A separate hydrogenation catalyst, often ruthenium based, is used to perform the hydrogenation to the alcohol. Cobalt has been used as an alternative to rhodium for hydroformylation catalysis, and indeed pre-dates the use of the precious metal. It has the advantages of being much cheaper than rhodium and can catalyse the final hydrogenation step as well as the initial hydroformylation. A well-studied catalyst is $[HCo(CO)_4]$ which is formed *in situ* from the widely available precursor $[Co_2(CO)_8]$ and H_2. A downside to using cobalt is that the catalysts often require harsh reaction conditions, especially high pressure. Phosphines are often used as ligands to improve catalyst stability and maintain performance when milder conditions are employed. The mechanisms for these reductive hydroformylation processes are well established with olefin substrates and can easily be adjusted for formaldehyde (Scheme 2.1).

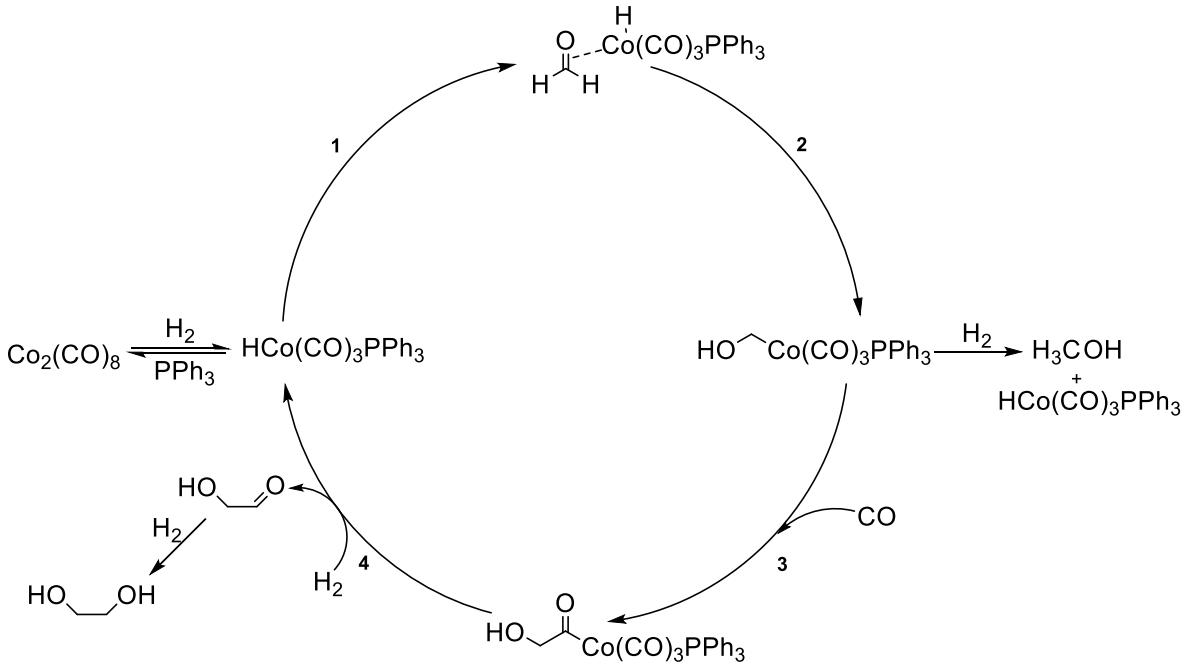

Scheme 2.1. Reductive Hydroformylation mechanism[2] adapted for formaldehyde

The $[Co_2(CO)_8]$ dissociates a CO ligand to form $[Co_2(CO)_7]$, which has a vacant site to react with H_2, forming $[HCo(CO_4)]$. The unsaturated substrate inserts into the Co – H bond (**2**) and CO is then subsequently inserted to form an acyl complex (**3**). ^{13}CO Labelling studies with $[MeMn(CO)_5]$ have shown that this CO comes from a bound ligand on the manganese centre rather than from the gas atmosphere.[3] It has been debated whether this step is an insertion of CO or a migration of the alkyl group to the CO ligand with the majority of the evidence suggesting the latter. The hydrogenation to the aldehyde (**4**) then requires dissociation of another CO ligand. Deuterium labelling experiments have shown that the hydrogenation can occur through two different mechanisms depending on which cobalt species are present. If there is a high concentration of $[HCo(CO)_4]$, this species will perform the reaction; however if the cobalt is predominantly as $[Co_2(CO)_8]$ then a direct hydrogenation with H_2 (or D_2) will occur (Scheme 2.2).[4] The phosphine ligands improve reactivity by acting as a nucleophile to stabilise the vacant sites after the CO dissociation steps.[5]

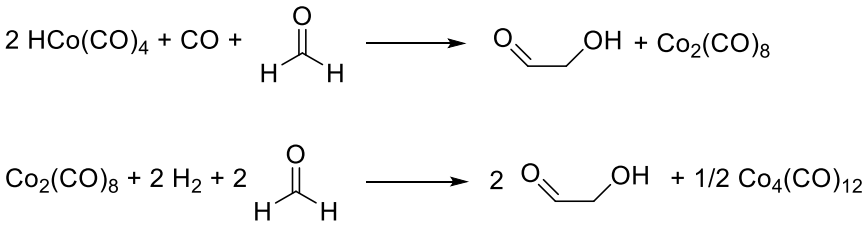

Scheme 2.2. Two different pathways to aldehyde formation

2.2 Cobalt – Phosphine Systems

2.2.1 – Initial Tests

The reductive hydroformylation of formaldehyde was attempted using *in situ* cobalt phosphine systems formed from dicobalt octacarbonyl, [$Co_2(CO)_8$] and a range of widely available phosphines. Triphenylphosphine was used for much of the work due to its low cost and ease of handling. Acetonitrile was selected as the solvent after work from Jacobson; this study reports a rhodium catalyst, in polar, aprotic solvents that can act as N-donors, in tandem with the phosphine ligands gives good conversion of formaldehyde to glycolaldehyde.[6] The results of these preliminary tests are shown below (Table 2.1).

Table 2.1. Hydroformylation of paraformaldehyde with Co-phosphine systems

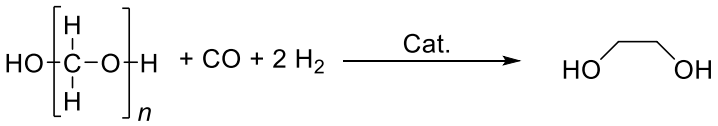

Run[a]	Phosphine	CO:H_2 ratio	%Yield EG	% Yield MeOH
1	PPh_3	1:2	9	78
2	PPh_3[b]	1:2	8	77
3	PPh_3	1:1	4	63
4	PPh_3	1:3	5	57
5	PPh_3	1:4	3	62
6	PPh_3[c]	1:2	3	41
7	PEt_3	1:2	3	30
8	1,1,1-Tris(diphenylphosphinomethyl)ethane	1:2	4	53

[a]conditions: 5 mmol paraformaldehyde, 10 mol% $Co_2(CO)_8$, 20 mol% phosphine, CH_3CN 10 mL, 40 bar, 180 °C, 3 h, [b]20 h, [c]DMF, 110 °C

None of the systems successfully achieved catalytic turnover. There was also no improvement from a 3 to 20 hour reaction time (compare Runs 1 to 2) under the same conditions. Kinetic studies reported in the literature had shown that increasing the hydrogen partial pressure increases the rate of hydroformylation whereas, above a threshold of 10 bar, increasing the CO partial pressure decreases the rate.[7] These studies were conducted using a rhodium catalyst, with cobalt, which is known as a better hydrogenation catalyst, it is likely that this increase in H_2 partial pressure increases the undesired hydrogenation of formaldehyde to methanol (Scheme 2.1). There was no improvement in EG production with increased H_2 partial pressure with a 1:2 CO:H_2 ratio, which corresponds to the ratio of these reagents in the reaction stoichiometry, giving the highest yield (Runs 1, 3 ,4 ,5). It may

be the case that a high CO partial pressure is required to form the catalyst species and suppress the formation of methanol.

The reactions all produced significant quantities of methanol. This could be formed in two ways; (1) through the hydrogenation of the syngas or (2) *via* the direct hydrogenation of the paraformaldehyde substrate, (Figure 2.1). To test the first route, a control experiment with no formaldehyde, but 40 bar 1:2 CO/H_2 syngas and the $[Co_2(CO)_8]/PPh_3$ system was performed. This produced 3 mmol of MeOH equivalent to a 60% yield in the formaldehyde tests. In both this test and those using the paraformaldehyde substrate in Table 2.1, a large amount of a metallic solid product was formed. It may be that the syngas pressures used for these reactions are not high enough to keep the cobalt complexes generated in the solution phase. The metallic Co solid could have played a role in the hydrogenation of syngas *via* a heterogeneous pathway. Cobalt species have been previously reported as part of a heterogeneous catalyst system for the conversion of syngas to methanol e.g. a Co doped CuZrCr catalysed prepared by co-precipitation reported by Calafat and Laine .[8,9]

Direct hydrogenation of formaldehyde could have occurred if the cobalt had bound to the substrate through the oxygen atom rather than the carbon (Figure 2.1). This would have given a bound methoxy complex which would not react with CO to give the desired acyl complex but could have been susceptible to hydrogenation releasing methanol and reforming the cobalt-hydride catalyst.

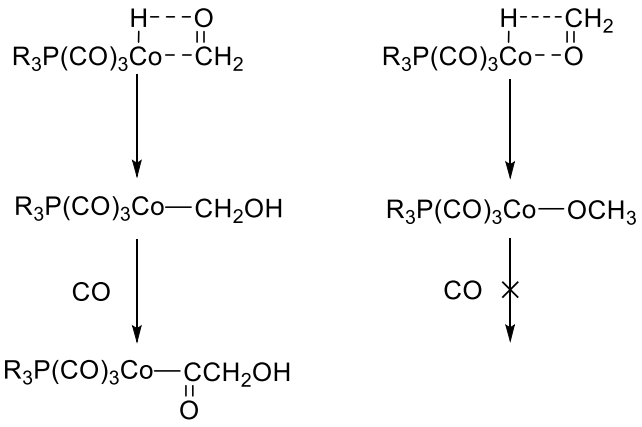

Figure 2.1. Possible Co to formaldehyde binding arrangements

In an attempt to enhance the Co – C bonding, electron-donating substituents on the phosphine ligand were selected and tested. It was proposed that this would have made the Co atom more electron rich increasing its affinity for the electron poor carbonyl carbon over the oxygen atom. The two ligands selected were triethylphosphine (PEt_3) and tri-*tert*-butylphosphine (P^tBu_3). The former did give a marked decrease in the amount of methanol produced but showed no improvement for EG formation when compared to triphenylphosphine (Run 7, Table 2.1). This test produced around half the yield of methanol as the PPh_3 tests (Runs 1-5), but a significant quantity (30%) is still present. This suggests that the methanol formed is as a result of a combination of direct hydrogenation of syngas and by Co-O binding with the formaldehyde. P^tBu_3 produced no EG, possibly due to the large steric bulk of the ligand precluding any sort of substrate binding.

The methanol production can also be rationalised by work published by Spencer with rhodium carbonyl phosphine complexes.[10] It was noted that while higher temperatures improved glycolaldehyde yield they also lead to large quantities of methanol being formed. A large increase in methanol formation was seen at 120 °C, believed to be caused by thermal degradation of the formaldehyde. It was stated that the highest selectivity was obtained at 110 °C with an *N*-substituted amide solvent featuring two small alkyl groups, e.g., DMF (Run 8, Table 2.1), but when tested this gave no improvement on the performance seen with CH_3CN at 180 °C. Furthermore, a thermal stability

experiment conducted with paraformaldehyde in CH_3CN at 180 °C for 3 hours revealed no methanol formation or other degradation at all.

Much of the literature work used high syngas pressures with the best results achieved above 120 bar.[6,10,11] To replicate these conditions, the apparatus in the high-pressure lab at the University of Bristol was used to achieve syngas pressures higher than those permitted in the synthetic labs. The autoclave was pressurised to 80 bar which yielded a reaction pressure of between 105 and 110 bar at the reaction temperature of 180 °C.

Table 2.2. High pressure experiments

Run[a]	Catalyst Loading (mol%)	Solvent	%Yield EG	%Yield MeOH
1	5	CH_3CN	6	26
2	5	DMF	5	53
3	5	PhCl	5	40
4	10	PhCl	8	76

[a]conditions: 5 mmol *para*formaldehyde, 1:1 Co:PPh_3, 10 mL solvent, 180 °C, 80 bar 2:1 H_2: CO, 3 h

The results (Table 2.2) reveal that the increased pressure gave no improvement on performance with all the values indicating less than one full turnover. During the first test there was substantial gasification of the acetonitrile solvent, attributed to a hydrogenation to ethylamine. DMF and PhCl, which is high boiling and inert to the reaction conditions, also gave poor turnover (Runs 2-4). Earlier tests using toluene had shown that the cobalt precursor [$Co_2(CO)_8$] was completely insoluble in this solvent.

To try to establish if there was any interaction between the cobalt precursor and the phosphines, [$Co_2(CO)_8$] and PPh_3 were stirred under the reaction conditions given in (Table 2.1) without substrate. The product mixture was analysed by $^{31}P\{^1H\}$ NMR spectroscopy (Figure 2.2). The resonance at -4.8 ppm is from unreacted PPh_3, but the signal at 24.6 ppm could be caused by a cobalt phosphine

complex. The peak appears as a singlet, so is not coupling to any nearby ^{31}P nuclei. The $[Co(CO)_3PPh_3]$ species, referred to in the literature for Co hydroformylation systems, is an unstable 17 electron species so is unlikely to have been observed. It is also d^9 and paramagnetic so would not give a sharp peak in the $^{31}P\{^1H\}$ NMR spectrum. The corresponding dimer complex $[Co_2(CO)_6(PPh_3)_2]$ featuring a cobalt-cobalt bond *cf.* $[Co_2(CO)_8]$ is a more likely candidate.[5]

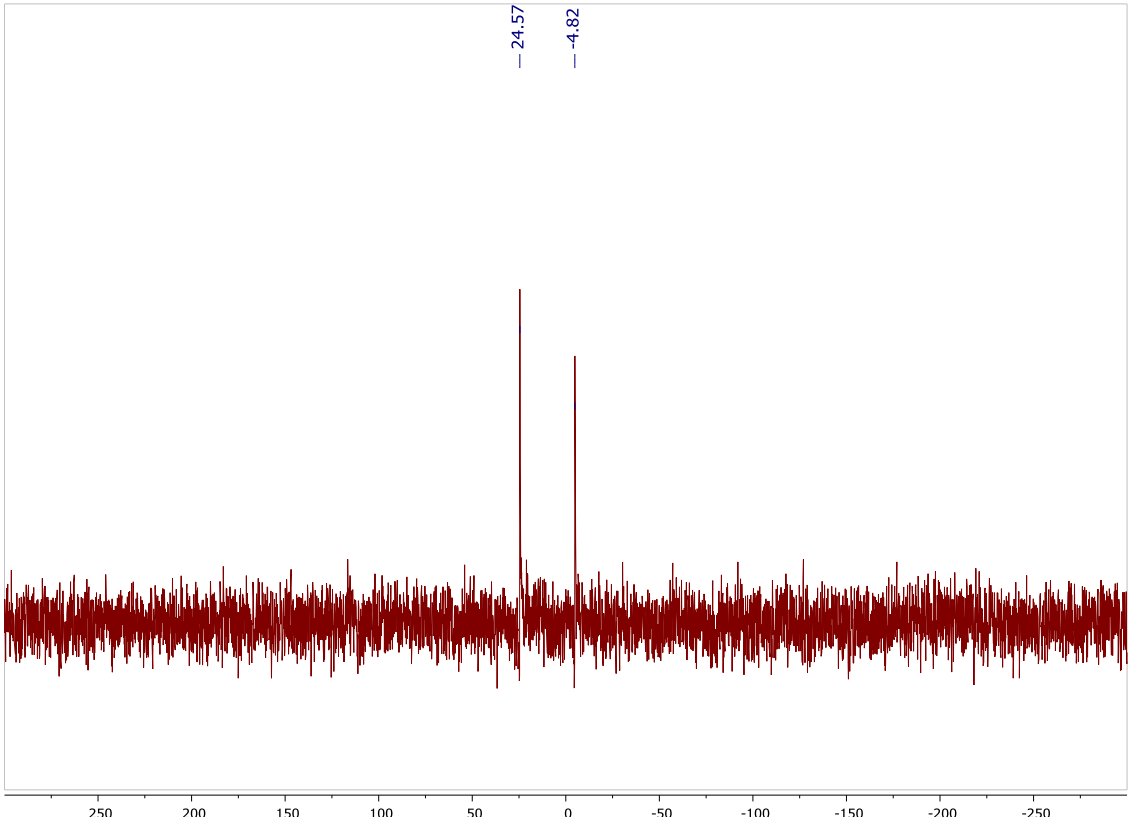

Figure 2.2.- $^{31}P\{^1H\}$ NMR (300 MHz, $CDCl_3$) catalyst pre-form test

A typical post-reaction $^{31}P\{^1H\}$ NMR spectrum for a $[Co]/PPh_3$ test is shown below (Figure 2.3). Three clear resonances are present; free triphenylphosphine at -4.7 ppm, with two other singlets at 27.9 and 55.6 ppm. The peak at 27.9 almost certainly corresponding to triphenylphosphine oxide. The phosphorus species generating a peak at 55.6 ppm is only present in this sample with the significant downfield shift highlighting a more electron poor phosphine environment.

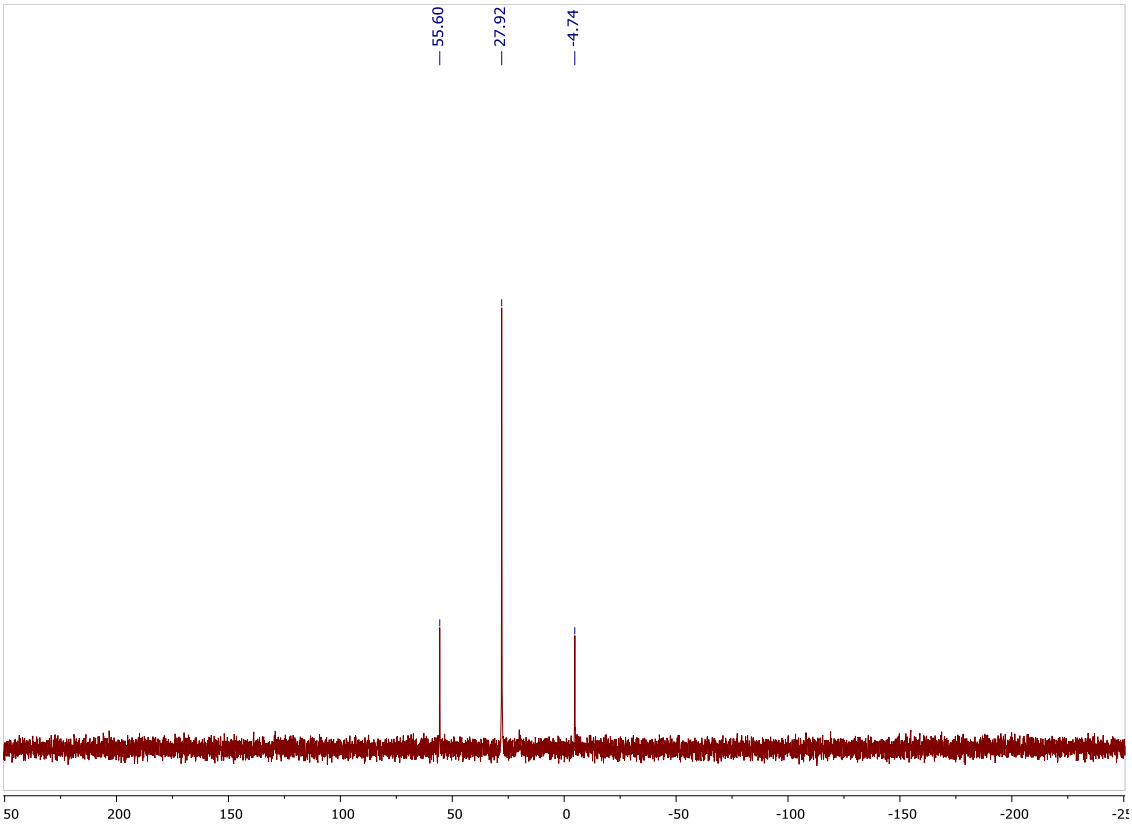

Figure 2.3. Example $^{31}P\{^{1}H\}$ NMR (162 MHz, $CDCl_3$) of Co/PPh_3 post reaction mixture

2.2.2 – Hydrogenation of Glycolaldehyde

The reductive hydroformylation route discussed above in Section 2.2.1 consists of two separate reactions; firstly, a hydroformylation of formaldehyde to glycolaldehyde which is then followed by a hydrogenation of this intermediate to EG. As attempts to perform both steps in one-pot with the same catalyst were unsuccessful the two reactions were examined independently. The first to be investigated was the hydrogenation of glycolaldehyde to EG. Glycolaldehyde is known to dimerise in the solid and liquid phase to a cyclic compound shown below (Scheme 2.3).

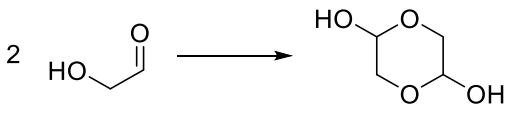

Scheme 2.3. Dimerisation of glycolaldehyde

The direct hydrogenation of the dimer was attempted using the $[Co_2(CO)_8]/PPh_3$ catalysts system with 40 bar H_2, which yielded only 10% EG. Cleavage of the dimer into its more reactive aldehyde components was subsequently tried using HCl. The resulting product mixture was analysed by GC-MS which revealed a number of species present including the desired glycolaldehyde and starting dimer. The structure with the highest occurrence could not be identified exactly but appears to correspond to a C3 fragment containing two oxygen atoms. The other compounds present are shown below (Figure 2.4).

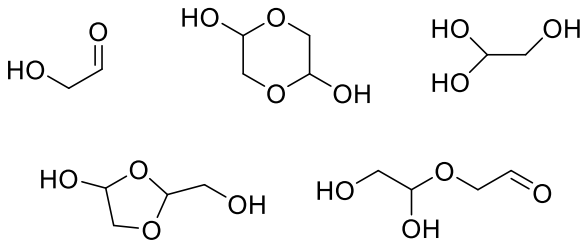

Figure 2.4. Observed glycolaldehyde species

The results from Section 2.2 show that despite testing a range of conditions including pressure, solvent, and H_2:CO ratio the cobalt/phosphine systems gave only a low level of activity for the reductive hydroformylation of formaldehyde not achieving a full catalytic turnover. Significant quantities of methanol are produced in each reaction which could originate from three reactions. The experimental results suggest that the majority of this methanol is likely to come from a direct hydrogenation of the syngas itself rather than from hydrogenation of the formaldehyde or thermal degradation of paraformaldehyde. A hydrogenation of glycolaldehyde was also attempted using the cobalt/phosphine catalyst which only gave a 10% yield. This reaction may have been hindered by the large array of compounds formed by glycolaldehyde in solution.

2.3 – Rhodium Catalysed Hydroformylation

Much of the work concerning the hydroformylation of formaldehyde has been based on rhodium systems so this was the second metal to be investigated. The target product for this study was glycolaldehyde, rather than EG since rhodium has little track record of tandem hydroformylation/hydrogenation. As mentioned above in Section 2.2.2 the analysis of a solution containing glycolaldehyde is not trivial, so a trapping reagent was used to calculate production. Phenylhydrazine was added to the post-reaction mixture to form the corresponding phenylhydrazone with glycolaldehyde, which was suitable for quantitative GC analysis (Scheme 2.4).

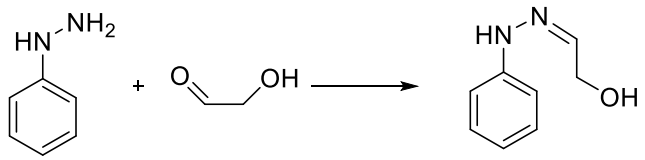

Scheme 2.4. Trapping glycolaldehyde with phenylhydrazine

The rhodium catalyst selected was [RhCl(CO)(PPh_3)$_2$] which had provided the highest activity in the reported literature.[10,11] The most successful system used DMF at 110 °C. A 0.5 mol% loading with 40 bar 2:1 H_2:CO syngas were also selected. Unfortunately, after the hydrazine addition none of the desired hydroxyethyl phenylhydrazone was produced, only an unwanted species formed from the reaction of the phenylhydrazine with formaldehyde starting material rather than glycolaldehyde. Jacobson reported that the Rh catalysts can be improved by using a phosphinoamide ligand as part of an *in situ* system.[6] A phosphinoamide was synthesised according to a literature procedure (Scheme 2.5).[12] This was then tested with the same Rh precursor at 0.5 mol% loading under the same conditions. Again, none of the desired phenylhydrazine product with glycolaldehyde was observed, only evidence of unreacted formaldehyde.

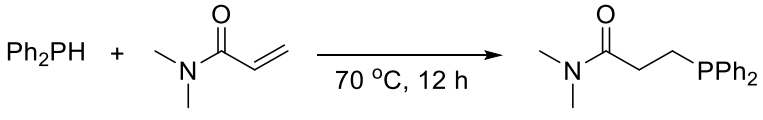

Scheme 2.5. Synthesis of phosphinoamide ligand

The disappointing performance of both the cobalt and rhodium systems was most likely due to the low syngas pressures used in the reactions. Even with the more active rhodium complexes pressures of 120 bar or greater are often required to achieve significant turnover to glycolaldehyde. These pressures were simply not feasible with the equipment available, so an alternative method was examined.

2.4 – Lewis Acid – Cobalt Carbonyl Systems

2.4.1 – Introduction

Coates has reported a catalyst system based around a Lewis acid cation with the cobalt tetracarbonyl anion, known to be active for hydroformylation reactions, for the reaction of epoxides and CO_2 to produce polycarbonates.[13] It was proposed that these Lewis acids, based around an aluminium centre with a tetradentate salen ligand, could activate the formaldehyde substrate offering a pathway to the hydroformylation reaction at lower syngas pressures (Figure 2.5).

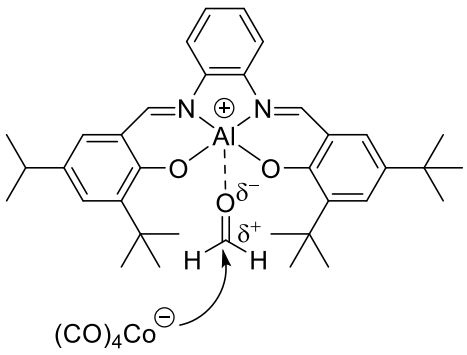

Fig. 2.5. Proposed activation of formaldehyde by Lewis Acid

A hypothesised mechanism is shown below (Scheme 2.6). The Lewis acid cation would be expected to coordinate to the oxygen atom of the formaldehyde drawing electron density from the C=O bond making the carbon more electron poor. This would increase the affinity of the $[Co(CO)_4]^-$ anion for this carbon atom and therefore increasing the likelihood of this cobalt-substrate interaction. This cooperative ion pair mechanism is very similar to Frustrated Lewis Pair (FLP) chemistry which has been

used for numerous reactions with small, unsaturated molecules such as CO reduction in syngas[14] and CO_2 capture.[15] Aluminium Lewis acids have even been used for the activation of small alkenes, ethylene and propylene.[16]

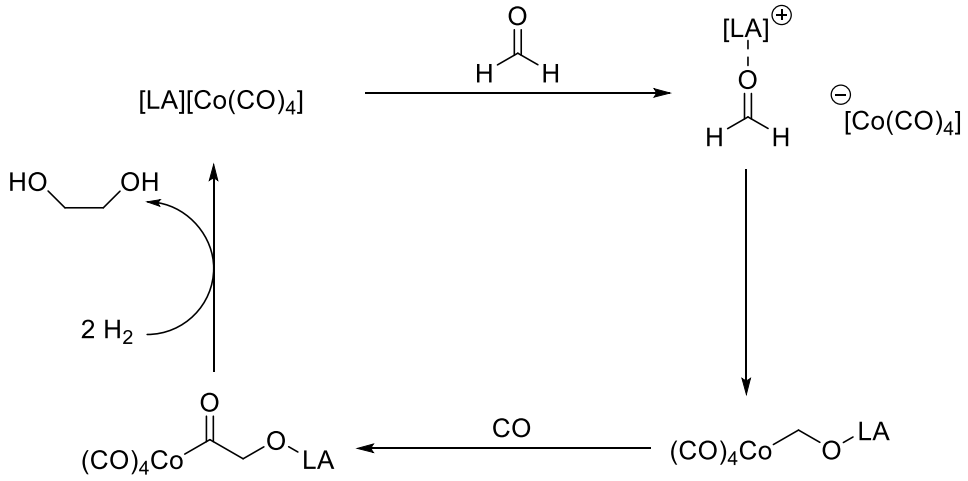

Scheme 2.6. Proposed mechanism for reductive hydroformylation of formaldehyde with [LA][Co(CO)$_4$]

2.4.2 – Catalyst Synthesis

The best performing system published by Coates uses a symmetric salophen ligand with a large delocalised π-system.[17] The ligand helps to stabilise the positively charged aluminium centre in the final complex. This was prepared from the condensation reaction of 1,2-phenylenediamine with 3,5-Di-tert-butyl-2-hydroxybenzaldehyde (Scheme 2.7).[18] The *tert*-butyl groups improve the solubility of the final compound in a wider range of solvents which gives more possibilities for reaction conditions in catalysis. The ligand was isolated with the ^{1}H NMR values matching those reported in the literature, clearly showing the imine protons at 11.6 ppm.

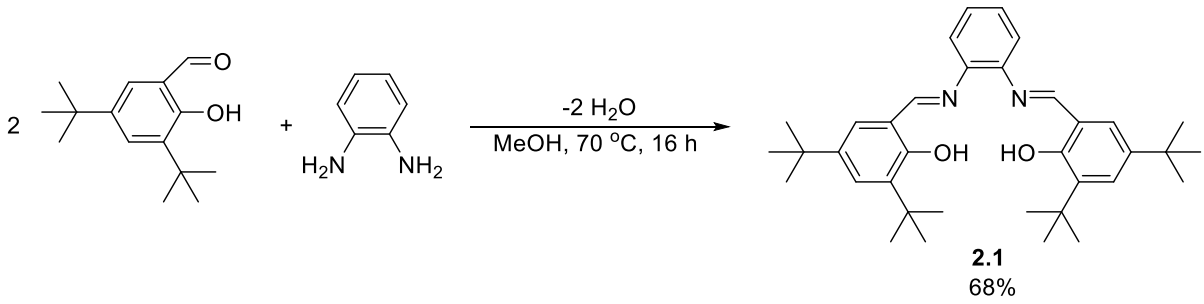

*Scheme 2.7. Synthesis of salophen ligand **2.1***

The ligand was then metallated with aluminium (Scheme 2.8) to give the neutral Al(III) chloride complex.[17] This gave the ^{1}H NMR results in agreement with the literature and ESI-MS gave the expected molecular ion peak at 598 m/z units with a peak at 565 indicating the loss of the chloride ligand. The rigidity of the salophen ligand means it is likely that the complex takes on a square pyramidal configuration with the metal halide bond coming out of the plane of the *O,N,N,O* arrangement. The aluminium atom is also very slightly displaced out of the plane of the ligand which can be vital for catalysis.[19] The displacement removes steric hindrance around the aluminium centre creating more space for the metal-substrate interaction.

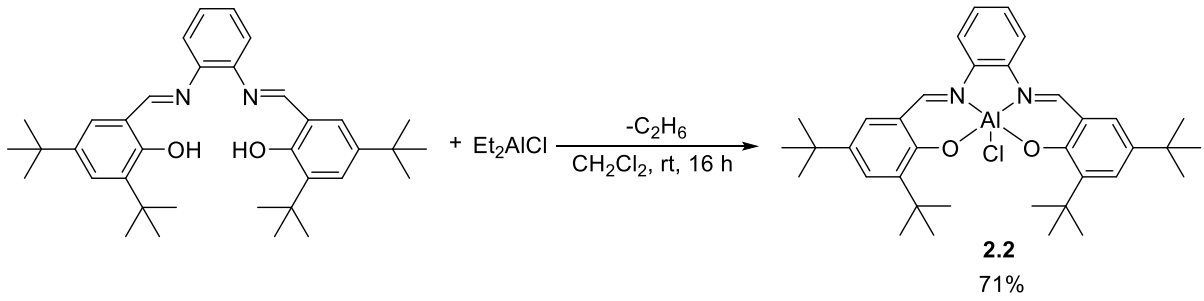

*Scheme 2.8. Synthesis of (salophen)AlCl **2.2***

The cobalt carbonyl precursor **2.3** was formed from $[Co_2(CO)_8]$ with NaOH (Scheme 2.9).[20] The Co(-I) salt, while more robust in solution, is extremely air sensitive as a solid and any exposure to air will change the colour from white to red indicating oxidation of the cobalt. A solution phase ATR-IR of the product in THF gave the desired ν(CO) at 1889 cm^{-1}.

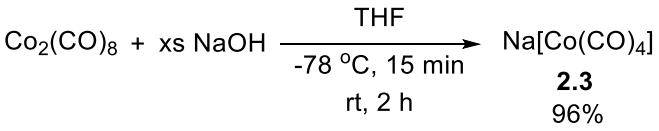

Scheme 2.9. Synthesis of $Na[Co(CO)_4]$ ***2.3***

The full ion pair was then prepared by reacting **2.2** and **2.3** together in THF (Scheme 2.10).[17] The ^1H NMR spectrum of the isolated complex was identical to that of the aluminium precursor except that it shows the bound THF molecules and the carbonyl stretching frequency at 1889 cm^{-1} was still present showing the $[Co(CO)_4]^-$ anion was intact.

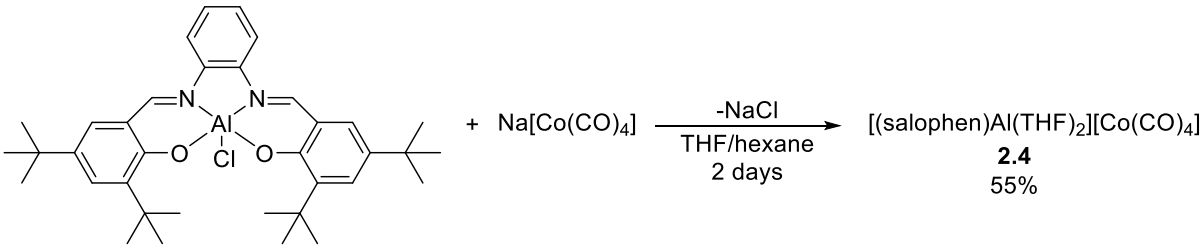

Scheme 2.10. Synthesis of complete ion pair ***2.4***

2.4.3 – Catalyst Testing

With the ion pair compound successfully synthesised it was tested for the reductive hydroformylation of formaldehyde. The results are shown below in Table 2.3.

*Table 2.3. Attempted reductive hydroformylation of formaldehyde with **2.4***

Run[a]	Catalyst	Solvent	%Yield EG	%Yield MeOH
1	**2.4**	THF	0	88
2	**2.4**[b]	THF	0	67
3	**2.4**[b]	DMF	0	69
4	**2.4**	PhCl	0	102
5	$Na[Co(CO)_4]$	THF	0	60
6	$[PPh_4][Co(CO)_4]$	THF	0	116
7	$H[Co(CO)_4]$	DME	0	137

[a]conditions: 5 mmol paraformaldehyde, 0.5 mol% catalyst, 10 mL solvent, 180 °C, 40 bar 2:1 H_2:CO, 20 h [b] 110 °C

The complex gave no turnover to EG with the formaldehyde remaining unreacted (Runs 1-4). None of the species formed from glycolaldehyde identified in Section 2.2.2 were observed by GC-MS. The MeOH yields of over 100% (Runs 4,6 and 7) were found, as with the cobalt/phosphine systems (Section 2.2.1), to be caused by direct syngas to methanol chemistry without the involvement of formaldehyde. While lowering the reaction temperature to 110 °C (Runs 2 and 3) did lower the quantity of MeOH produced it made no improvement on EG. The use of DMF as a solvent (Run 3), previously shown to be beneficial with rhodium catalysts, also did not have any effect on EG yield. The sodium salt of the cobalt carbonyl anion was tested along with another non-Lewis acidic tetraphenylphosphonium compound which also gave no reactivity (Runs 5 and 6).[21] Finally, the hydride species, which is an active hydroformylation catalyst, was prepared *in situ* from $[Ph_3Si][Co(CO)_4]$ and tosylic acid in DME; however this species also gave no turnover (Run 7).[22] Perhaps unsurprisingly as it features a protic component it resulted in the highest degree of syngas to methanol hydrogenation. It is clear from these results that these ion pair complexes could not catalyse the required chemistry so further modifications to the system were investigated.

2.4.4 – Appended Ammonium Salt Arm Salophen Complex

In 2017 Peters *et al*. published the use of an aluminium salen compound with an appended quaternary ammonium salt arm for the carboxycyanation of aldehydes. [23] The aluminium Lewis acid activated the substrate while the arm guided the cyanide anion for a selective attack in the correct position (Figure 2.6) which vastly improved TON and yield. As the desired hydroformylation reaction also features an anionic component ($[Co(CO)_4]^-$) perhaps this assistance could provide some turnover.

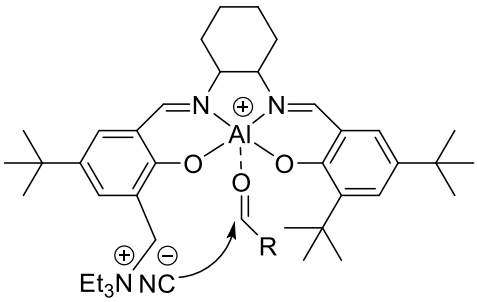

Figure 2.6. Mode of action of appended arm salophen catalyst for carboxycyanation of aldehydes

The ligand was prepared in several steps following the literature procedure (Scheme 2.11).[23] 5-*tert*-butyl-2-hydroxylbenzaldehyde was reacted with a formaldehyde solution and diethylamine through an aromatic substitution reaction with a corresponding condensation, Scheme 2.10, to form the product with an amine arm. The ^{1}H NMR spectrum concurs with the literature. The CH_2 protons in the chain arm are visible as a singlet at 3.78 ppm with the *N*-ethyl groups visible as a quartet at 2.61 ppm for the CH_2 protons and a triplet at 1.10 ppm for the CH_3 signal with an integration ration of 2:3.

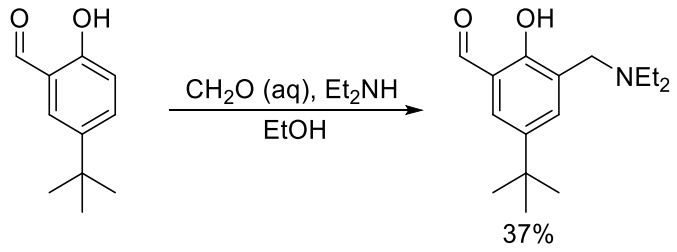

Scheme 2.11. Synthesis of amine arm ligand fragment

To ensure the desired asymmetric ligand was obtained one of the amine sites of the 1,2-diaminocyclohexane was protected by conversion to the mono-hydrochloride salt (Scheme 2.12).

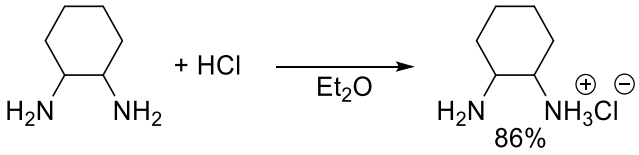

Scheme 2.12. Synthesis of monoamine hydrochloride salt

The two benzaldehyde precursors were added sequentially, the di-*tert*-butyl variant first then, the amine arm compound was added along with triethylamine to re-form the cyclohexylamine from the hydrochloride salt (Scheme 2.13). After purification, the product ^{1}H NMR was in accordance with the literature, crucially showing two ^{1}H signals at 8.26 and 8.30 ppm corresponding to the two imine protons.

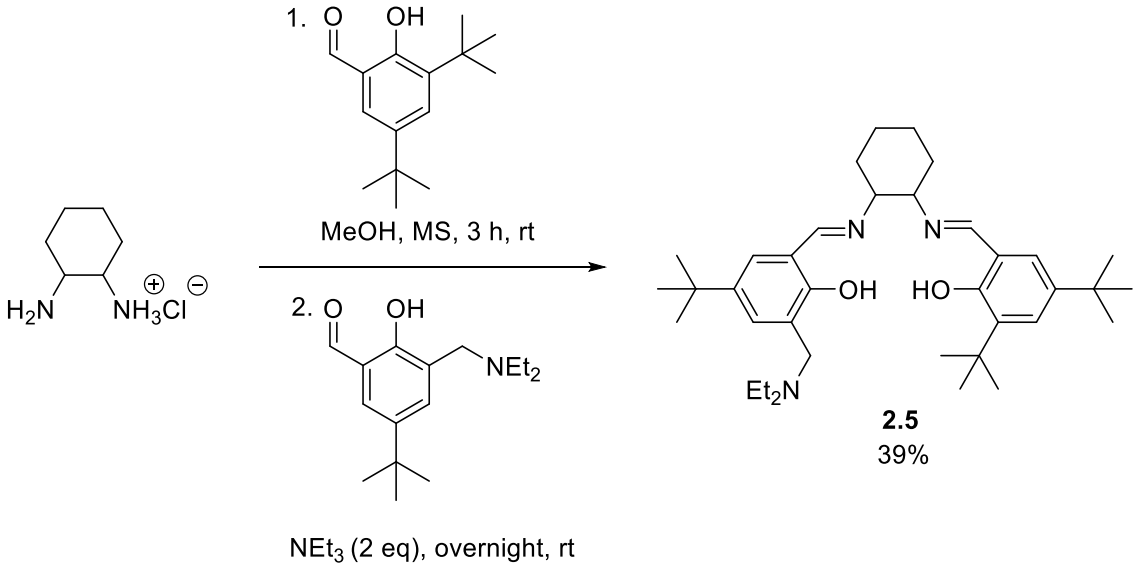

*Scheme 2.13. Synthesis of amine arm pro-ligand **2.5***

To form the final ligand containing the ammonium salt the pro-ligand was reacted with triethyloxonium tetrafluroroborate (Scheme 2.14). This strong alkylation agent effectively acts as a source of Et^{+} which reacts with the amine forming a salt with a BF_4^{-} counterion and Et_2O as a by-

product. The attached strongly electron-accepting phenyl system weakens the nucleophilicity of the amine site. This necessitated the use of a powerful, strongly electrophilic alkylating agent for the reaction.[24]

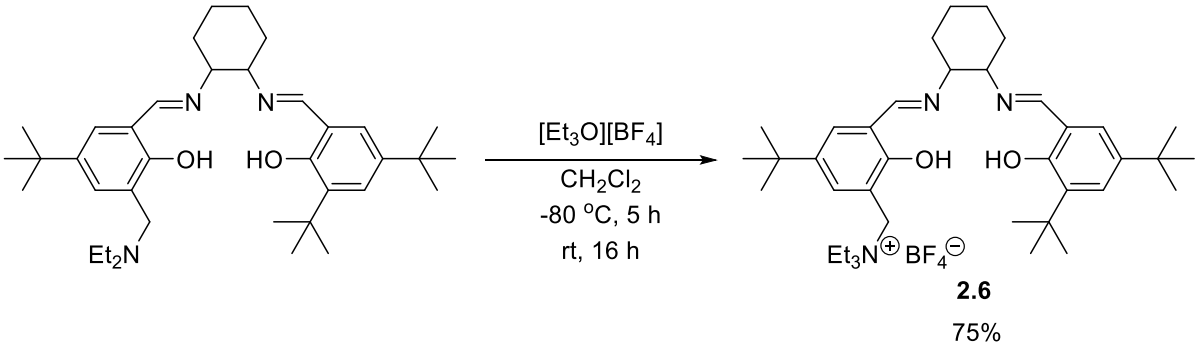

*Scheme 2.14. Synthesis of appended ammonium salt salen ligand **2.6***

The ^{19}F NMR spectrum showed the expected peaks at -152.35 and -152.41 caused by the $^{10}BF_4^-$ and $^{11}BF_4^-$ anions respectively. These two isotopes have different spin values, 3 and 3/2, so they are observed as two distinct peaks at very slightly different chemical shifts. Both isotopes are quadrupolar so their nuclei have fast relaxation times causing the resulting signals to appear broad. The protons signals derived from the ethyl groups on the newly formed ammonium salt have shifted downfield significantly and are now found as part of a large overlapping series of peaks with the 1,2-cyclohexyl protons adjacent to the imines between 3.15 and 3.48 ppm.

The ligand was metallated using [Et_2AlCl] as with the salophen ligand (**2.1**) (Scheme 2.15) to give the Al(III) chloride complex. The resulting ^1H NMR spectrum showed the loss of the hydroxide protons at 10.4 ppm from the ligand and the ESI-MS gave an expected molecular ion peak at 308.4 m/z corresponding to an $[M\text{-}Cl]^+$ fragment.

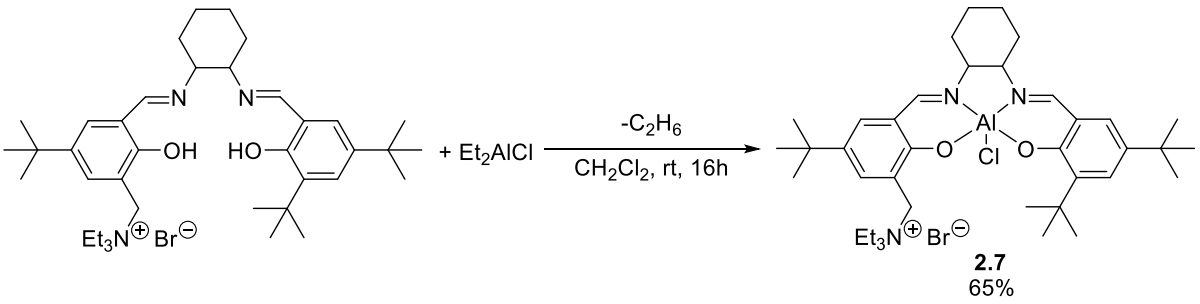

*Scheme 2.15. Synthesis of Al precursor complex with ammonium ligand **2.7***

Instead of preparing the full ion pair as with the salophen complex (**2.4**) the catalyst was formed *in situ* from the Al complex above and $Na[Co(CO)_4]$ (**2.3**). This was to remove any issues around the crystallisation of the ion pair complex and to minimise handling of the air sensitive cobalt anion. This system was tested for the hydroformylation of paraformaldehyde under identical conditions to **2.4** (40 bar 2:1 H_2:CO syngas at 180 °C for 20 hours, Table 2.3). It failed to produce any EG or glycolaldehyde-based products. 80 mol% MeOH was obtained and there was the presence of a large quantity of unreacted formaldehyde.

The results from Section 2.4 show that using an aluminium Lewis acid component with the cobalt carbonyl anion $[Co(CO)_4]^-$ does not give any turnover to EG from paraformaldehyde under the conditions used. The $H[Co(CO)]_4$, a known hydroformylation catalyst, also showed no catalytic activity. Modifying the salophen ligand to include an appended ammonium salt arm also gave no improvement. The lack of activity shown by the systems may be due to the Lewis acid-formaldehyde interaction being too weak. The catalyst complexes feature THF adducts, and it may be that the formaldehyde is not a strong enough nucleophile to displace these adducts. If the formaldehyde – LA interaction does occur it may be too weak and not lower the kinetic barrier to nucleophilic attack from the $[Co(CO)_4]^-$ anion enough. These catalysts were designed for the carbonylation of epoxides. The strained ring structure of epoxides means that the α-carbon atoms are highly susceptible to an attack by a nucleophile so may require less assistance from the Lewis acid – oxygen interaction for the reaction to occur. Formaldehyde does not have this strong structural effect driving the reaction at the carbon atom which may be why these catalysts were unsuccessful.

2.4.5 – Anisaldehyde Model Reaction

Due to the lack of success in using the complexes in Section 2.4 for the hydroformylation of formaldehyde, a different approach was taken. Using formaldehyde as a substrate posed several synthetic challenges including the polymerisation in high concentrations, the glycolaldehyde intermediate which makes analysis difficult (Section 2.2.2) and the high pressures required for the reaction. To determine whether the salophen ion pair complex **2.4** could show any activity as a hydroformylation catalyst a different substrate was needed. Anisaldehyde was chosen as it avoided the issues associated with formaldehyde. It was soluble in the reaction solvents tested and the methoxy group gave a useful handle for quantitative ^{1}H NMR analysis.

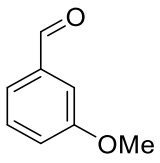

Figure 2.7. m-Anisaldehyde

The reductive hydroformylation of *m*-anisaldehyde was attempted using [(salophen)Al(THF)$_2$][Co(CO)$_4$] (**2.4**) (Scheme 2.16). The post-reaction mixture was analysed by both ^{1}H NMR and GC-MS. 92% of the anisaldehyde starting material remained unreacted with around 6% having been directly hydrogenated to the corresponding alcohol. A trace amount of the hydroformylation product aldehyde was observed by GC-MS, but there was too little present for quantitative analysis. None of the diol from hydroformylation and hydrogenation, analogous to EG production from formaldehyde, was detected by either GC-MS or ^{1}H NMR.

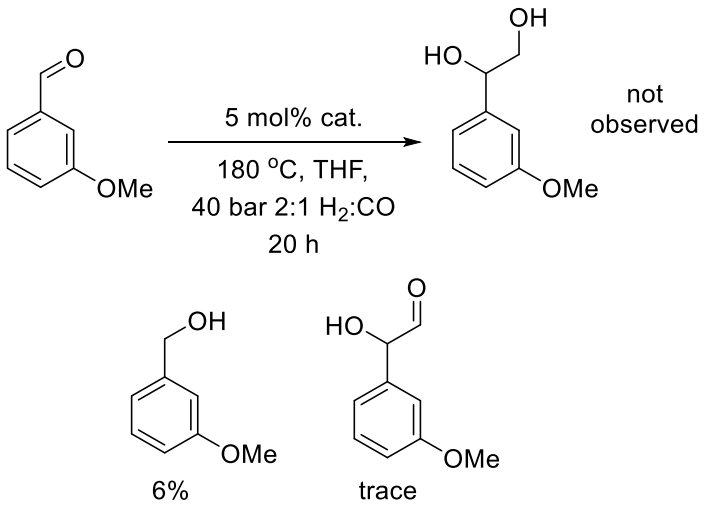

Scheme 2.16. Attempted reductive hydroformylation of m-anisaldehyde

2.4.6 – Electrophilic Phosphonium Cations

With the metallic Lewis acid – cobalt carbonyl catalysts showing no activity for EG formation stronger Lewis acid components were examined. Stephan has published a range of strongly electrophilic fluorinated phosphonium cations.[25] Unlike traditional Lewis acids which have a vacant orbital, these compounds are coordinatively saturated with the acidity coming from a σ* acceptor orbital opposite a fluoride.

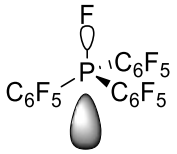

Figure 2.8. LUMO σ orbital of phosphonium cation*

If these cations could be paired with the $[Co(CO)_4]^-$ anion they could have a much stronger coordination to the formaldehyde and lower the energy barrier for a nucleophilic attack of the cobalt anion to the carbon atom (Scheme 2.17).

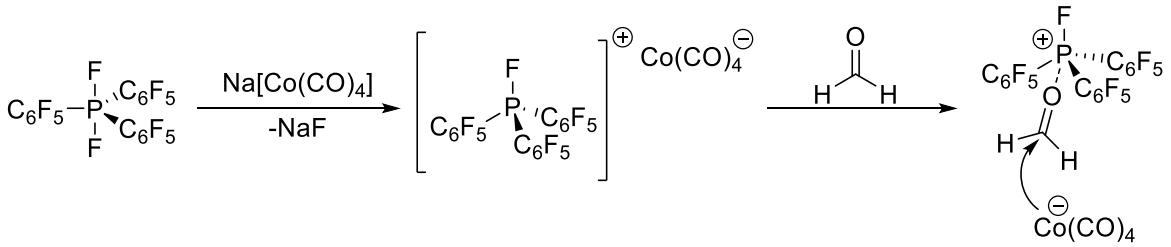

Scheme 2.17. Proposed route to ion pair with phosphonium cation and activation of formaldehyde

The synthesis of these compounds followed the literature preparation.[25] Tris(pentafluorophenyl)phosphine was oxidised with xenon difluoride to give the P(V) difluorophosphorane compound **2.8** (Scheme 2.18). The ^{19}F NMR spectrum gave the expected signal at 0.6 ppm for the PF_2 fluorides with resonances at -132.8, -146.7 and -159.6 ppm for the *ortho-, para-* and *meta-* fluorine atoms of the pentafluorophenyl groups respectively.

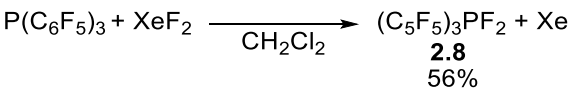

*Scheme 2.18. Synthesis of electrophilic difluorophosphorane **2.8***

The formation of the cation was attempted using two counterions to abstract a fluoride ion from the phosphorane (Scheme 2.19). **2.8** was stirred in chlorobenzene with $Na[Co(CO)_4]$ or $[Ph_3Si][Co(CO)_4]$. The formation of the NaF salt should provide a thermodynamic driving force for the reaction and Si-F bonds are extremely strong with an energy of around 580 kJ/mol due to the high electronegativity of fluorine.[26] Unfortunately, no reaction occurred in either case with the $^{31}P\{^1H\}$ and ^{19}F spectra showing no change from the starting material even after having been stirred for several days. As discussed above, the formation of NaF or SiF salts should have provided a strong driving force for the reaction. The fault, therefore, may lie with the ion pair. The cobalt carbonyl anion may not have a strong enough Lewis basicity to pair with the highly electrophilic phosphonium cation.

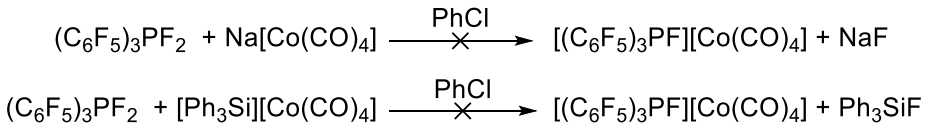

Scheme 2.19. Attempted synthesis of phosphonium cation cobalt carbonyl ion pair

The results from Section 2.4 show that using an aluminium Lewis acid component with the cobalt carbonyl anion $[Co(CO)_4]^-$ does not give any turnover to EG from *para*formaldehyde under the conditions used. The $H[Co(CO)]_4$, a known hydroformylation catalyst, also showed no catalytic activity. Modifying the salophen ligand to include an appended ammonium salt arm also gave no improvement. Replacing the formaldehyde substrate with anisaldehyde, largely to alleviate experimental difficulties, also saw no hydroformylation. Most of the anisaldehyde was unreacted with a small percentage undergoing direct hydrogenation. The lack of activity shown by the systems may be due to the Lewis acid-aldehyde interaction being too weak. The catalyst complexes feature THF adducts, it may be that the formaldehyde is not a strong enough nucleophile to displace these adducts. If the formaldehyde – LA interaction does occur it may be too weak and not lower the kinetic barrier to nucleophilic attack from the $[Co(CO)_4]^-$ anion enough. These catalysts were designed for the carbonylation of epoxides. The strained ring structure of epoxides means that the α-carbon atoms are highly susceptible to an attack by a nucleophile so may require less assistance from the Lewis acid – oxygen interaction for the reaction to occur. Formaldehyde does not have this strong structural effect driving the reaction at the carbon atom which may be why these catalysts were unsuccessful. With this in mind the synthesis of an ion pair featuring a much more electrophilic phosphonium cation was attempted, but the desired complex was not formed.

2.5 – Summary and Future Work

The reductive hydroformylation of paraformaldehyde to ethylene glycol was attempted using a $[Co_2(CO)_8]/PPh_3$ catalyst system. No turnover to EG or glycolaldehyde was observed through testing a range of reaction conditions, including high syngas pressure. The hydroformylation to glycolaldehyde with rhodium catalysts was also attempted but was unsuccessful.

A cooperative ion pair catalyst $[(salphen)Al(THF)_2][Co(CO)_4]$ **(2.4**), reported by Coates for the ring opening and carbonylation of epoxides was synthesised and also tested for the reductive hydroformylation of *para*formaldehyde. Both these tests and those with a model aldehyde, *m*-anisaldehyde, were unsuccessful. Modifying the Lewis acid component by incorporating an appended ammonium salt or completely replacing it with a highly electrophilic phosphonium catalyst gave no improvement.

Much of the experimentation in the literature discussed in Sections 1.4, 2.1 and 2.2 used high syngas pressures often in excess of 120 bar for the hydroformylation of *paraf*ormaldehyde. These conditions appear crucial for achieving any reactivity. Unfortunately, the equipment available was not suitable to test these for the catalysts prepared. A potential area of future work could be to examine a wider range of Lewis Acids for formaldehyde activation. Stoichiometric reactions between the Lewis acid paraformaldehyde could be conducted with resulting mixtures analysed by IR and NMR. If successful interaction were to occur, a decrease in the v(CO) stretching frequency compared to formaldehyde indicating a weakening of the C=O bond would be seen in the IR spectrum. There may also be an accompanying downfield shift in the ^{13}C NMR resonance of the carbon atom. A potential obstacle for this study is the poor solubility of paraformaldehyde in most laboratory solvents, base is normally required to dissolve the polymer, while commercial formalin solutions are aqueous, and the water may cause unwanted reactivity with many Lewis acids. If a suitable methodology is developed which identifies a Lewis acid capable of activating formaldehyde then this could be tested alongside known hydroformylation catalysts, both cobalt and rhodium based. These tests could then determine if the

Lewis acid – formaldehyde interaction does lower the required syngas pressure for a successful reaction.

2.6 – References

1. M. Beller, B. Cornils, C. D. Frohning, and C. W. Kohlpaintner, *J. Mol. Catal. A Chem.*, 1995, **104**, 17–85.

2. J. Pospech, I. Fleischer, R. Franke, S. Buchholz, and M. Beller, *Angew. Chem. Int. Ed.*, 2013, **52**, 2852–2872.

3. K. Noack and F. Calderazzo, *J. Organomet. Chem.*, 1967, **10**, 101–104.

4. R. Tannenbaum and G. Bor, *J. Phys. Chem. A*, 2004, **108**, 7105–7111.

5. M. Green and D. C. Wood, *J. Am. Chem. Soc.*, 1966, **88**, 4106–4107.

6. S. E. Jacobson, *J. Mol. Catal.*, 1987, **41**, 163–183.

7. G. Natta, R. Ercoli, S. Castellano, and F. H. Barbieri, *J. Am. Chem. Soc.*, 1954, **76**, 4049–4050.

8. A. Calafat and J. Laine, *J. Catal.*, 1994, **147**, 88–95.

9. Y. Sun, T. Lin, L. Zhong, F. Yu, X. Qi, W. Lu, K. Li, J. Li, Y. Xiao, and B. Liu, 2016, CN106268852.

10. A. Spencer, *J. Organomet. Chem.*, 1980, **194**, 113–123.

11. A. S. C. Chan, W. E. Carroll, and D. E. Willis, *J. Mol. Catal.*, 1983, **19**, 377–391.

12. Y. Moglie, M. J. González-Soria, I. Martín-García, G. Radivoy, and F. Alonso, *Green Chem.*, 2016, **18**, 4896–4907.

13. V. Mahadevan, Y. D. Y. L. Getzler, and G. W. Coates, *Angew. Chem. Int. Ed.*, 2002, **41**, 2781–4.

14. R. Dobrovetsky and D. W. Stephan, *J. Am. Chem. Soc.*, 2013, **135**, 4974–4977.

15. C. M. Mömming, E. Otten, G. Kehr, R. Fröhlich, S. Grimme, D. W. Stephan, and G. Erker, *Angew. Chem. Int. Ed.*, 2009, **48**, 6643–6646.

16. G. Ménard, L. Tran, J. S. J. McCahill, A. J. Lough, and D. W. Stephan, *Organometallics*, 2013, **32**, 6759–6763.

17. Y. D. Y. L. Getzler, V. Mahadevan, E. B. Lobkovsky, and G. W. Coates, *J. Am. Chem. Soc.*, 2002, **124**, 1174–1175.

18. J. Wöltinger, J.-E. Bäckvall, and Á. Zsigmond, *Chem. Eur. J.*, 1999, **5**, 1460–1467.

19. P. G. Cozzi, *Chem. Soc. Rev.*, 2004, **33**, 410–421.

20. D. J. Harrison, A. L. Daniels, I. Korobkov, and R. T. Baker, *Organometallics*, 2015, **34**, 4598–4604.

21. C. H. Wei, T. M. Bockman, and J. K. Kochi, *J. Organomet. Chem.*, 1992, **428**, 85–97.

22. J. W. Kramer, D. Y. Joh, and G. W. Coates, *Org. Lett.*, 2007, **9**, 5581–5583.

23. D. Brodbeck, F. Broghammer, J. Meisner, J. Klepp, D. Garnier, W. Frey, J. Kästner, and R. Peters, *Angew. Chem. Int. Ed.*, 2017, **56**, 4056–4060.

24. V. G. Granik, B. M. Pyatin, and R. G. Glushkov, *Russ. Chem. Rev.*, 1971, **40**, 747–759.

25. C. B. Caputo, L. J. Hounjet, R. Dobrovetsky, and D. W. Stephan, *Science*, 2013, **341**, 1374–1377.

26. R. Walsh, *Acc. Chem. Res.*, 1981, **14**, 246–252.

Chapter 3 – Hydrogenation of C2 Oxalates with Ruthenium/Tridentate Phosphine Catalysts

3.1 – Introduction

The first hydrogenation of DMO to EG using a ruthenium/tridentate phosphine system was reported by Elsevier and Teunissen in 1997.[1] The catalyst, formed *in situ* from the ruthenium precursor [$Ru(acac)_3$] and the commercially available tripod ligand (**L1**, Scheme 3.1), gave 100% DMO conversion with 84% EG yield over 16 hr at 100 °C with 70 bar H_2. This demonstrated a vast improvement on the previously reported ruthenium carbonyl complex, [$Ru(CO)_2(CH_3COO)_2(P^nBu_3)_2$] reported by Matteoli *et al.* which only yielded 27% EG at much more forcing conditions of 130 bar H_2 for 144 hours.[2] The tripod system used zinc metal as an additive, to reduce the [$Ru(acac)_3$] precursor, with the TOF reduced by almost a half when not used. A range of other phosphine ligands, including triphenylphosphine, $Ph_2PCH_2PPh_2$ and the flexible, tridentate ligand triphos (**L10**, bis(diphenylphosphinoethyl)phenylphosphine), were also tested, none of which gave any conversion to EG. This led to the conclusion that for an efficient hydrogenation of DMO through MG to EG, a tridentate, facially capping phosphine ligand is required.

3.2 – Hydrogenation of DMO

3.2.1 – Benchmarking

The Elsevier system was benchmarked using lower H_2 pressures and a range of temperatures with the results shown below in Table 3.1. Perhaps unsurprisingly, the most forcing conditions of 30 bar and 180 °C (Run 1) gave the best results. Increasing the reaction time from 3 hours to 20 made no appreciable difference (compare Runs 1 and 2) and there was a clear drop in catalyst performance when the pressure was reduced from 20 to 10 bar H_2 (Runs 3 and 4) and the temperature lowered from 150 to 120 °C (Runs 5 and 6). As with the Elsevier work, methanol was used as the solvent, changing to toluene giving poor turnover to EG (Run 7). This appeared to be caused by poor catalyst

solubility; the initial complex did not dissolve in toluene and a black metallic solid, most likely Ru(0), was present in the post-reaction mixture indicating catalyst decomposition. This did not occur in the other tests.

Table 3.1. Conditions Screen for Hydrogenation of DMO with [Ru(acac)$_3$]/Tripod

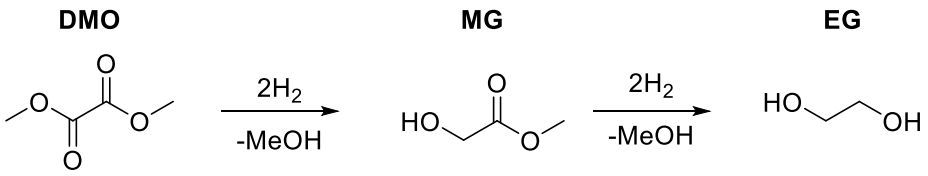

Run[a]	H_2 Pressure (Bar)	Temperature (°C)	%Yield MG	%Yield EG
1	30	180	12	43
2	30[b]	180	16	45
3	20	180	13	36
4	10	180	37	4
5	30	150	7	38
6	30	120	12	4
7	30[c]	180	53	2

[a]conditions: 5 mmol DMO, 10 mL MeOH, 0.5 mol% [Ru(acac)$_3$], 0.5 mol% tripod ligand, 2 mol% Zn, 3 h, [b] 20 hr, [c] toluene solvent

3.2.2 – C-Centred Tripod Systems

With conditions established, the catalyst system was then examined, to determine specifically whether the zinc additive could be removed. This metal reducing agent, which forms zinc oxide during the reaction, presents clear disadvantages for scale-up and catalyst recycling. Alessio *et al.* have reported the facile synthesis of a Ru(II) dimer salt **3.1** from [$RuCl_2(DMSO)_4$] and the tripod ligand **L1** (Scheme 3.1).[3]

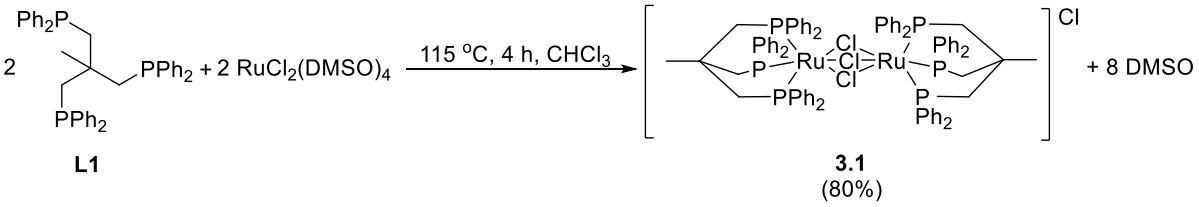

*Scheme 3.1 Synthesis of **3.1***

Following Alessio's method, complex **3.1** was synthesised as a yellow solid in 80% yield. The product gives a singlet at 36 ppm in the $^{31}P\{^{1}H\}$ NMR spectrum, consistent with that reported and contrasting to the free tripod ligand at -28 ppm. The ^{1}H and ^{13}C NMR spectra are also concordant with the literature. A test showed that the complex is air stable for at least 5 days in the solid state, with no change in the $^{31}P\{^{1}H\}$ NMR spectrum at all after this time. Fully oxidised Tripod oxide exhibits a peak at 32 ppm.[4] The crystal structure of the dimeric cation with a $[BPh_4]^-$ counterion has been reported by Bachechi *et al.*[5] The Ru-phosphine units are eclipsed while the bridging chlorides have a staggered arrangement compared to the phosphines. The whole dimer cation has a co-facial bioctahedral geometry with an axis of symmetry running through the two apical carbon atoms in the tripod ligand. There is little distortion in the tripod ligands; however, there is more of a discrepancy between the ideal and observed geometry around the two Ru centres. The Ru-Cl-Ru angles are wider than usual (87.8(1)° compared to 75.0(1)°) with the corresponding Cl-Ru-Cl angles smaller than ideal to a similar extent (77.2(1)°/90.0(1)°). With **3.1** synthesised, it was then tested for the hydrogenation of DMO under the same conditions as the *in situ* system, but with no zinc additive. The catalyst loading was also halved to 0.25 mol% to keep the overall Ru concentration the same. This gave an improved performance of 60% EG and 20% MG with 93% DMO conversion in the liquid phase. ^{1}H and ^{13}C NMR spectroscopy were also used to confirm the presence of EG in the product solution with signals at 3.72 and 64 ppm respectively. The remaining conversion (13 mol%) can be attributed to the formation of small quantities of other side products which could not be identified by NMR spectroscopy or GC-MS. The error associated with the GC analysis of around 5% should also be considered. Catalyst loading was then investigated (Table 3.2). As expected, the EG yield reduced with decreased catalyst loading from 0.25 mol% (compare Runs 2-4). Interestingly the yield also lowered when the loading was

increased to 0.75 mol% (Run 1). This mirrors some observations with other ruthenium complexes believed to be caused by the formation of Ru nanoclusters, which have fewer active sites than a true homogeneous catalyst, at higher concentrations.[6]

*Table 3.2. Catalyst loading screen for DMO Hydrogenation with **3.1***

Run[a]	Catalyst Loading (mol%)	%Yield MG	%Yield EG
1	0.75	26	47
2	0.25	20	60
3	0.1	33	40
4	0.05	33	6

[a]conditions: 5 mmol DMO, 10 mL MeOH, 180 °C, 30 bar H_2, 3 h

With the phenyl substituted system showing good catalytic activity, the synthesis of a range of other catalysts using the Tripod scaffold was attempted. The ethyl substituted ligand, ETripod (**L2**), previously prepared using literature methods[7] was successfully complexed to Ru to give the corresponding dimer complex $[Ru_2Cl_3\mathbf{L2}_2]Cl$ (**3.2**,Scheme 3.2). Unlike **3.1** , it took several days for any product to be formed, the yellow solid precipitated out of the toluene solution; even after 90 hours the solution and washings still showed a large amount of free ligand with a single peak at -32 ppm in the $^{31}P\{^1H\}$ NMR spectrum. The dimeric complex gave a singlet at 44 ppm in the $^{31}P\{^1H\}$ NMR with the ethyl groups also visible in the ^1H NMR spectrum at 1.12-1.26 and 1.66 -1.86 ppm. The peaks are broad multiplets most likely due to a degree of distortion or asymmetry in the dimer structure rendering the ethyl groups inequivalent creating several overlapping signals at similar chemical shifts. ESI-MS analysis also confirmed the presence of the dimer.

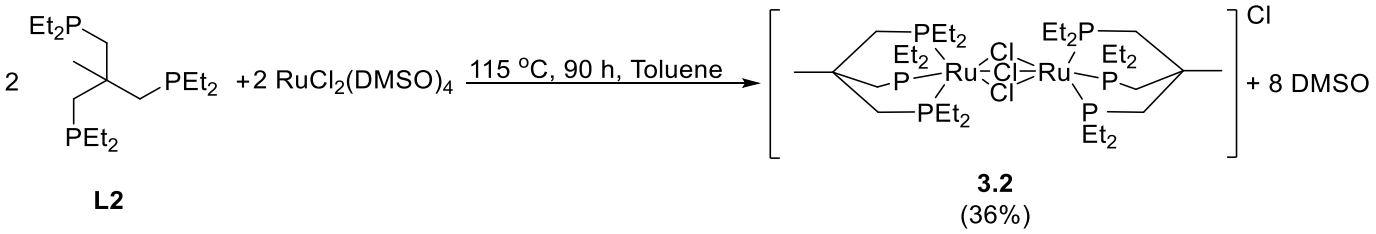

L2

3.2
(36%)

*Scheme 3.2. Synthesis of **3.2***

The ethyl analogue **3.2** was then tested against **3.1** for DMO hydrogenation with the results in Table 3.3 below. No EG was produced and the yield of MG and conversion of DMO were only approximately half that seen for **3.1.**

*Table 3.3. Hydrogenation of DMO with **3.1** and **3.2***

Run[a]	Catalyst	% Yield MG	% Yield EG	% Conv DMO[b]
1	**3.1**	20	60	93
2	**3.2**	11	0	44

[a]conditions: 5 mmol DMO, 0.25 mol% catalyst, 10 mL MeOH, 180 °C, 30 bar H_2, 3 h [b] in liquid fraction

The cyclohexyl tripod analogue was then targeted to better investigate the effects of ligand sterics and electronics on catalytic activity. A synthetic route was devised which consisted of lithiating the chlorinated tripod scaffold then reacting this product with the secondary chlorophosphine (Scheme 3.3). However, this reaction was unsuccessful giving a mixture of products none of which were the desired trisubstituted dicyclohexylphosphine ligand. Another unsuccessful procedure involved the deprotonation of dicyclohexylphosphine with KO^{t}Bu to form the corresponding phosphide which was then reacted with the trichloride tripod frame (Scheme 3.3). After work up, $^{31}P\{^1H\}$ NMR spectroscopic analysis of the product mixture showed a single peak at -29 ppm due to dicyclohexylphosphine. The deprotonation had been unsuccessful. The only literature preparation for this ligand is a direct hydrogenation of tripod (**L1**) using forcing conditions and a niobium aryloxide catalyst.[8]

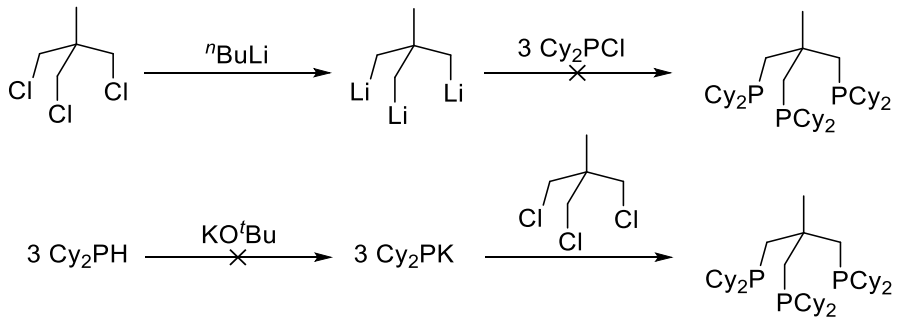

Scheme 3.3. Unsuccessful synthetic routes to cyclohexyl tripod ligand

3.2.3 – N-Centred Tripod Systems

With difficulties encountered trying to prepare a range of different analogues of the tripod framework other alternatives were investigated. The nitrogen centred, N-Tripod (**L3**), first reported by Hanton, Miller *et al* was an obvious target.[9] The ligand is prepared *via* a two-step Mannich reaction through a bis(hydroxymethyl)phosphonium chloride salt and, unlike the carbon centred variants, the final ligand precipitates out of the reaction solution for easy isolation and purification. **L3** was prepared following the literature procedure (Scheme 3.4).[10] The final product had the reported shift of -29 ppm in the $^{31}P\{^{1}H\}$ spectrum.

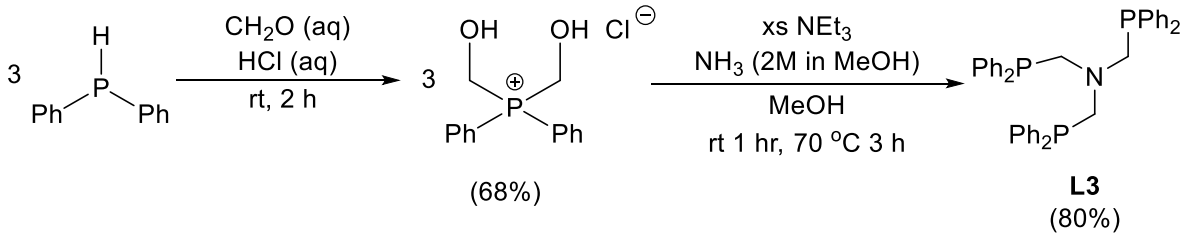

*Scheme 3.4. Preparation of **L3***

The dimer complex **3.3** was prepared in a similar method to the C-centred alternatives (Scheme 3.5). The ligand and $[RuCl_2(DMSO)_4]$ precursor were heated in toluene and the complex precipitated as a yellow solid. This gave the expected singlet at 18 ppm in the $^{31}P\{^{1}H\}$ NMR spectrum. As with **3.1**, the crystal structure of **3.3** has been reported using the $[BPh_4]^-$ counterion.[11] The phosphines are confirmed as having facial geometry, but there is some significant asymmetry in the bridging chlorides,

also seen with **3.1**. All Ru-Cl distances are shorter for one Ru atom than the other with the N-Ru distance also shorter for this same atom. The reasons for this distortion are not known.

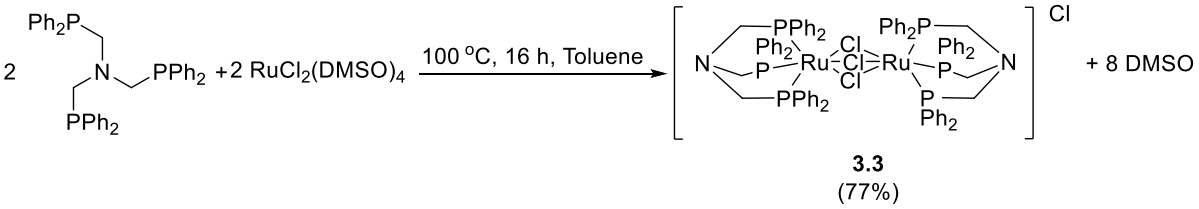

*Scheme 3.5. Preparation of **3.3***

With this synthetic route established as successful and straightforward, other N-tripod variants were prepared. Initial studies focussed on the ethyl (**L4**), for comparison with **L2,** and the cyclohexyl (**L5**) analogues. The synthesis of **L4** followed that reported in the literature[9] with the procedure for **L5** simply adapted from that for **L3**.

Ligand **L4** was prepared using a slightly different method to the other N-centred tripods (Scheme 3.6). Diethylphosphine was dissolved in MeOH and reacted with aqueous formaldehyde to give (hydroxymethyl)diethylphosphine which then underwent a Mannich reaction with ammonia. No chloride salt was formed. This resulted in a biphasic mixture with the oily ligand underneath a layer of methanol which was decanted *via* cannula.

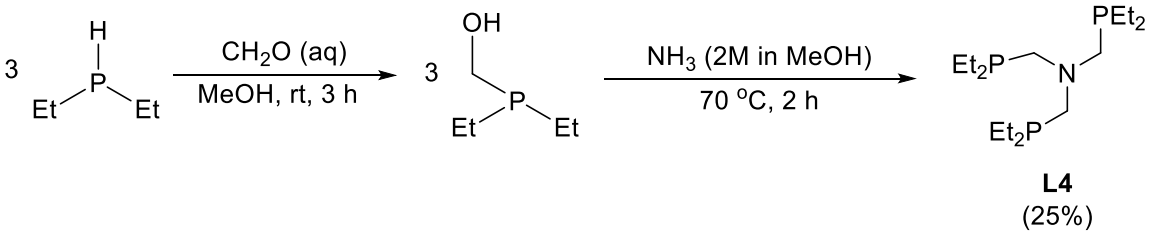

*Scheme 3.6. Preparation of **L4***

The crude ligand was reacted with the Ru(II) precursor in a similar way to the preparation of **3.3** (Scheme 3.7). Complex **3.4** was isolated as an orange solid. The $^{31}P\{^{1}H\}$ NMR showed the expected peak at 27 ppm and the desired molecular ion peak was observed by ESI-MS.

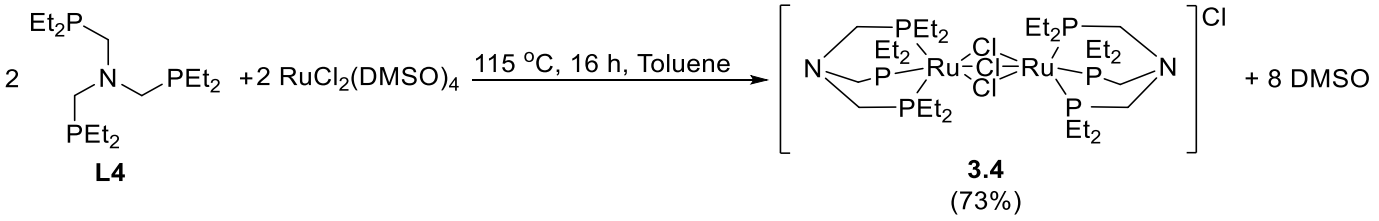

*Scheme 3.7. Synthesis of **3.4***

Compared to the unsuccessful attempts to prepare a cyclohexyl variant of the C-centred tripod, the synthesis of the cyclohexyl N-Tripod ligand (**L5**) was facile. Dicyclohexylchlorophosphine was used as the starting material and was converted to the secondary phosphine using $LiAlH_4$. This yielded a colourless solution with the desired $^{31}P\{^1H\}$ NMR shift of -28 ppm. **L5** was then prepared in the same way as **L3** to give the desired ligand as a white solid (Scheme 3.8). The $^{31}P\{^1H\}$ NMR spectrum showed a single peak at -17 ppm which was in the region expected for this ligand. The cyclohexyl groups are much more electron donating than the phenyl groups of **L3** making the central phosphorus atom more electron rich causing a downfield shift.

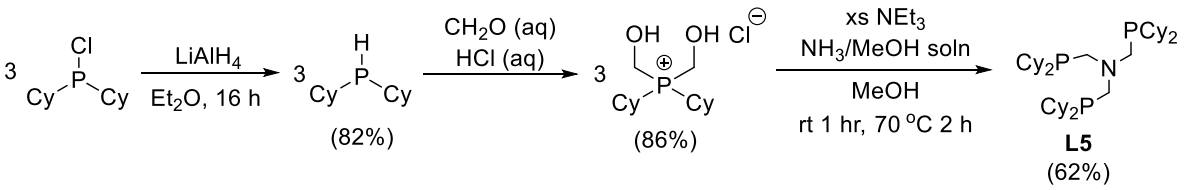

*Scheme 3.8. Synthesis of **L5***

The previously unreported dimer complex **3.5** was then prepared in the same manner as the other N-tripod ruthenium complexes (Scheme 3.9). The yellow solid obtained exhibited two singlets at 48.9 and 50.2 ppm in the $^{31}P\{^1H\}$ NMR spectrum with approximately equal intensities. No coupling appeared to be present between these signals suggesting that they were derived from two separate species. There was potentially to be restricted rotation around the P-Cy bonds due to the bulky groups which could mean that two complexes with separate ligand arrangements were formed. This could explain why two signals are seen in the spectrum compared to one, for example, in **3.3** where the smaller phenyl groups induce less steric clashing. As mentioned previously, the crystal structure

reported for **3.3** shows a small amount of discrepancy in the Ru-phosphine end caps with two different Ru-N distances so this may be exacerbated with the much larger cyclohexyl groups present. The dimer complex is likely to have the same face-sharing bioctahedron structure as **3.3**, which could have two different isomers through the $Ru(\mu^2\text{-}Cl)_3Ru$ bridge. Further characterisation of the compound is needed. Variable temperature $^{31}P\{^1H\}$ NMR spectroscopy experiments where the sample is heated could be performed. If a degree of broadening or coalescence is seen with the two peaks at higher temperature then the presence of two isomers which are unable to interconvert at room temperature is likely. If the peaks remain separate this suggests two unrelated species which give similar chemical shift values. The ^1H NMR spectrum also showed a series of broad multiplets in the alkyl region at 0.73-0.83, 1.17-1.23 and 1.53-1.88 which most likely correspond to the cyclohexyl protons. As with the $^{31}P\{^1H\}$ NMR it may be that restricted rotation caused similar signals from different configurations to appear on top of each other giving the broad multiplets. There are also 7 different proton environments, some of which are chemically very similar, which would also contribute to the overlapping signals in the spectrum. ESI-MS analysis confirmed that the desired complex had been obtained.

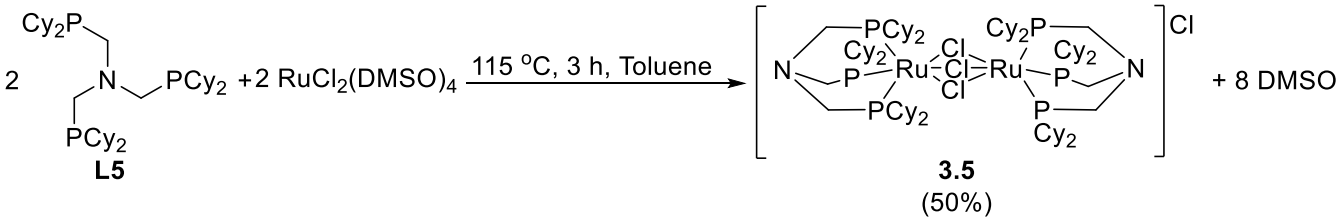

*Scheme 3.9. Synthesis of **3.5***

With a range of nitrogen centred tripod dimers now prepared they were tested for the hydrogenation of DMO and compared to the carbon centred tripod complex **3.1** (Table 3.4).

*Table 3.4. Hydrogenation of DMO with **3.1** and **3.3-5***

Run[a]	Catalyst	% Yield MG	% Yield EG	%Conv DMO
1	**3.1**	20	60	93
2	**3.3**	17	60	95
3	**3.3**[b]	21	52	99
4	**3.4**	0	2	5
5	**3.5**	64	3	91
6	**3.5**[b]	40	50	99

[a]conditions: 5 mmol DMO, 0.25 mol% catalyst, 10 mL MeOH, 180 °C, 30 bar H_2, 3 h [b] 20 h

3.3 showed similar catalytic activity to the carbon-based analogue **3.1** giving the same yield of both EG and MG and DMO conversion within error (Compare Runs 1 and 2). The ethyl variant **3.4** showed no catalytic competence (Run 4). An interesting result was observed with the cyclohexyl dimer **3.5**; after 3 hours only MG had been formed with little EG present suggesting that only the first hydrogenation step had been catalysed (Run 5). However, when left overnight for a total of 20 hours the reaction proceeded through the second hydrogenation to give EG in a 50% yield, only 10% less than the best systems (Run 6). When left for 20 hours, **3.3** showed no improvement in EG yield; in fact a small decrease in yield is observed potentially caused by other organic side reactions or oligomerisation (Run 3).

The steric and electronic properties of the corresponding phosphine ligands are shown below in Table 3.5. For **3.1/3.3** and **3.4**, $PEtPh_2$ and PEt_3 were used respectively with the ethyl group providing an approximation of the ligand arm. Unfortunately, data for the cyclohexyl analogue for comparison with **3.5** has not been published so PCy_3 was used instead, which gives a much cruder approximation. The electronic parameter is the A_1 carbonyl stretching frequency of the $Ni(CO)_3L$ complex, the lower this value the more electron donating the ligand.[12] Both **3.5** and **3.4** are more electron donating than **3.3** which could offer an explanation as to why they showed less catalytic activity. However, **3.5** which is

the most electron rich still showed good turnover to EG after 20 hours whereas **3.4**, which is between **3.5** and **3.3,** did not. It appears that a steric factor is also important, but from this ligand set the nature of this is unclear with **3.3** between **3.5** and **3.4** in terms of steric bulk.

Table 3.5. Catalyst, yields and respective phosphine ligand parameters

Catalyst	**% Yield EG**	**Phosphine Cone Angle, θ (°)**[12]	**Phosphine Tolman electronic parameter ν (± 0.3 cm^{-1})**[12]
3.5	3	170	2056.4
3.1/3.3	60	140	2066.7
3.4	2	132	2061.7

From the above results, it was clear that a wider range of ligands needed testing. As the best catalyst had been **3.3** which features phenyl groups a series of substituted phenyl ligands and their corresponding dimer complexes were synthesised to better determine any kind of structure activity relationship. Four ligands were targeted; *ortho*-tolyl (**L6**), *para*-tolyl (**L7**), *para*-anisolyl (**L8**) and *para*-fluoro (**L9**) variants of N-Tripod.

L6 was prepared in the same fashion as **L5** converting the chlorophosphine to the secondary phosphine before forming the ligand. For **L7-9** the relevant chlorophosphines were either unavailable or available only in small quantities not appropriate for the multi-step process. Instead a route reported by Beller *et al* was used for the synthesis of the secondary phosphines (Scheme 3.10).[13] The appropriate brominated phenyl starting material was reacted with magnesium in the presence of a small quantity of iodine to form an *in situ* Grignard reagent. This was then reacted with diethyl phosphite to give the corresponding secondary phosphine oxide which was reduced with DIBAL-H to yield the secondary phosphine.

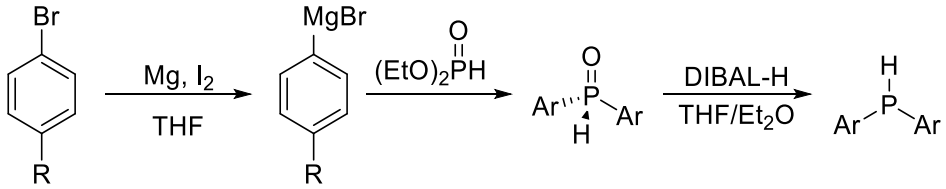

Scheme 3.10. General synthesis of aryl secondary phosphines via Grignard reagents

With the phosphines prepared the tripod ligands could then be produced using the same procedure as for **L3** (Figure 3.1). The $^{31}P\{^{1}H\}$ NMR spectrum for **L6** showed two singlets at very similar chemical shift values in a 1:2 ratio (Figure 3.2). The methyl protons of the tolyl groups also appeared as two peaks with the same 1:2 ratio at 2.31 and 2.35 ppm in the ^{1}H NMR spectrum. This implies that perhaps two of the di-*o*-tolylphosphine units are inequivalent to the third. As discussed with complex **3.5,** variable temperature NMR spectroscopy studies could show whether these two different environments interconvert at higher temperature. If merging of the two peaks is seen this could suggest that the bulky *ortho*-tolyl groups are restricting rotation in the ligand at room temperature.

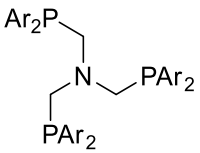

L6 Ar - *o*-tolyl (17%) $^{31}P\{^{1}H\}$ -45,-46 ppm
L7 Ar - *p*-tolyl (16%) $^{31}P\{^{1}H\}$ -29 ppm
L8 Ar - *p*-anisolyl (19%) $^{31}P\{^{1}H\}$ -32 ppm
L9 Ar - p(C_6H_4F) (23%)$^{31}P\{^{1}H\}$ -21, ^{19}F -112 ppm

*Figure 3.1. Ligands **L6-9***

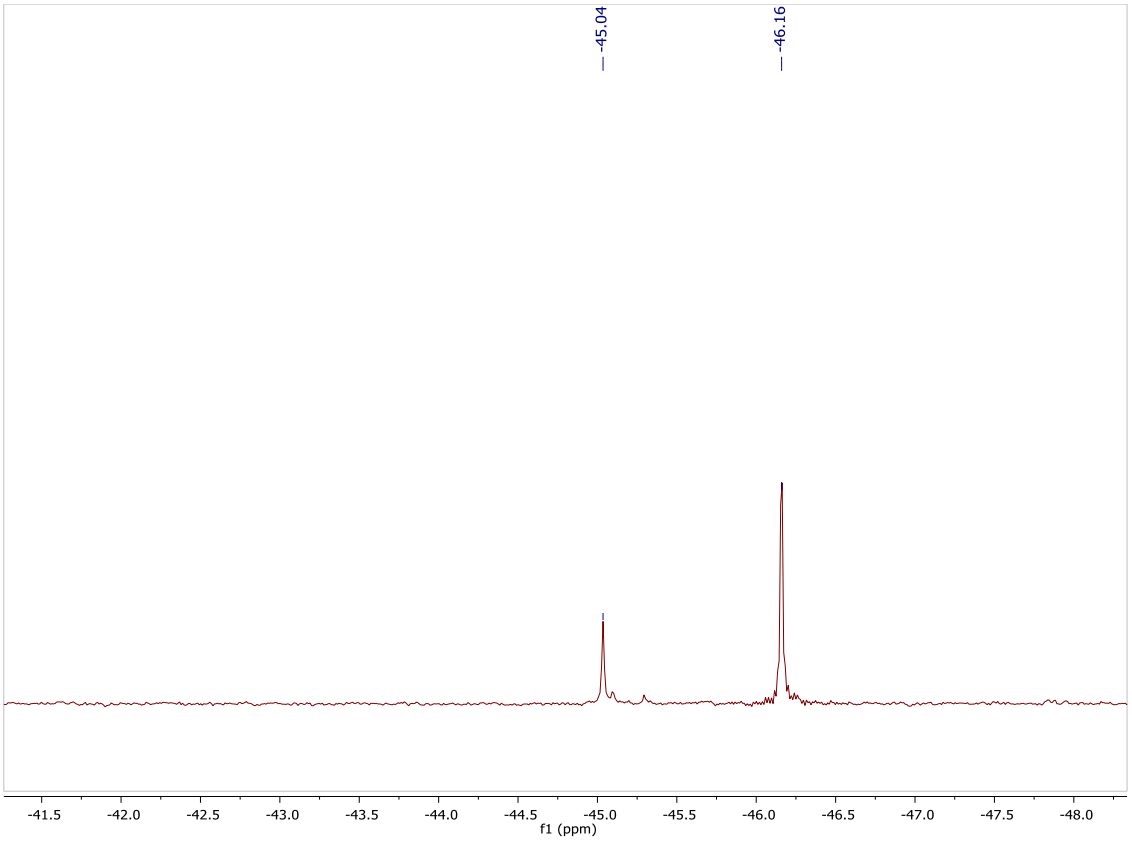

*Figure 3.2. $^{31}P\{^{1}H\}$ NMR (300 MHz, $CDCl_3$) of **L6***

The previously unreported complexes **3.6**, **3.7** and **3.8** were then prepared as with the other N-tripod dimer complexes, by a reflux with the ruthenium precursor in toluene. The ^{1}H NMR spectra showed the expected structures with singlets at 2.20 ppm for the tolyl protons in **3.6** and **3.7** and a singlet at 3.69 ppm for the anisole protons in **3.8** clearly visible. ESI-MS also confirmed synthesis of the desired dimers. When **L9** was reacted with $[RuCl_2(DMSO)_4]$, no complex between Ru and the ligand was formed, even after several days at reflux. The $^{31}P\{^{1}H\}$ NMR spectrum showed the same singlet at -21 ppm as with the free ligand. It may be the case that the electron-withdrawing fluorine atoms on the ligand limit the electron donating capability of the phosphine to such an extent that bonding cannot occur.

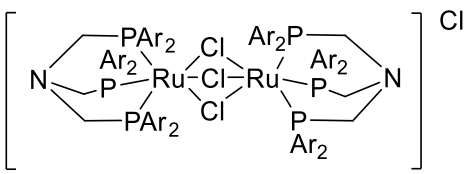

3.6 Ar - *o*-tolyl (64%) $^{31}P\{^{1}H\}$ 32 ppm
3.7 Ar - *p*-tolyl (62%) $^{31}P\{^{1}H\}$ 34 ppm
3.8 Ar - *p*-anisole (73%) $^{31}P\{^{1}H\}$ 17 ppm

Figure 3.3. Complexes 3.6-8

Complexes **3.6-8** were then tested for DMO hydrogenation with the results shown below in Table 3.6. As with **3.5,** the cone angle and electronic parameter for the related $PEtAr_2$ phosphines was unavailable so the tridentate PAr_3 values were used instead giving only a very rough approximation of the steric and electronic factors.

*Table 3.6. DMO hydrogenation with **3.6-8***

Run[a]	Catalyst	% Yield MG	% Yield EG	% Conv DMO	Phosphine θ (°)[12]	Phosphine ν (± 0.3 cm^{-1})[12]
1	**3.3**	20	60	93	140	2066.7
2	**3.6**	41	0	95	194	2066.6
3	**3.7**	36	32	99	145	2066.7
4	**3.8**	33	33	99	-	2066.1

[a]conditions: 5 mmol DMO, 0.25 mol% catalyst, 10 mL MeOH, 180 °C, 30 bar H_2, 3 h

3.6 failed to produce any EG within 3 hours (Run 2). This result, together with those for **3.5** suggest that increased steric bulk in the ligand hinders the formation of EG. Both **3.7** and **3.8** with *para*-electron donating groups catalyse the hydrogenation of DMO to EG (Runs 3 and 4). **L7** has the same cone angle as **L3** and it can be assumed that **L8** is very similar, although not listed. Across the series of N-tripod catalysts the activity follows the trend **3.3**>**3.7/3.8**>>**3.5**>**3.6** which roughly mirrors the bulk of the respective ligands containing phenyl or larger groups. There is not enough evidence to comment on whether electron-donating or -withdrawing groups have a significant impact on activity. A complex featuring a strong withdrawing group would have to be synthesised and tested. A hydrogenation using **L9**, $[Ru(acac)_3]$, and zinc *via* the Elsevier *in situ* method yielded no MG or EG. Another potential candidate for an electron-withdrawing group was a nitro-substituted ligand. However, under these reaction conditions it is likely that this would have been hydrogenated to an amine so was deemed unsuitable. A ligand featuring a CF_3 group would also be strongly electron-withdrawing, but this could potentially suffer from the same difficulties with complexation as seen with **L9**.

3.2.4 – Triphos systems

The triphos ligand (**L10**, bis(diphenylphosphinoethyl)phenylphosphine), which does not formally adopt a facial structure when bound to Ru, was one of the other phosphine ligands tested by Elsevier. Although not producing any EG in that study it produced a significant quantity of MG, 67% with 76% DMO conversion,[1] and so was the best performing ligand aside from tripod (**L1**). A complex of **L10** and Ru was prepared following a procedure reported by Venanzi *et al.* (Scheme 3.11).[14] As with the tripod species, the product, **3.9**, is a cationic Ru dimer with a κ^3 triphos ligand on each Ru centre, 3 bridging chlorine atoms and a chloride counterion. The $^{31}P\{^1H\}$ NMR spectrum gave the expected peaks; a triplet at 98 ppm for the central phosphorus atom and a doublet at 68 ppm for the two terminal phosphorus atoms. The crystal structure of the dimer with a triflate anion was also reported. All 3 P-Ru distances are shorter than in tripod dimer **3.1**, with the central Ru-P bond shorter than those with the two terminal phosphines. These two terminal Ru-P are also unequal, although only by 0.002(3) Å suggesting only some very slight distortion in the phosphine ligand. The Ru-Ru distance is also shorter in **3.9** than **3.1** with shorter Ru-Cl-Ru bonding and smaller corresponding angles, an average of 84° compared to 88°.

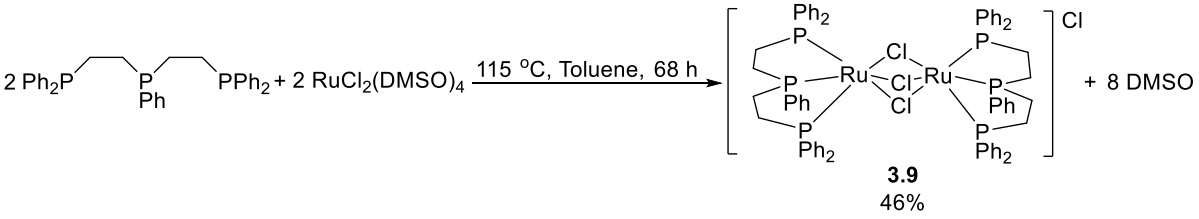

*Scheme 3.11. Synthesis of **3.9***

3.9 was tested for the hydrogenation of DMO and gave 27% EG, 51% MG with 95% conversion. To try to improve on the activity of **3.9**, two different triphos based ligands were prepared (Scheme 3.12). The first, **L11**, featured ^{t}Bu groups on the terminal phosphines and was synthesised according to the literature procedure.[15] The second, the novel ligand **L12**, contained terminal ethyl groups and was prepared by adapting the **L11** synthesis. These ligands were selected to try to alter the geometry of the ligand binding to the Ru atoms in the final complexes. The bulky ^{t}Bu groups should force the ligand

to adopt more of a meridional arrangement where these terminal groups are spaced further apart to avoid clashing. With smaller ethyl groups the ligand might adopt more facial type bonding akin to the tripod systems which could improve the activity for ester hydrogenation.

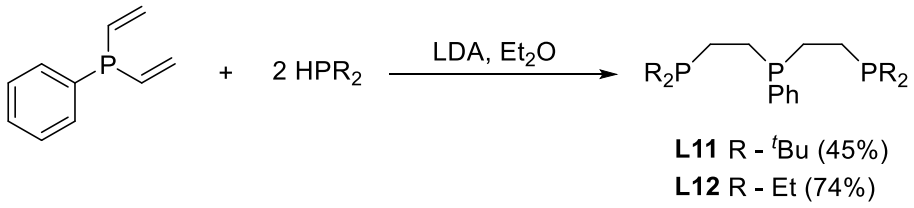

*Scheme 3.12. Synthesis of **L11** and **L12***

Divinylphenylphosphine was reacted with 2 equivalents of the relevant secondary phosphine with lithium diisopropylamide. The two ligands were both isolated as orange oils with **L11** exhibiting $^{31}P\{^{1}H\}$ NMR shifts of a doublet at 34 ppm for the terminal P atoms and a triplet at -16 ppm for the central P. **L12** gave a triplet at -16 ppm and a doublet at -19 ppm which are also in the expected region *cf.* tri-*tert*-butylphosphine and triethylphosphine which have $^{31}P\{^{1}H\}$ shifts of 60 and -20 ppm respectively.

The ligands were then complexed to Ru to form the two dimer complexes **3.10** and **3.11** (Figure 3.4). The complexation was conducted in the same manner for **3.9** by a reflux in toluene with the $[RuCl_2(DMSO)_4]$ precursor. Unfortunately, with **L11** the desired product was not obtained. The resulting $^{31}P\{^{1}H\}$ NMR spectrum showed two singlet peaks at 27 and -5 ppm in a 4:1 ratio of intensities, the origin of which was not ascertained. Conversely, **L12** gave the expected result with peaks at 103 and 76 ppm in a ratio of approximately 1:2.5 (Figure 3.6). The latter appears as a complex collection of signals rather than simply a doublet suggesting that the two terminal phosphines are in different chemical environments. The phenyl analogue **3.9** is known to occur in two different configurations, staggered and eclipsed (Figure 3.5) which can also be thought of as transoid and cisoid respectively. The former should generate three sets of doublets of doublets while the latter should give a doublet and a triplet. The spectrum below (Figure 3.6) suggests that there may be a mixture of these species present with the eclipsed more prevalent. There are twice as many of the PEt_2 groups at similar chemical shifts and the resulting signals from both the staggered and eclipsed arrangements could

have appeared on top of each other giving the multiplet at 76 ppm. The expected doublet of doublets for the PPh from the minor staggered arrangement may have been lost in baseline noise. This would also explain why the intensity of the phosphine signals for the PEt_2 environments is slightly greater than twice that for the central PPh signal.

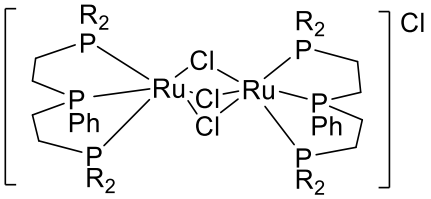

3.10 R - ^{t}Bu unsuccessful

3.11 R - Et (48%)

Figure 3.4. ***3.10*** *and* ***3.11***

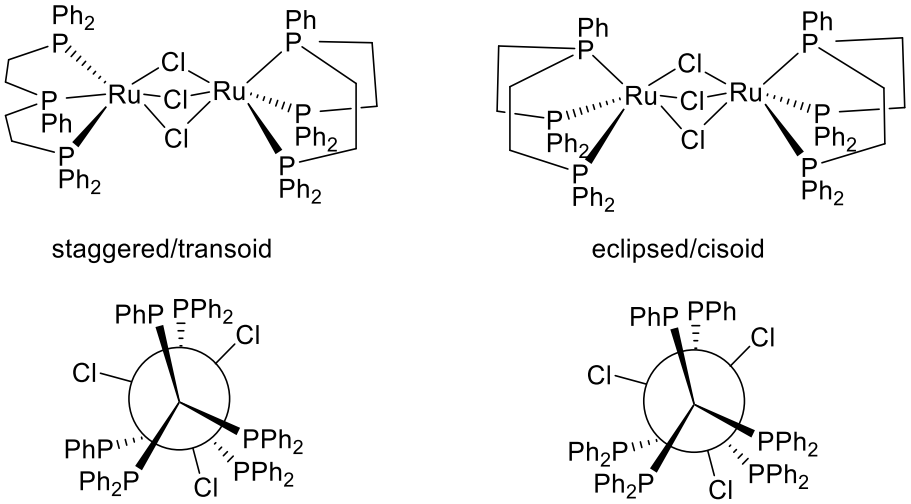

Figure 3.5. Staggered and eclipsed arrangements of ***3.9*** *(charge and counterion omitted)*

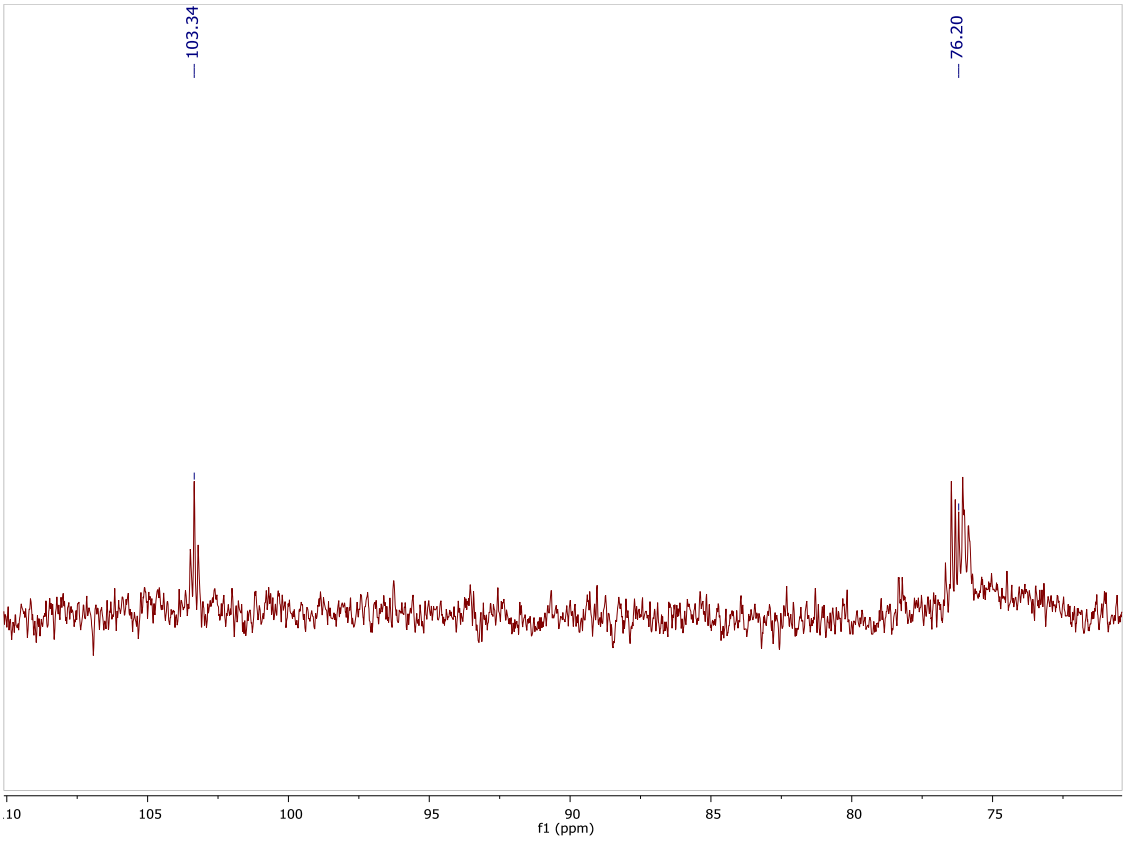

*Figure 3.6. $^{31}P\{^{1}H\}$ ($CDCl_3$, 162 MHz) NMR spectrum of **3.11** $[RuCl_{1.5}$**(L12)**$]_2Cl$*

3.11 was then tested for the hydrogenation of DMO. Unfortunately, it showed no catalytic activity with neither EG nor MG produced and only 5% DMO conversion. The product reaction mixture contained a substantial quantity of a black metallic solid, assumed to be Ru(0). Possibly, the ligand has de-coordinated from the metal centre, leading to decomposition. This is unusual behaviour for a tridentate triphos-type ligand and not observed with the other complexes tested; it is not clear why this specific derivative should lead to decomposition.

3.2.5 – Other Phosphorus-Based Ligands

With the tripod systems, especially **3.1** and **3.3**, showing success for DMO to EG hydrogenation other ligands and their corresponding Ru complexes were identified and prepared. The first was a bidentate equivalent of **L3**, with a butyl chain replacing one of the phosphine arms. This was to examine whether a successful catalyst had to feature a tridentate phosphine.

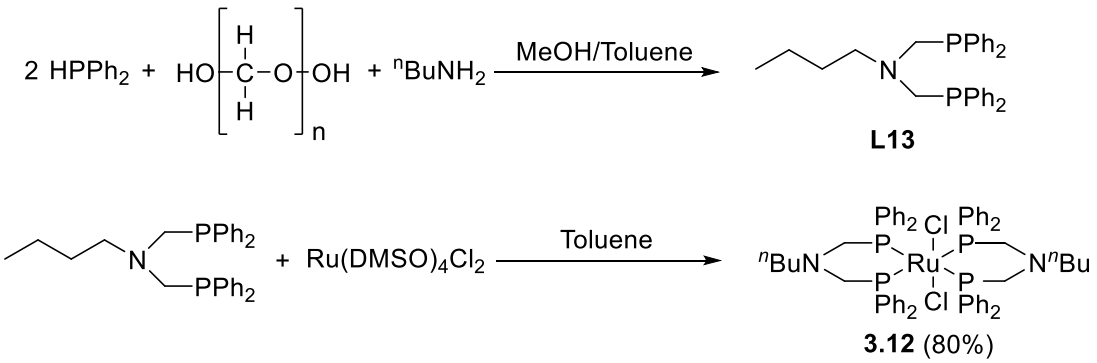

*Scheme 3.13. Synthesis of **L13** and **3.12***

The ligand was prepared following the procedure reported by Li and Wu using a similar Mannich reaction to the synthesis of **L3** (Scheme 3.13).[16] The product was a viscous, white oil which gave a peak at -28 ppm in the $^{31}P\{^{1}H\}$ NMR spectrum. When reacted with the Ru precursor in toluene a yellow solid was formed giving a singlet at -3.5 ppm. ESI-MS analysis showed that the complex was in fact a monometallic, bis-chelate complex rather than a dimer.

An analogue of **L3** with longer alkyl arms, an ethyl link instead of a methyl, was also synthesised and complexed to ruthenium (Scheme 3.14). The ligand synthesis followed a literature procedure[17] and began by reacting triethanolamine with thionyl chloride to give a trichloroethylamine hydrochloride salt. This salt was then added to a solution of diphenylphosphine in THF with the secondary phosphine having been deprotonated by KO^{t}Bu. The ligand **L14** was isolated as a white solid ($^{31}P\{^{1}H\}$ -20 ppm) and was complexed to Ru in the same manner as the other N-Tripod ligands (Scheme 3.14). The $^{31}P\{^{1}H\}$ NMR spectrum of the Ru complex formed showed a doublet at 27 ppm and a triplet at 47 ppm with a 2:1 ratio of intensities. ESI-MS gave a signal at 825.7 which corresponds to a 5 co-ordinate, dichloride complex. The d^6 Ru centre would be paramagnetic with a trigonal bipyramidal geometry, which wouldn't give the sharp peaks observed in the $^{31}P\{^{1}H\}$ NMR spectrum so a square pyramidal arrangement is more likely. It is also possible that an octahedral complex with a DMSO ligand was formed and that this ligand was removed during the ESI-MS experiment. There is a small peak (5% intensity per proton compared to the phenyl protons) in the ^{1}H NMR spectrum at 3.10 ppm which is

consistent with an *O*-bound DMSO ligand suggesting that this complex is present, but only as a minor component of the isolated product.

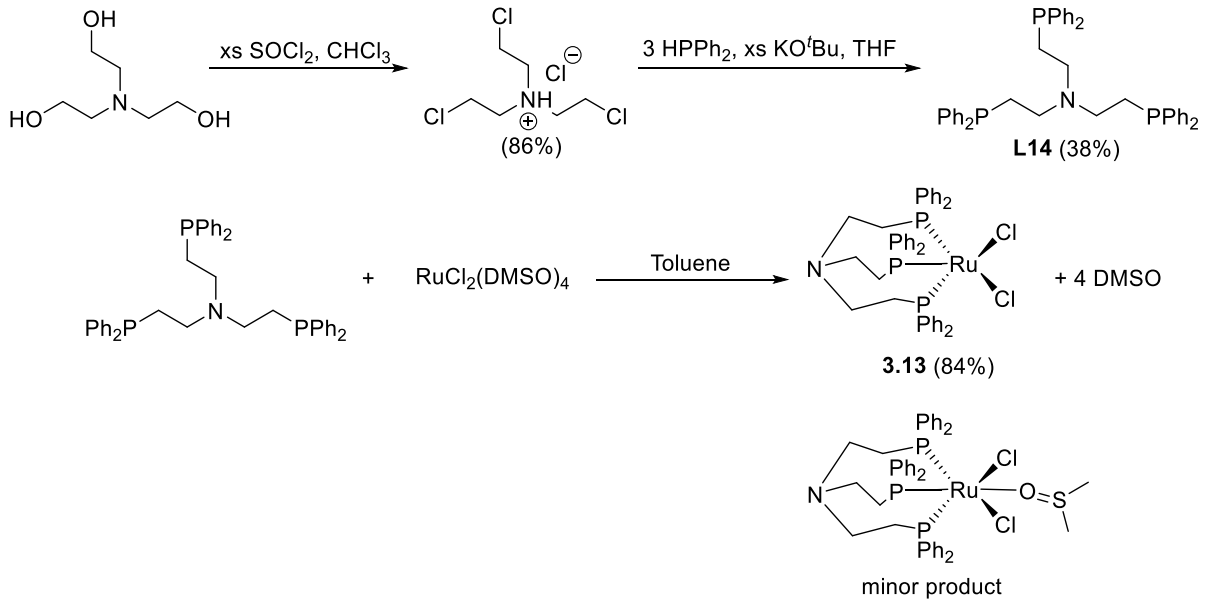

*Scheme 3.14. Synthesis of **L14** and **3.13***

The related tripodal phosphinite (**L15**) was synthesised from the methoxy tripod scaffold with 3 equivalents of chlorodiphenylphosphine (Scheme 3.15). Phosphinites are more air stable than their phosphine analogues, but are not stable with moisture, the P-O bond being susceptible to hydrolysis. In the case of the carbon centred tripods, phosphinites could provide a simpler synthetic route to a range of ligands. The diphenylphosphinite tripod was isolated with a single peak at 114 ppm in the $^{31}P\{^{1}H\}$ NMR spectrum. The ligand was then complexed to Ru with the product, **3.14**, isolated as an orange solid. The $^{31}P\{^{1}H\}$ spectrum NMR showed two broad peaks at 150 and 145 ppm in a 1:2 ratio, consistent with the literature.[18]. As with **3.13**, the complex is likely to form a square pyramidal structure, consistent with the ESI-MS analysis which showed a peak at 809 which corresponds to $[M\text{-}Cl]^{+}$. It is also possible that an octahedral arrangement with a coordinated DMSO molecule has been formed, but the large peak at 3.08 ppm in the ^{1}H NMR for the $-CH_2-$ protons of the ligand obscure the region where a signal for coordinated DMSO is likely to occur. In the solid phase 3.14 is reported to form a dimeric complex $[Ru_2Cl_3(\mathbf{L15})_2]Cl$ as with the other complexes prepared.

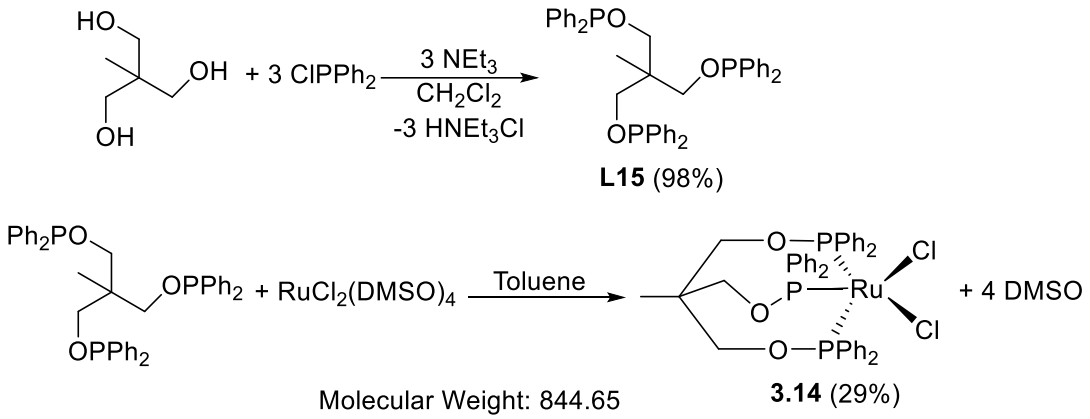

*Scheme 3.15. Synthesis of **L15** and **3.14***

These three complexes were all tested for the hydrogenation of DMO.

*Table 3.7 DMO Hydrogenation with **3.12-14***

Run[a]	Catalyst	% Yield MG	% Yield EG	% Conv DMO
1	**3.12**	38	0	85
2	**3.13**	42	13	90
3	**3.14**	53	0	70

[a]conditions: 5 mmol DMO, 0.25 mol% catalyst, 10 mL MeOH, 180 °C, 30 bar H_2, 3 h

The only catalyst to give any conversion to EG was the elongated N-tripod complex **3.13** (Run 2). Both **3.12** and **3.14** gave some turnover for the first hydrogenation to MG but were unsuccessful with the second step (Runs 1 and 3). There was also some evidence of catalyst decomposition with the phosphinite complex **3.14** i.e. black metallic solid was formed during the reaction. This reinforces the concept that for a successful hydrogenation from DMO through to EG the catalyst must be based around a ligand that is firstly, tridentate in its coordination to the metal centre and secondly, that coordination must be through phosphine groups.

A number of other Ru based catalysts reported for ester, ketone and aldehyde hydrogenation were examined for DMO to EG (Scheme 3.16). These included the commercially available Shvo's catalyst (**3.15**),[19] two Noyori catalysts,[20] one with two coordinating triphenylphosphine ligands (**3.16**), the

other with a bidentate BINAP ligand (**3.17**), a pyridinyl centred PNP complex reported by Milstein (**3.18**)[21] and the related complex featuring amines in the alkyl linkers used by Kirchner (**3.19**).[22]

All these complexes were tested using both the optimum conditions established for the Tripod systems and conditions from their respective literature reactions. The latter included adding an alkoxide base, either NaOMe or KO^{t}Bu, and, for the Noyori catalysts, using ^{i}PrOH as a solvent and hydrogen transfer agent. None of these catalysts showed any activity for the hydrogenation of DMO, producing no MG or EG and leaving the substrate unconverted. This again reiterates the idea that for a successful hydrogenation of DMO a system which contains a tridentate, facial capping phosphine ligand is required.

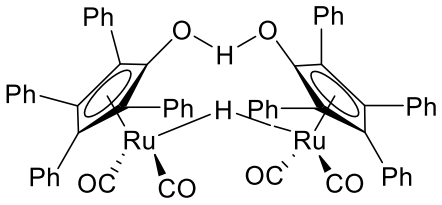

3.15

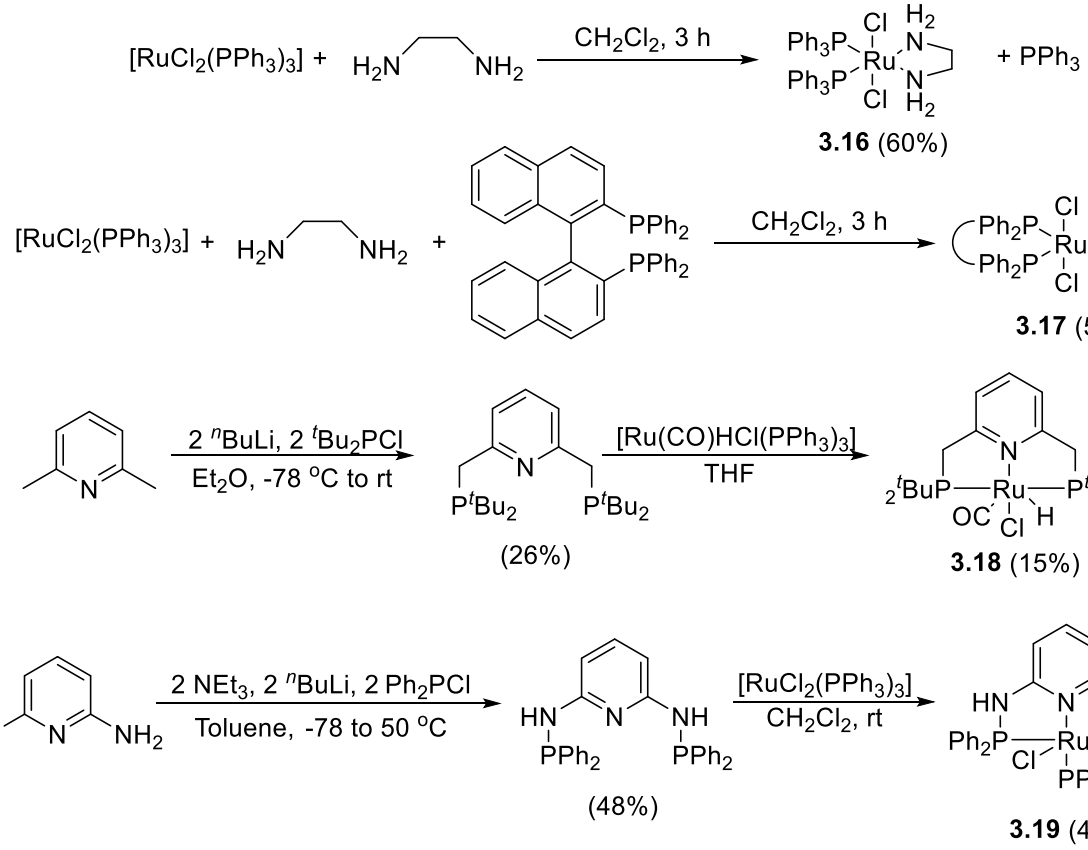

*Scheme 3.16. complex **3.15** and syntheses of **3.16-19***

3.2.6 – First Row Transition Metal Complexes

Given the scarcity and high cost of precious metals such as ruthenium, a large body of research has been carried out in recent years to devise effective catalyst systems using the cheaper and more abundant first row transition metals. Iron[23] and cobalt[24] catalysts have been investigated to this end for several years while, more recently, manganese systems have been developed as an alternative to ruthenium for hydrogenation reactions and borrowed hydrogen processes.[25,26] Mn and Ru are situated diagonally from each other on the periodic table so the Mn(I) atom, which features in all known active Mn catalysts published so far, is electronically and sterically similar to a Ru(II) centre often utilised in

catalysis. Often, to circumvent the lack of latent reactivity with these metals, higher catalyst loadings, longer reaction times, harsh conditions or co-catalysts and additives are needed.

Tripod complexes of Fe (**3.20**),[27] Co (**3.21**)[28] and Mn (**3.22, 3.23**)[29] were prepared using literature procedures and tested for the hydrogenation of DMO (Scheme 3.17). An [Fe(acac)$_3$] with Zn *in situ* system similar to the Elsevier Ru catalyst was also tested. Unfortunately, at a higher 5 mol% loading, none of these systems gave any MG or EG.

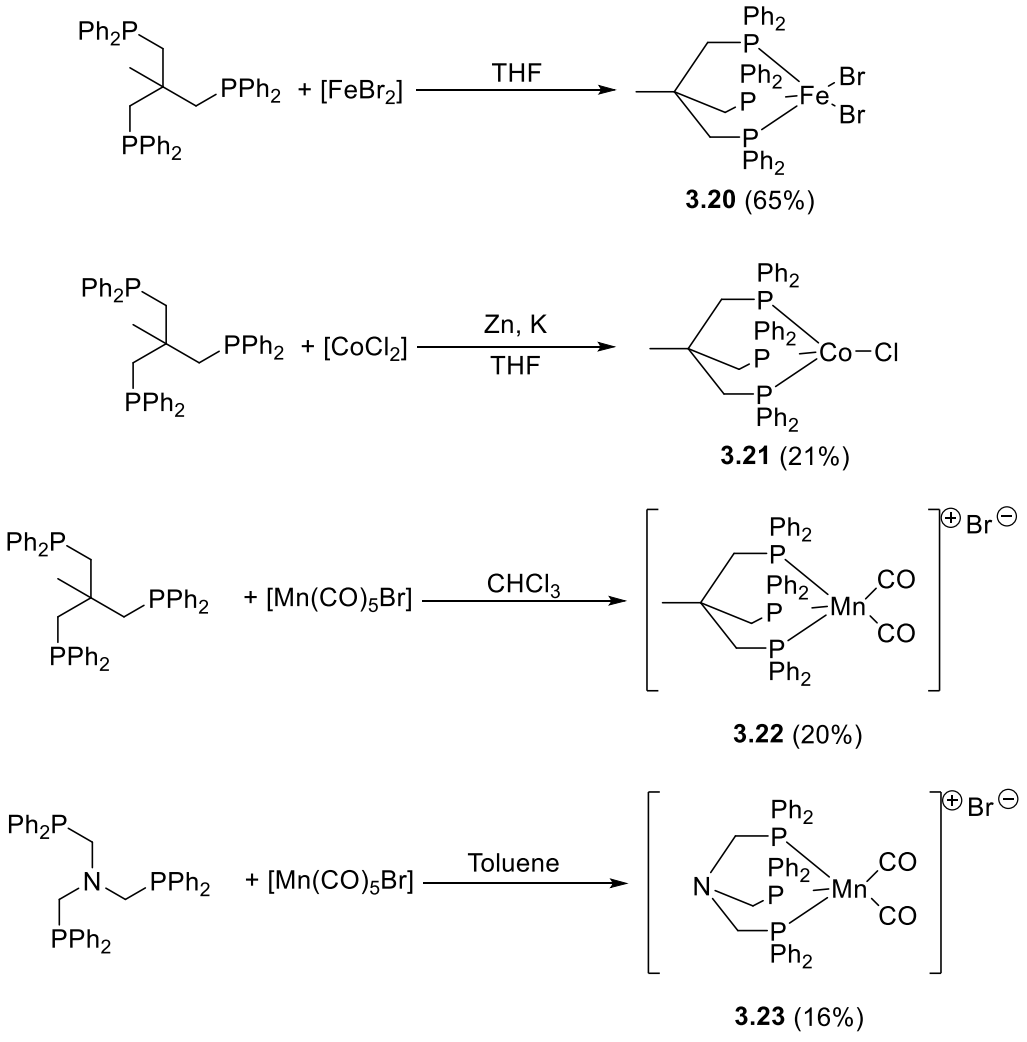

*Scheme 3.17. Synthesis of first row transition metal tripod complexes **3.20-23***

The lack of success of the Mn complex can perhaps be explained by the nature of the tripod ligand. The successful published catalysts tend to use a “non-innocent” ligand. As suggested the ligands in these complexes have some form of interaction with the substrate to assist the metal, either as

present in the complex or a deprotonated form produced using base. As yet there has been no evidence of these tripod ligands acting in a non-innocent fashion (see mechanistic discussion, Section 3.5) which could explain why they can only be used successfully with a more reactive precious metal i.e. ruthenium.

3.2.7 – Catalyst Recycling

To study the potential for recycling the catalysts, a test was performed with **3.1** and **3.3** (Table 3.8). The DMO hydrogenation was performed as normal, but after cooling the sample an aliquot was taken for GC analysis before another 5 mmol of DMO substrate was added and the autoclave re-pressurised with H_2 and returned to the heating block for another 3-hour reaction (Runs 1B and 2B). This did not change the yield of EG, but the amount of MG in the reaction mixture increased. The catalyst had clearly not been fully deactivated as there was fresh turnover from DMO to MG. An excess of DMO or MG could perhaps have slowed the MG to EG hydrogenation or potentially altering the composition of the reaction mixture changed the equilibrium of the reaction to favour the first hydrogenation step over the second.

*Table 3.8. Recycle tests with **3.1** and **3.3***

Run[a]	Catalyst	% Yield MG	% Yield EG
1A	**3.1**	20	58
1B[b]		82	55
2A	**3.3**	37	50
2B[b]		60	49

[a]conditions: 5 mmol DMO, 0.25 mol% catalyst, 10 mL MeOH, 180 °C, 30 bar H_2 [b]conditions: As for [a] then cooled and vented, additional 5 mmol DMO added, run for 3 h conditions as for [a]

3.3 – Hydrogenation of Glycolic Acid

Glycolic acid (GA) is another substrate that can be hydrogenated to EG. Most GA production occurs through the reaction of formaldehyde with synthesis gas and water,[30] although it is also naturally occurring in many plants and can be prepared by a hydrogenation of oxalic acid.[31] The hydrogenation of GA to EG has previously been reported using heterogeneous Ru catalysts (Ru metal, RuO_2, Ru/C) on supports such as silica, alumina and silicon carbide.[32] The best performing Ru/tripod complexes synthesised and tested with DMO were evaluated for the hydrogenation of GA to EG by homogeneous catalysis (Table 3.9).

Table 3.9. Hydrogenation of GA with Ru/Tripod catalysts

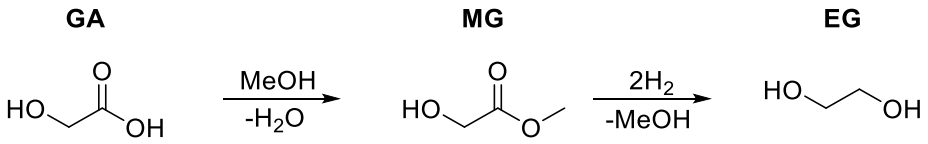

Run[a]	Catalyst	% Yield MG	% Yield EG
1	**3.1**	7	80
2[b]	**3.1**[b]	0	0
3	**3.2**	85	1
4	**3.3**	9	72
5	**3.4**	91	0
6	**3.5**	79	6
7	**3.6**	90	0
8	**3.7**	23	76
9	**3.8**	28	64
10	**3.9**	43	50
11	**3.11**	94	0
12	-	93	0

[a]conditions: 5 mmol GA, 0.25 mol% catalyst, 10 mL MeOH, 180 °C, 30 bar H_2, 3 h [b] 10 mL THF

The reaction proceeds through a transesterification of GA to MG which is then hydrogenated to EG. A catalyst free run showed that under the reaction conditions the transesterification was self-catalysed by GA and gave a high yield of MG (Run 12). A test using THF, which has a similar polarity and boiling point to methanol and can solubilise all the reaction components, but crucially cannot form an ester with GA gave no MG or EG (Run 2). This implies that the transesterification route is the only pathway to EG with no direct hydrogenation of GA. The results matched those seen with the DMO hydrogenation; the carbon-based tripod complex **3.1** (Run 1) performed best with **3.3** and its para-substituted analogues also showing good activity (Runs 4, 8 and 9). The triphos dimer **3.9** gave a reasonable yield of EG (Run 10) while **3.11,** the ethyl variant, again gave no turnover and appeared to decompose during the reaction (Run 11). The cyclohexyl complex **3.5** gave limited EG over 3 hours but was much slower than **3.1** as seen with DMO (Run 6).

As this reaction was shown to progress through a transesterification of the GA substrate with the alcohol solvent, the effect of solvent on the reaction was studied. As mentioned above, changing to THF, which cannot form an ester with GA, precluded all reactivity. A range of other alcohol solvents were tested with **3.1** and GA. All formed the relevant esters *in situ* although full quantitative analysis was not possible. Ethanol and *n*-propanol were the only solvents that yielded enough EG to be within the quantitative range for GC analysis (9% and 8%) respectively. However, by looking at the raw data from the GC trace a rough trend can be established; MeOH>>EtOH≈^{n}PrOH>BnOH>^{i}PrOH. This relationship follows the size of the alcohols which suggests that as the alcohol solvent gets bulkier either the corresponding glycolate ester is formed in a smaller quantity or more slowly, or that the ester is more resistant to hydrogenation.

3.4 – Hydrogenation of MG

As the hydrogenation of both substrates studied so far, DMO and GA, occur via the MG intermediate, the hydrogenation of MG itself was examined. Four of the tripod-based catalysts were selected with the results given below (Table 3.10).

Table 3.10. Hydrogenation of MG with Ru/Tripod catalysts

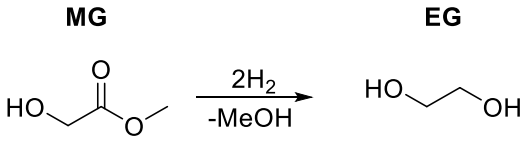

Run[a]	Catalyst	% Yield EG	% Conv MG
1	**3.1**	51	81
2	**3.2**	1	22
3	**3.3**	38	42
4	**3.5**	4	5

[a]conditions: 5 mmol MG, 0.25 mol% catalyst, 10 mL MeOH, 180 °C, 30 bar H_2, 3 h

The pattern of reactivity is the same as observed with DMO and GA. **3.1** and **3.3** (Runs 1 and 3) performed well with **3.5** (Run 4) only providing a few turnovers and essentially no activity from **3.2** (Run 2). Interestingly, there was a much bigger discrepancy between MG conversion and EG yield with the C-centred ligands than the N-centred ligands suggesting the formation of more side products with **3.1** and **3.2**. The GC analysis did show several small peaks at comparable retention times to MG and EG perhaps suggesting some similar organic molecules were formed. There were a few peaks in the product ^{1}H NMR spectrum with a similar chemical shift to EG, perhaps suggesting the formation of some oligomeric glycols. Further analysis would be needed to confirm this. It is also possible that the EG itself is reacting on to form by-products. A stability test was conducted using **3.1** and EG to see if the product was stable to the catalyst and reaction conditions. The full amount of EG was retained;

however, this only shows stability with respect to itself and the catalyst. EG could potentially still react with another organic compound formed in the reaction mixture from the MG substrate.

3.5 – Mechanistic Studies

Both **3.1** and **3.3** were studied further to try to identify active catalyst species or intermediates. A catalyst run was conducted using **3.1** with methanol-d_4 (CD_3OD) as the solvent. The product mixture was kept under inert conditions for NMR and ESI-MS analysis. The resulting $^{31}P\{^1H\}$ NMR spectrum showed a single peak at 37 ppm due to the dimer complex. The ^1H NMR spectrum showed peaks corresponding to the complex, DMO, MG and EG as well as a few other small peaks in the same region as the organic compounds. Crucially, there is no evidence of either a bound hydrogen or Ru-hydride complex present, the latter being particularly easy to observe having a characteristic chemical shift below -5 ppm. It is possible that a hydride complex was formed and was converted to a deuteride complex by exchange with the solvent. The ESI-MS gave a large peak at 783.1 m/z units which could correspond to a $[Ru(\mathbf{L1})(CO)_2H]^+$ species. The isotope pattern of the peak confirms a monometallic structure with the expected peaks 783.1 (100%), 785.1 (59%), 782.1 (54%) (Figure 3.7). This species contradicts the NMR data which showed no evidence of a ruthenium hydride. To form the carbon monoxide for the carbonyl ligands either decarbonylation of the DMO substrate or the methanol-$_{d4}$ solvent must have occurred.

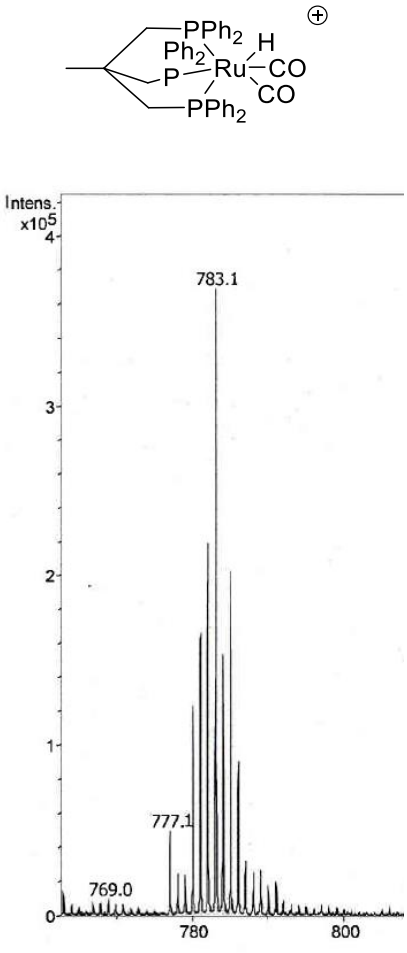

Figure 3.7. Potential structure from ESI-MS and trace showing isotope pattern

Complex **3.3** with the N-tripod ligand was subjected to the same analysis. A catalyst run with no DMO substrate gave a single $^{31}P\{^{1}H\}$ NMR peak at 18.8 ppm which corresponds to the complex **3.3**. However, unlike with **3.1**, the NMR spectrum changed when the autoclave run was conducted using the substrate. Two peaks were then present in the $^{31}P\{^{1}H\}$ NMR spectrum, one at 36.6 ppm and a larger peak at 25.8 ppm. The former could be oxidised ligand. Previous studies with an *in situ* N-Tripod/Ru system have shown a degree of catalyst decomposition with accompanying ligand oxidation during DMO hydrogenation.[9] However, the origin of the peak at 25.8 ppm is unknown.

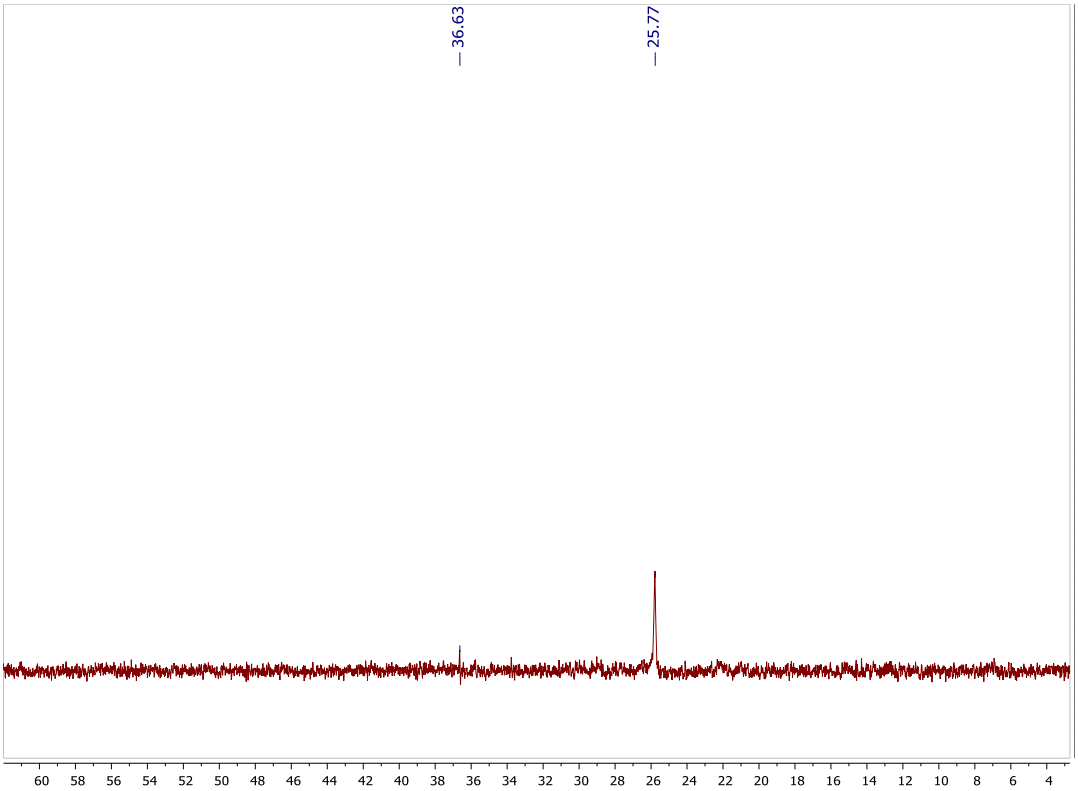

*Figure 3.8. $^{31}P\{^{1}H\}$ (MeOD-d_4, 162 MHz) spectrum of reaction mixture of **3.3** with DMO*

The ESI-MS analysis shows two obvious peaks at 930.2 and 805.1 m/z. A potential structure for the 805 fragment is a monomeric Ru complex with a chelating ethylene glycol molecule with a coordinating methoxide (Figure 3.9). This has a mass of 806.17 so would require the loss of a proton. Another possibility is the dicarbonyl chloride species also shown, which has an exact mass of 804.07. The 930.2 peak could be caused by the bimetallic complex [Ru(**L3**)$(CO)_4H_2$] which has a mass of 929.01. The ESI-MS trace shows the expected isotope pattern for the bimetallic structure; $[M-2]^+$ (92%), $[M-1]^+$ (85%), but this proposed structure is unlikely the Ru centres do not have an 18 electron count.

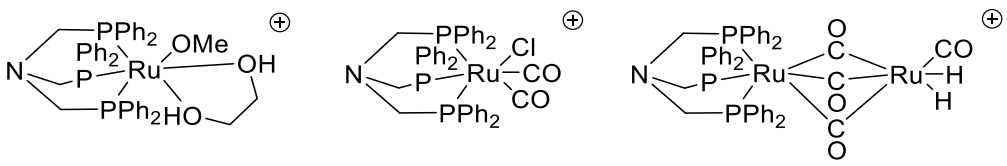

Fig 3.9. Potential structures for ESI-MS fragment at m/z 805 and 930

3.6 – Kinetic Studies

Kinetic investigations were undertaken to better understand the mechanism through which the DMO hydrogenations occur. A series of catalyst runs over set time periods were conducted with both **3.1** and **3.3** to see how the amount of the three key components; DMO, MG and EG change over the 3-hour time period until maximum yield is obtained.

The data for **3.1** (Figure 3.10) indicates that the first hydrogenation reaction to MG was well underway within 0.5 hours. The lack of induction period suggests that the process follows a homogenous pathway rather than nanoparticles or soluble nanoclusters. The yield of EG built steadily from 1 to 2 hours with the amount obtained being similar to that of MG. Between 2 and 2.5 hours there was a sharp increase in the rate of EG production with a TOF of approximately 240 turnovers h^{-1}. During this period there was also a net consumption of MG demonstrating that at this stage the rate of the second hydrogenation had overtaken that of the first. The DMO substrate was essentially fully consumed within 2.5 hours.

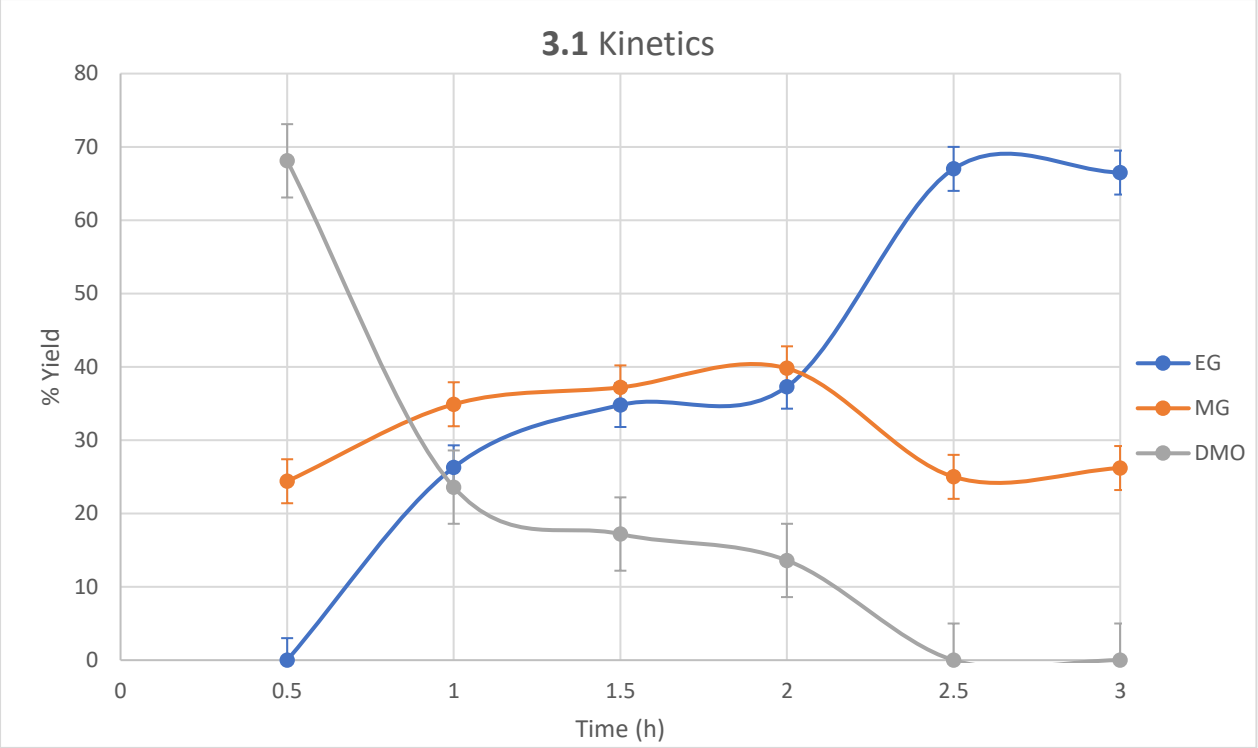

*Figure 3.10. Plot of %yield vs time for catalyst **3.1** Conditions: 5 mmol DMO, 0.25 mol% catalyst, 10 mL MeOH, 180 °C, 30 bar H_2. Each data point measured by individual timed runs*

The results for **3.3** show a similar pattern (Figure 3.11). The first hydrogenation reaction began rapidly suggesting no nanoparticle formation. The formation of EG appeared to occur at a steadier rate of around 160 turnovers h^{-1} from 1 to 2 hours compared to the plateau then sharp increase seen with **3.1.** There is a clear crossover point between 1.5 hours and 2 hours where the rate of the second hydrogenation outstrips that of the first. The reaction almost reached completion at 2.5 hours with little change in EG or MG yields during the final 0.5 hours. Interestingly the DMO is consumed within 2 h with **3.3**, faster than with **3.1**. Previous studies by Miller and Hanton examining the kinetics using hydrogen uptake observed that after an induction period, minimal in this work as pre-formed catalysts were used, the Tripod catalyst had a TOF around 20 times than that of the N-Tripod analogue.[9] This contrasts drastically to the results presented here as the dimer complexes appear to show a much more similar rate of DMO hydrogenation.

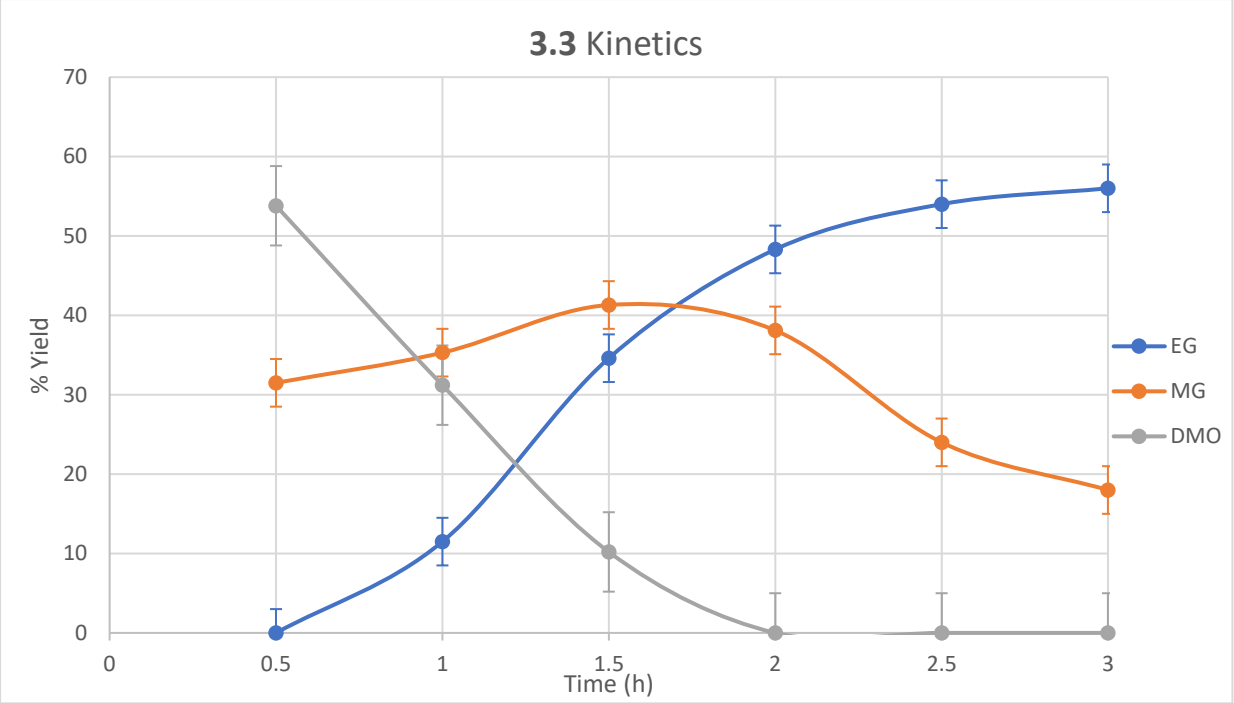

*Figure 3.11. Plot of %yield vs time for catalyst **3.3.** Conditions: 5 mmol DMO, 0.25 mol% catalyst, 10 mL MeOH, 180 °C, 30 bar H_2. Each data point measured by individual timed runs*

3.7 – Hydrogenation of DMO and MG in flow

The following work was conducted during a visit to BP at the Centre of Expertise for Applied Chemistry and Physics, Saltend HRTC, Hull under the supervision of industrial supervisor Prof. Glenn Sunley and Dr Greg Price.

The hydrogenation of DMO to EG was investigated in flow using an H-Cube and Phoenix flow reactor (See Chapter 6 for more experimental details). A solution of catalyst, **3.1** and **3.3** were tested, and substrate in methanol was prepared and flowed through the apparatus. The reactor coil was pre-heated to the desired temperature and a hydrogen pressure generated *in situ* by the H-Cube. After the required residence time in the reactor an aliquot of the product mixture was collected and analysed by GC. As well as allowing an examination of the catalysis in flow versus in batch autoclave reactions, this equipment allowed more forcing conditions than could be used with the autoclaves and different reaction conditions could be tested during the course of one run. The first test was the hydrogenation of DMO (Table 3.11).

The values below are approximate yield calculated using relative peak areas.

*Table 3.11. Hydrogenation of DMO with **3.1** in flow*

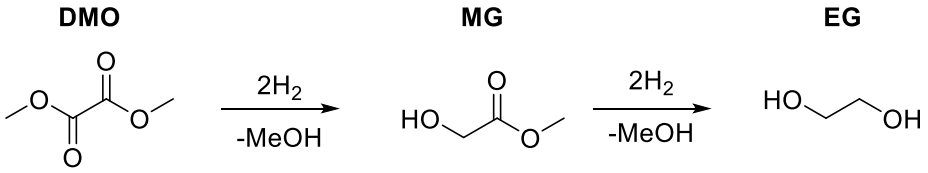

Sample[a]	Temperature (°C)	% DMO	% MG	% EG
1	180	70	22	0
2	200	25	35	37

[a]conditions: 0.3 mol% **3.1**, 20 mmol DMO, 200 mL MeOH, 90 bar H_2, 0.1 mL/min, 90 min residence time

When 180 °C was used there was only partial conversion of the DMO to MG (Sample 1). However, when the temperature was increased to 200 °C some conversion all the way through to EG was observed (Sample 2). This revealed that the reaction can work under flow conditions and also that the catalyst **3.1** is stable and may in fact perform better at temperatures higher than those used previously. With these results in mind, the hydrogenation of MG was then conducted (Table 3.12).

*Table 3.12. Hydrogenation of MG with **3.1** in flow*

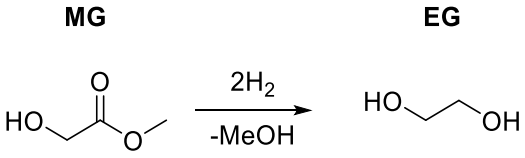

Sample[a]	Temperature (°C)	% MG	% EG
1	180	99	0
2	200	79	21
3	220	47	53

[a]conditions: 0.3 mol% **3.1**, 20 mmol MG, 200 mL MeOH, 90 bar H_2, 0.1 mL/min, 90 min residence time

As with the DMO test previously, there was no MG conversion at 180 °C (Sample 1), but increasing to 200 °C gave some turnover to EG (Sample 2). Raising the temperature further to 220 °C gave an even larger increase in EG formation (Sample 3). The yellow solution turning paler was observed during the reaction at 220 °C suggesting a degree of catalyst decomposition. No other signs of degradation such as a black or metallic solid were noted.

It was thought that EG itself may poison the catalyst, react to other products or perhaps even back to MG or limits the overall conversion of the reaction in another way. To investigate this, two tests were performed using DMO and MG as substrates with an equivalent of EG added to the reaction solution. The results are shown below (Tables 3.13 and 3.14).

*Table 3.13. Hydrogenation of DMO by **3.1** with EG*

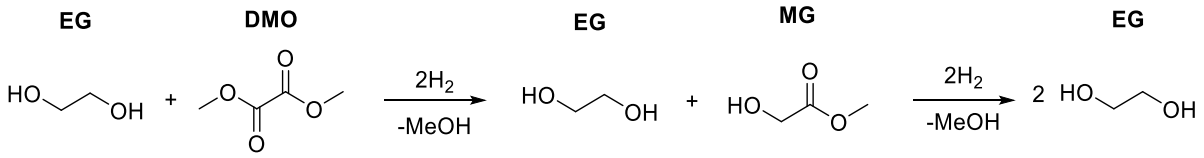

Sample[a]	Temperature (°C)	% DMO	% MG	% EG
1[b]	25	54	0	46
2	180	27	14	59
3[c]		27	14	59
4	200	0	5	95
5[c]		0	5	95
6	220	22	16	62
7[c]		22	16	62

[a]conditions: 0.3 mol% **3.1**, 20 mmol DMO, 20 mmol EG, 200 mL MeOH, 90 bar H_2, 90 min residence time [b] feed sol^n [c] reaction aliquot left at rt for 24 hours

The reaction aliquots were left for 24 hours at room temperature to see if any reactivity occurred without the applied temperature and H_2 pressure. In all cases there was no difference between these samples and those analysed immediately after the reaction. The results at 180 °C (Samples 2 and 3) support those from the previous tests showing some DMO to MG conversion, but very little from MG to EG. At 200 °C however, there is almost complete conversion from DMO through MG to EG (Samples 4 and 5). This illustrates that the presence of EG does not have a negative impact on the turnover of these ester hydrogenations. At 220 °C, the catalytic activity has decreased, and the results are similar to those obtained at 180 °C (Samples 6 and 7). This supports the idea that the catalyst may degrade at this temperature. As with the previous test the reaction mixture had lost its yellow colour during this reaction. These results are very promising, but it must be reiterated that these were from one test using a fairly crude GC-MS analysis. The experiment must be repeated and examined more thoroughly to obtain more reliable data.

*Table 3.14. Hydrogenation of MG by **3.1** with EG*

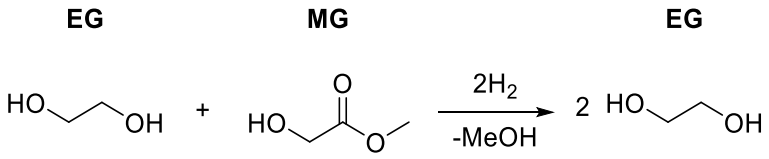

Sample[a]	Temperature (°C)	% MG	% EG
1	180	36	64
2	200	15	85
3	220	22	78

[a]conditions: 0.3 mol% $[Ru(Tripod)Cl_{1.5}]_2Cl$, 20 mmol MG, 20 mmol EG, 200 mL MeOH, 90 bar H_2, 90 min residence time

These results compliment those presented above (Table 3.13). A low conversion of MG to EG is seen at 180 °C (Sample 1) with much improved catalytic performance at 200 °C (Sample 2). As with DMO hydrogenation turnover worsened when the temperature was increased from 200 to 220 °C potentially due to catalyst decomposition.

The DMO hydrogenation in flow was also attempted using catalyst **3.3** with the results shown below (Table 3.15).

*Table 3.15. Hydrogenation of DMO by **3.3** in flow*

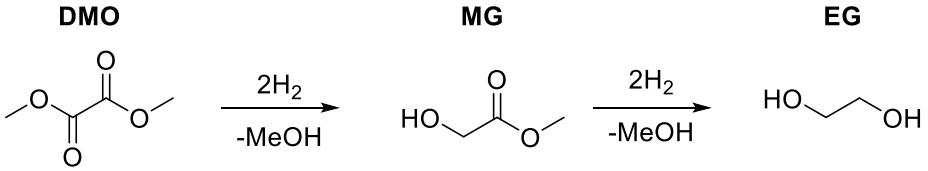

Sample[a]	Temperature	% DMO	% MG	% EG
1	180	25	41	16
2	200	76	23	0
3	220	91	9	0

[a]conditions: 0.3 mol% $[Ru(NTripod)Cl_{1.5}]_2Cl$, 2.45 g DMO, 200 mL MeOH, 90 bar H_2, 90 min residence time

The 180 °C gave some turnover to EG (Sample 1), unlike with **3.1**. However, at 200 and 220 °C catalyst performance was significantly worse with no EG formed and DMO to MG conversion decreased with increased temperature (Samples 2 and 3). These two samples also appeared colourless, compared to the bright yellow of the feed solution. It may be that this complex decomposed at the higher temperatures and lacked the thermal stability showed by **3.1** at 200 °C.

3.8 – Summary

A range of ruthenium catalysts with phosphorus-based ligands were synthesised and tested for the hydrogenation of DMO, GA and MG. The dimer complex, **3.1**, incorporating the widely available tripod ligand was the most successful while the related N-Tripod complex **3.3** also showed good activity. It was established that for the best reactivity the ligand must contain a tridentate phosphine which binds to the metal with a facial geometry. It also appears that increasing steric bulk in the ligand can slow or halt the ester hydrogenation. Attempts were made to apply these ligands to first row transition metals, but they proved unsuccessful for catalysis.

Brief mechanistic investigations illustrate that both **3.1** and **3.3** perform the hydrogenation reactions through a homogeneous mechanism and there is some evidence to suggest that both **3.1** and **3.3** break down into monomeric complexes during the course of the reaction.

Attempts to perform the hydrogenation of DMO and MG with **3.1** and **3.3** in flow showed success. With **3.1** high catalytic activity was observed at 200 °C suggesting a high thermal stability not explored in previous studies. **3.3** did not show this stability and the performance of both catalysts decreased at 220 °C accompanied by possible signs of degradation.

3.9 – Future Work

The active catalyst species is currently unidentified. Despite not seeing any evidence of this with **3.1** in the mechanistic experiments discussed above, it is likely that the dimer splits into two monomeric ruthenium components with the loss of the chloride ligand. In the early Elsevier work it was suggested that the MeOH solvent acted as a donor ligand, but no evidence for this was presented.[1] This is the only obvious way to generate an active site for substrate – metal binding. As mentioned previously, the tripod ligands have never exhibited any sort of substrate interaction, any reactivity must occur through the metal centre. It is also unlikely, due to the chelate effect, that one of the phosphines is released from the metal. This would also bring about an obvious change to the $^{31}P\{^{1}H\}$ NMR spectrum,

with a clear phosphine resonance at around -15 ppm. This also has not been observed at any point during these studies. The synthesis of a monomeric tripod-Ru complex with more labile ligands to replace the bridging chlorides or using an additive with the dimers may give better insights into the catalyst' s mode of operation. Monomeric complexes with ruthenium and **L1** or **L3** have been reported, but they lack the air and moisture tolerance of the dimers studied here. The other ligands are also chlorides or CO which give no improvement in lability.[10,11] Preparing a complex using less strongly binding ligands e.g. donor solvents such as MeCN or DMSO or potentially even simple phosphines such as PPh_3 could improve catalyst activity. It is likely that the octahedral, Ru(II) arrangement will be required for catalyst activity so this must be taken into account for any catalyst design.

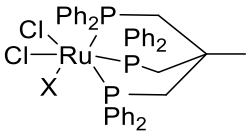

X - labile ligand e.g. donor solvent, PR_3

*Figure 3.12. Monomeric variant of **3.1** with labile ligand*

Using a base, Lewis acid or silver salt with the dimer may help to break up the catalyst into two monomers and strip the chloride ligands from the metal centres. This obviously adds another, highly reactive, component to the reaction so the necessary tests to ensure that these additives cause no unwanted side effects would have to be performed.

It is possible that EG, and MG, can chelate to the metal centre. This was identified in a plausible ESI-MS structure above. These would form thermodynamically stable 5-membered rings with the ruthenium atom, potentially poisoning the catalyst. This could explain why no improvement is seen from 3 to 20 hours and why the recycling test yielded no improvement in EG yield. Stochiometric reactions with the catalyst will show how readily these complexes are formed. Also, experiments where the reaction mixture is spiked with EG could also be carried out to investigate whether it acts as a catalyst poison.

The ester hydrogenations in flow could pave the way for a substantial body of work. The data presented in Section 3.7 are approximate values so these experiments should be repeated and analysed using a more rigorous GC analysis with quantities determined using an external standard. A more thorough screen of reaction conditions; H_2 pressures, temperatures and flow rates, which determines residence time, could be conducted to determine both the optimum conditions and limits of what the catalysts can tolerate. There was some evidence of catalyst decomposition at 220 °C which could be further investigated using ^{31}P NMR and ESI-MS studies to identify the ruthenium complexes present in the reaction mixture.

3.10 – References

1. H. T. Teunissen and C. J. Elsevier, *Chem. Commun.*, 1997, 667–668.
2. U. Matteoli, G. Menchi, M. Bianchi, and F. Piacenti, *J. Organomet. Chem.*, 1986, **299**, 233–238.
3. E. Iengo, E. Zangrando, E. Baiutti, F. Munini, and E. Alessio, *Eur. J. Inorg. Chem.*, 2005, **2005**, 1019–1031.
4. A. M. J. Lees and A. W. G. Platt, *Polyhedron*, 2005, **24**, 427–433.
5. L. F. Rhodes, C. Sorato, L. M. Venanzi, and F. Bachechi, *Inorg. Chem.*, 1988, **27**, 604–610.
6. J. Lee, PhD Thesis, 2015.
7. W. Hewertson and H. R. Watson, *J. Chem. Soc.*, 1962, 1490.
8. J. S. Yu and I. P. Rothwell, *J. Chem. Soc. Chem. Commun.*, 1992, 632–633.
9. M. J. Hanton, S. Tin, B. J. Boardman, and P. Miller, *J. Mol. Catal. A Chem.*, 2011, **346**, 70–78.
10. A. Phanopoulos, N. Long, and P. Miller, *J. Vis. Exp.*, 2015, e52689.

11. A. Phanopoulos, A. J. P. White, N. J. Long, and P. W. Miller, *ACS Catal.*, 2015, **5**, 2500–2512.

12. C. A. Tolman, *Chem. Rev.*, 1977, **77**, 313–348.

13. W. Liu, B. Sahoo, A. Spannenberg, K. Junge, and M. Beller, *Angew. Chem. Int. Ed.*, 2018, **57**, 11673–11677.

14. A. Albinati, Q. Jiang, H. Ruegger, and L. M. Venanzi, *Inorg. Chem.*, 1993, **32**, 4940–4950.

15. R. Gilbert-Wilson, L. D. Field, and M. M. Bhadbhade, *Inorg. Chem.*, 2012, **51**, 3239–3246.

16. W. Wu and C.-J. Li, *Chem. Commun.*, 2003, 1668.

17. M. I. García-Seijo, A. Habtemariam, P. del Socorro Murdoch, R. O. Gould, and M. E. García-Fernández, *Inorg. Chim. Acta*, 2002, **335**, 52–60.

18. E. Dulière, M. Devillers, and J. Marchand-Brynaert, *Organometallics*, 2003, **22**, 804–811.

19. R. Karvembu, R. Prabhakaran, and K. Natarajan, *Coord. Chem. Rev.*, 2005, **249**, 911–918.

20. H. Doucet, T. Ohkuma, K. Murata, T. Yokozawa, M. Kozawa, E. Katayama, A. F. England, T. Ikariya, and R. Noyori, *Angew. Chem. Int. Ed.*, 1998, **37**, 1703–1707.

21. J. Zhang, G. Leitus, Y. Ben-David, and D. Milstein, *Angew. Chem. Int. Ed.*, 2006, **45**, 1113–1115.

22. D. Benito-Garagorri, E. Becker, J. Wiedermann, W. Lackner, M. Pollak, K. Mereiter, J. Kisala, and K. Kirchner, *Organometallics*, 2006, **25**, 1900–1913.

23. S. Chakraborty, H. Dai, P. Bhattacharya, N. T. Fairweather, M. S. Gibson, J. A. Krause, and H. Guan, *J. Am. Chem. Soc.*, 2014, **136**, 7869–7872.

24. T. J. Korstanje, J. I. Van Der Vlugt, C. J. Elsevier, and B. De Bruin, *Science*, 2015, **350**, 298–302.

25. N. A. Espinosa-Jalapa, A. Nerush, L. J. W. Shimon, G. Leitus, L. Avram, Y. Ben-David, and D. Milstein, *Chem. Eur. J.*, 2017, **23**, 5934–5938.

26. S. Fu, Z. Shao, Y. Wang, and Q. Liu, *J. Am. Chem. Soc.*, 2017, **139**, 11941–11948.

27. T. K. Mukhopadhyay, M. Flores, R. K. Feller, B. L. Scott, R. D. Taylor, M. Paz-Pasternak, N. J. Henson, F. N. Rein, N. C. Smythe, R. J. Trovitch, and J. C. Gordon, *Organometallics*, 2014, **33**, 7101–7112.

28. C. P. Richers, J. A. Bertke, and T. B. Rauchfuss, *Dalton Trans.*, 2017, **46**, 8756–8762.

29. A. M. Bond, R. Colton, A. Van den Bergen, and J. N. Walter, *Inorg. Chem.*, 2000, **39**, 4696–4703.

30. L. D. John, 1936, US2152852.

31. P. P. T. Sah and S. L. Chien, *J. Am. Chem. Soc.*, 1931, **53**, 3901–3903.

32. W. Gresham, 1949, US2607805A.

Chapter 4 – Glycerol to Ethylene Glycol

4.1 – Introduction

Glycerol is produced in large quantities from biodiesel manufacture and a burgeoning field of chemistry is the conversion of this cheap, widely available product into useful, higher value chemicals (Introduction, Section 1.7). We envisaged a new potential route from glycerol to ethylene glycol (Scheme 4.1). The glycerol would first be converted to glycerol carbonate (GLC) which is then reacted to ethylene carbonate (EC) which can be hydrogenated to EG. The first and final reactions have been reported in the literature, therefore GLC to EC is the key step of the process. This transformation is essentially the removal of a hydroxymethyl group and presents much more of a synthetic challenge which may require a several step approach.

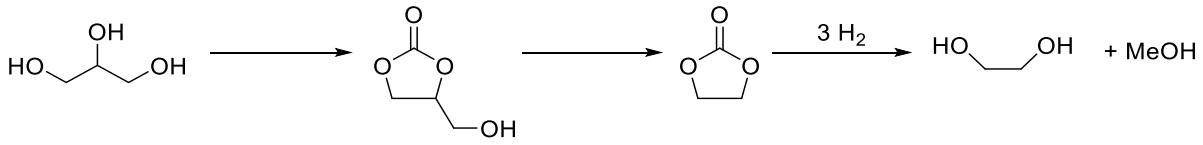

Scheme 4.1. Proposed overall route from glycerol to ethylene glycol

4.2 – Glycerol to Glycerol Carbonate

The preparation of GLC followed that published by Pyo and Hatti-Kaul (Scheme 4.2).[1] Dimethyl carbonate (DMC) is used as both reagent and solvent. The glycerol undergoes a methoxycarbonylation at one of the alcohol groups before ring closing to form the thermodynamically stable 5-membered cyclic carbonate. 4Å molecular sieves were used to absorb the methanol produced helping to drive the reaction equilibrium through to the product side. The reaction was performed at 90 °C to prevent a second methoxycarbonylation occurring at the free alcohol site in GLC. Even an increase of 20 °C to 110 °C shifts the reaction to producing more of this unwanted by-product. The product was isolated as a colourless oil giving the expected ^{1}H NMR spectrum.

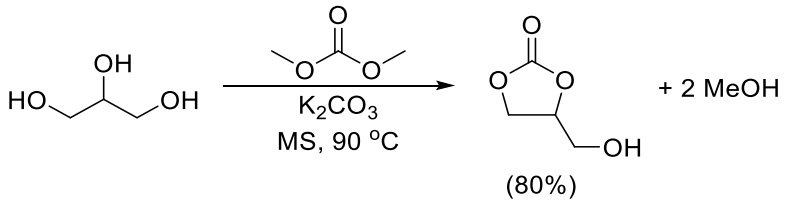

Scheme 4.2. Formation of GLC from glycerol

4.3 – Glycerol Carbonate to Ethylene Carbonate

4.3.1 – Direct Conversion

With the carbonate fragment in place acting as a protecting group for the 1,2-diol moiety, the removal of the hydroxymethyl component was then attempted. The first method was a direct removal of this group *via* an acceptorless dehydrogenative decarbonylation reported by Madsen *et al* (Scheme 4.3).[2]

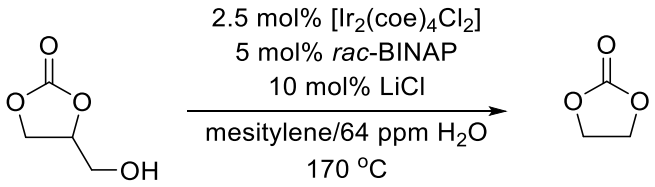

Scheme 4.3. Attempted dehydrogenative decarbonylation of GLC

This reaction has been reported for benzyl and naphthyl alcohols undergoing a two-step catalytic cycle (Scheme 4.4); the first dehydrogenation yielding the aldehyde and an equivalent of hydrogen through an octahedral Ir dihydride complex followed by a decarbonylation producing CO and the alkyl substituted arene. $[Ir_2(coe)_4Cl_2]$ and *rac*-BINAP were used to form the square planar active species [IrCl(CO)BINAP] *in situ.*

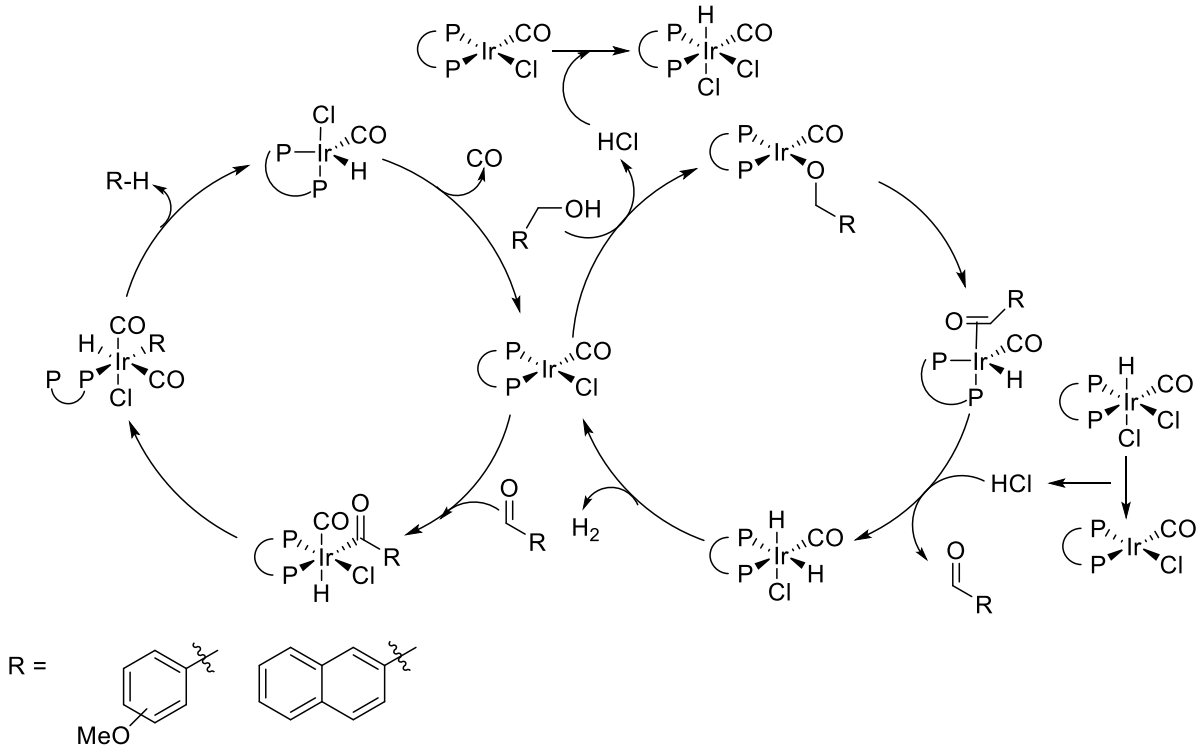

Scheme 4.4. Mechanism for dehydrogenative decarbonylation of benzyl or naphthylmethyl alcohols

This catalytic system was tested with GLC as a substrate using the reported conditions. These included 10 mol% LiCl to help phosphine dissociation generating a vacant site for substrate binding and 64 ppm H_2O in the mesitylene solvent for its mild basic properties. Unfortunately, the reaction was unsuccessful, the ^{1}H NMR spectrum showed a mass of poorly defined signals between 3.5 and 4.3 which is the same environment for glycerol/glycol type protons as well a broad singlet resonance at 1.9 ppm which must correspond to an alcohol (neither glycerol (4.4 ppm)) nor ethylene glycol (3.2 ppm)). The ^{13}C NMR spectrum showed no signals corresponding to EC or any carbonate. The boiling point of glycerol carbonate is 140 °C and above this temperature the carbonate unit can thermally decompose; this appears to have occurred in this case. The reaction was therefore repeated using toluene at 115 °C, well below the boiling point of GLC. Regrettably, no reaction occurred with the ^{1}H and ^{13}C NMR spectra both showing only the presence of the starting material. An explanation for this failure can be found in the initial Madsen work which states that electron rich alcohols react more readily with the iridium catalyst than electron poor alcohols.[2] The carbonate group of GLC has a

significant electron withdrawing effect pulling electron density away from the alcohol. Therefore, this could create too high a kinetic barrier for the reaction at this temperature.

With this dual step approach yielding no results, the use of two distinct stages was evaluated – converting the alcohol to an aldehyde or carboxylic acid then performing a decarbonylation or decarboxylation respectively to give EC.

4.3.2 – Glycerol Carbonate to Aldehyde

With the carbonate being sensitive to high temperatures, a mild oxidation route was sought. An attractive option was the (bipy)Cu^{I}/TEMPO system, with *N*-Methylimidazole base, reported by Stahl *et al.*[3] This catalyst has been shown to oxidise a range of primary alcohols at room temperature in air with excellent functional group tolerance. The reaction was conducted as per the reported procedure (Scheme 4.5). The GLC and other reagents were added to an acetonitrile solution and stirred overnight open to air. Following the prescribed work-up an orange oil was obtained. The resulting ^{1}H NMR spectrum showed no peaks in the aldehyde region of around 9.5 to 10.5 ppm. There was clearly some GLC starting material persistent in the sample as well as some new unidentifiable peaks including two broad multiplets at around 1.0 and 1.3 ppm. From the aromatic region it also appeared that some of the bipyridine complex or free ligand was present in this product mixture. GC-MS analysis also confirmed a lack of the desired aldehyde product. The Stahl work indicated that some alcohols featuring potential chelating groups were more resistant to oxidation.[3] A dioxolane compound similar to GLC remained mostly unconverted which was attributed to a chelation of this substrate to the copper catalyst rendering it inactive. It may be the case that a similar interaction occurs between the oxygen atoms of the carbonate fragment and the Cu centre giving the low conversion.

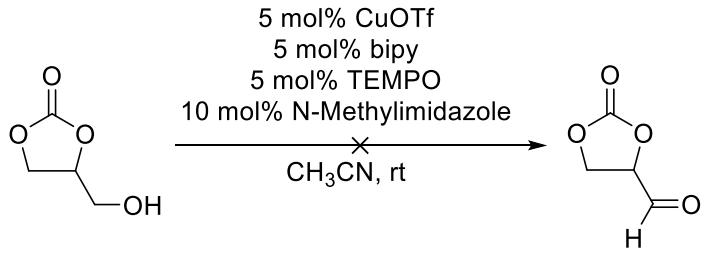

Scheme 4.5. Attempted oxidation of GLC using (bipy)Cu^{I}/TEMPO

With the Stahl preparation unsuccessful, a Swern oxidation of the GLC was also tested (Scheme 4.6). It involves the reaction of oxalyl chloride with DMSO to prepare a chloro(dimethyl)sulphonium chloride which then performs the oxidation of the alcohol to the aldehyde in the presence of triethylamine base.[4] This also yielded no aldehyde in the post reaction mixture. This is perhaps unsurprising as the Swern oxidation is traditionally used for secondary alcohols whereas GLC is a primary alcohol.

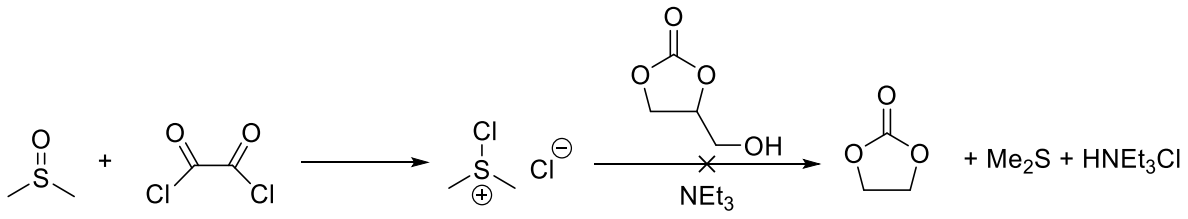

Scheme 4.6. Attempted Swern oxidation of GLC

A final attempt at preparing the aldehyde utilised the [$RuCl_2(dppm)_2$] complex used extensively in the Wass group for the preparation of the advanced biofuels *n*-butanol and *iso*butanol (Chapter 5, Section 5.1). In this process the alcohol is dehydrogenated by the ruthenium catalyst and a base before undergoing an aldol condensation and re-hydrogenation to the new alcohol. Due to the steric strain of the product it is unlikely that two glycerol carbonate molecules would undergo any sort of coupling and, if performed in an open system where the hydrogen produced can escape, the reaction may stop at the aldehyde. The reaction was performed in EtOH for catalyst solubility with sodium hydroxide as a base (Scheme 4.7). An orange oil was isolated and the resulting ^{1}H NMR showed a range of broad peaks and overlapping multiplets between 3.4 and 5.0 ppm (Figure 4.1), suggestive of some form of

oligomerisation. A likely explanation is that the catalyst has decarbonylated the GLC re-forming glycerol. This has then undergone aldol condensation and coupling with other glycerol molecules to form an oligomeric compound.

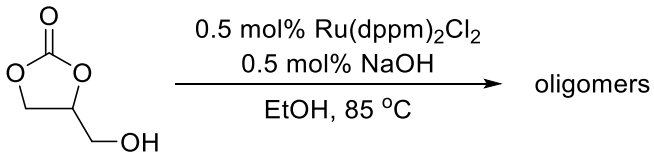

Scheme 4.7. Attempted oxidation of GLC using [$RuCl_2(dppm)_2$]

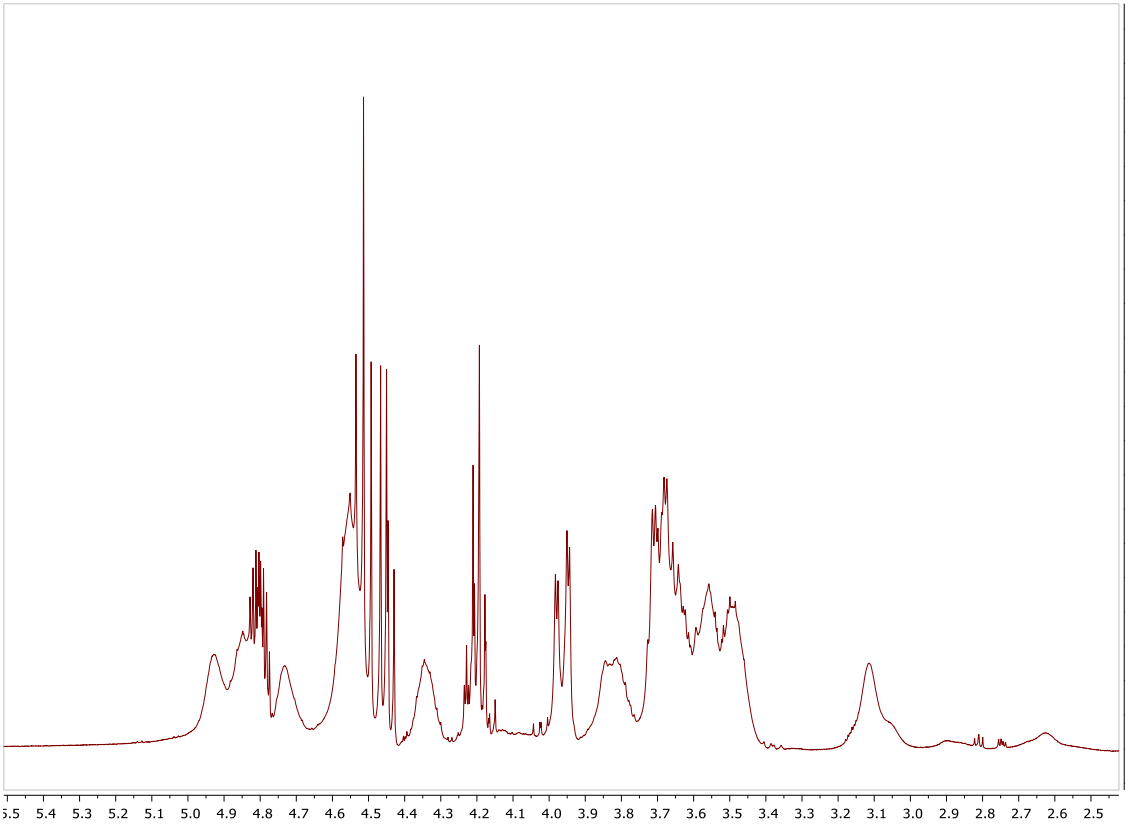

Figure 4.1. ^1H NMR (300 MHz, $CDCl_3$) of GLC with [$RuCl_2(dppm)_2$] test

A ruthenium free test was performed to see if the oligomerisation was caused by the strong sodium hydroxide base. Some similar peaks were present in the resulting ^1H NMR spectrum, but not to the same degree as with the ruthenium complex present.

4.3.3 – Glycerol Carbonate to Carboxylic Acid

With no success converting the alcohol of GLC to an aldehyde, transformation to the corresponding carboxylic acid was attempted instead. Since CO_2 is thermodynamically a better leaving group than CO this has the potential to be superior to the aldehyde route.

The procedure, reported in the patent literature (Scheme 4.8), uses trichloroisocyanuric acid (TCCA) and $NaHCO_3$ with catalytic amounts of TEMPO and NaBr.[5] After the prescribed work-up, a white solid was isolated. This was insoluble in all available deuterated NMR solvents so was analysed by ATR-IR. The GLC starting material had a clear OH alcohol stretching frequency at 3432 cm^{-1} which had been replaced by a peak at 2862 cm^{-1}, in the expected region for a carboxylic acid OH and consistent with the literature. The carbonyl C=O stretch at 1770 cm^{-1} for GLC had also shifted to 1705 cm^{-1} with a new peak at 1788 cm^{-1} for the C=O of the carboxylic acid. These ATR-IR results suggest that the reaction had yielded the desired carboxylic acid compound.

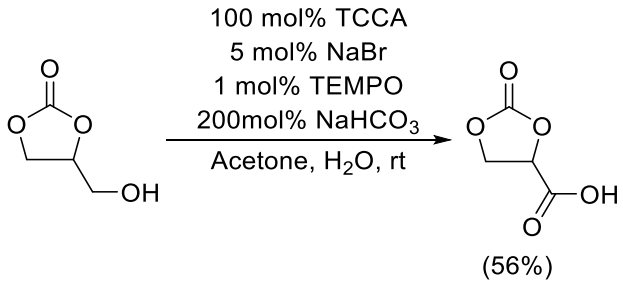

Scheme 4.8. Attempted oxidation of GLC using TCCA/TEMPO

The mechanism for the oxidation is shown below (Scheme 4.9). TEMPO reacts with a catalytic amount of the TCCA to form an *N*-oxoammonium ion which oxidises the alcohol to an aldehyde also giving a hydroxyamine. This hydroxyamine can react with TCCA again to regenerate the *N*-oxoammonium ion. The TCCA is hydrolysed by the water present to give hypochlorous acid which reacts with HCl produced earlier to give chlorine *in situ*. The chlorine can react with the aldehyde yielding an acyl chloride which is hydrolysed by another water molecule to give the carboxylic acid as the final product.[6]

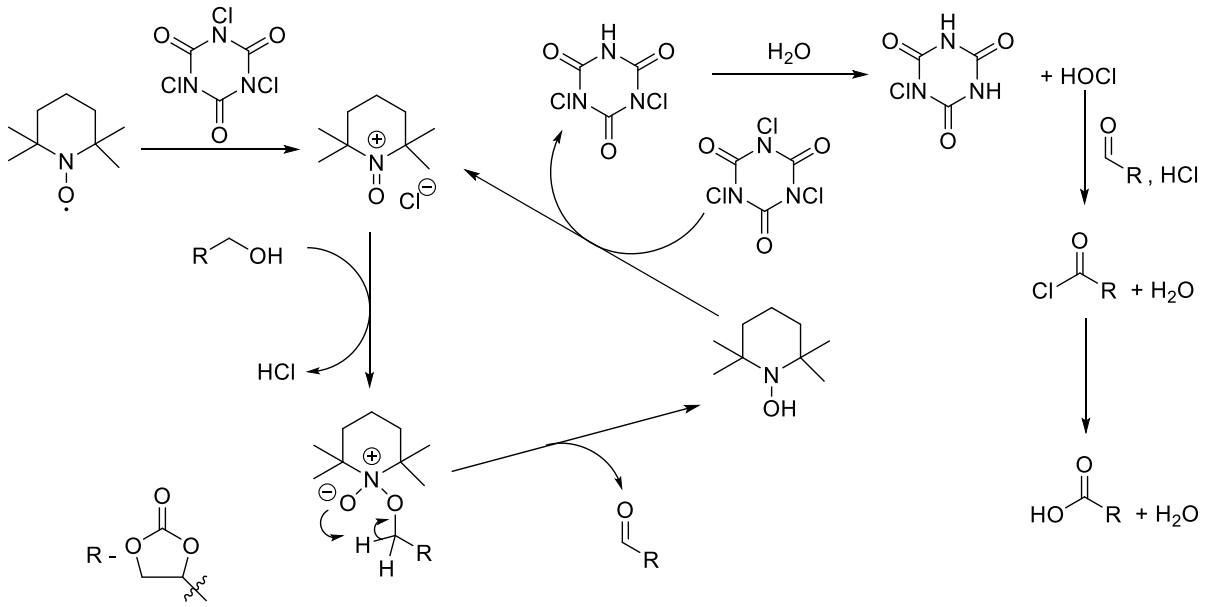

Scheme 4.9. Mechanism of oxidation of GLC using TCCA/TEMPO

4.3.4 – Decarboxylation of Carboxylic Acid

The decarboxylation of the carboxylic acid to EC was then attempted by dissolving the acid in boiling EtOH, the compound only appeared soluble in boiling alcohols or water, then adding a slight excess of strong base. The two bases tested were sodium hydroxide and potassium *tert*-butoxide. Both reactions were left at reflux overnight before analysis. Unfortunately, in both cases there was no conversion of the carboxylic acid to EC. On cooling the reaction mixture, the starting material precipitated out of solution with the mother liquor only containing base with no organic proton signals in the ^{1}H NMR spectrum, even after removal of the solvent. Many of the substrates that are successfully decarboxylated by this method feature an unsaturated group adjacent to the carboxylic acid to form a cyclic transition state. For a similar mechanism to take place with this substrate a double bond would have to be formed between the α-carbon to the acid and the neighbouring oxygen atom breaking the cyclic carbonate. Given the thermodynamic stability of this functional group it is unlikely that this would occur under the reaction conditions. A decarboxylation reagent that operates *via* a different mechanism is required. If a suitable decarboxylation reaction were to be found that would open a full synthetic pathway from glycerol to EC.

The first step of the conversion from glycerol to GLC (Scheme 4.1) was performed successfully following a literature procedure. The next step from GLC to EC was attempted *via* a direct route with a two-step process with an iridium catalyst. It was also attempted by first converting the GLC to the corresponding aldehyde, which was unsuccessful, and to the carboxylic acid which was successfully isolated. A decarboxylation of this carboxylic acid to EC was then investigated. Unfortunately, both this method and the direct approach were unsuccessful. Despite these difficulties, the final part of the glycerol to ethylene glycol route, the hydrogenation of the carbonate, was then studied in isolation.

4.4 – Hydrogenation of Ethylene Carbonate

The hydrogenation of EC and other cyclic carbonates has received notable attention in recent years. In addition to a synthetic route for diols, as here with EG, the process has been investigated for indirect CO_2 to methanol synthesis (Scheme 4.10). The cyclic carbonates are often prepared using CO_2 with an epoxide and are then hydrogenated to a diol and an equivalent of MeOH. This latter cyclic carbonate to alcohol step gives a net CO_2 to MeOH balance. With MeOH the subject of intense interest as both a fuel additive and chemical feedstock this process, which has a high atom efficiency and can produce a potentially useful diol by-product, is extremely attractive.

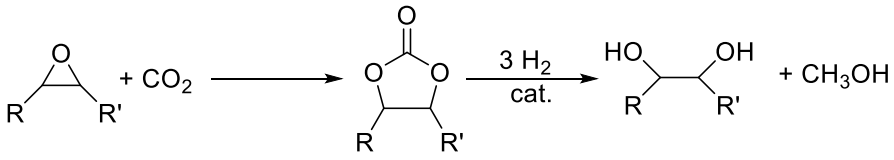

Scheme 4.10. General formation of cyclic carbonates from CO_2 and epoxides and hydrogenation to methanol and diols

Pioneering work for this reaction was carried out by Ding *et al.* using the (PNP)Ru^{II} (Figure 4.2) catalyst Ru-MACHO achieving full conversion to EG and MeOH at 50 bar H_2 and 140 °C.[7] The catalyst scope was then extended to a wider range of carbonate and formate substrates by Hong and Kim.[8] Within the last two years, this catalysis has been expanded to the first row transition metals with (PNP)Mn^{I} (Figure 4.2) complexes published by the groups of Leitner[9] and Rueping[10] and a $Co(BF_4)_2.6H_2O$/tripod system

from Beller[11] which give good conversions and yield but, as is often the case with non-precious metals (Introduction, Section 1.5), at much slower rates and with higher catalyst loading.

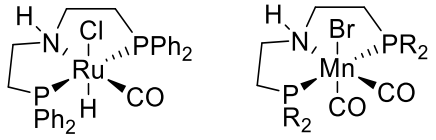

Figure 4.2. Ru and Mn based catalysts for EC hydrogenation

The Ru/tridentate phosphine complexes prepared in Chapter 3 were tested for this hydrogenation of EC. Initial benchmarking was done using the tripod complex **3.1** (Table 4.1).

*Table 4.1. Benchmarking for EC hydrogenation with **3.1***

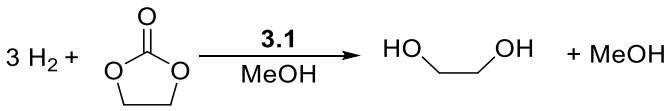

Run[a]	Temperature (°C)	H_2 Pressure (bar)	%Yield EG	%Conv EC
1	180	50	91	96
2	180	30	90	95
3	180	20	89	95
4	180	10	71	79
5	180	4	46	56
6	150	20	33	34
7	120	20	0	5
8	100	20	0	5
9[b]	180	20	89	95

[a]conditions: 5 mmol EC, 10 mL MeOH, 0.25 mol% **3.1**, 3 h, [b] 0.1 mol% **3.1**

These tests showed that an excellent EG yield of 89% could be obtained at 20 bar H_2 pressure with an increase to 50 bar making no appreciable difference (Runs 1,2 and 3). At 10 bar the conversion started to decrease and was reduced to 46% at 4 bar, although there was still substantial turnover (Runs 4

and 5). Altering temperature had a more severe effect with a marked drop of 56% EG yield from 180 to 150 °C and no conversion at 120 °C or lower (Runs 6, 7 and 8). As this reaction involves breaking a thermodynamically stable 5 membered ring it is perhaps unsurprising that the conversion shows a high temperature dependence. Lowering the catalyst loading from 0.25 to 0.1 mol% gave no reduction in yield, at optimum temperature and pressure, (Run 9) so the latter was then used as the loading for the rest of the catalytic tests (Table 4.2).

Table 4.2. EC hydrogenation with Ru/Tridentate phosphine complexes

Run[a]	Catalyst	%Yield EG	%Conv EC
1	**3.1**	89	95
2	**3.2**	96	96
3	**3.3**	88	95
4	**3.4**	98	98
5	**3.5**	84	88
6	**3.6**	97	99
7	**3.7**	96	96
8	**3.8**	93	94
9	**3.9**	92	94
10	**3.11**	92	93
11	**3.12**	88	95
12	**3.13**	94	95
13	**3.14**	85	85

[a]conditions: 5 mmol EC, 10 mL MeOH, 0.1 mol% catalyst, 20 bar H_2, 180 °C, 3 h

A wider range of ruthenium phosphorus complexes, introduced in Chapter 3, were evaluated for EC hydrogenation. The results (Table 4.2) clearly show that the ligand had no real effect on catalyst performance. The EG yields fall in the very narrow range of 85-98% suggesting that some other factors

are responsible for these results. To probe this further a range of control experiments using a variety of Ru precursors and a catalyst free test, using a clean PTFE insert, were conducted (Table 4.3).

Table 4.3. Control tests for EC hydrogenation

Run[a]	Catalyst	%Yield EG	%Conv EC
1	Average of complexes	92	94
2	$RuCl_2(DMSO)_4$	91	93
3	$RuCl_3$	99	9
4	Ru/C	98	99
5	Catalyst free	97	98
6[b]	Catalyst free	95	98

[a]conditions: 5 mmol EC, 10 mL MeOH, 0.1 mol% catalyst, 20 bar H_2, 180 °C, 3 h [b]20 bar Ar

The experiments above were designed to evaluate what facets of the ruthenium complexes are needed for catalytic competence. The $[RuCl_2(DMSO)_4]$ to test if any Ru(II) complex would be successful (Run 2), the $[RuCl_3]$ to see if the +2 oxidation state was necessary (Run 3) and Ru/C to determine whether a cheap and widely available heterogeneous catalyst could also perform the reaction (Run 4). These all gave a positive result, but more importantly so did the metal free run in a clean sleeve (Run 5). To investigate how this could be the case, the product mixtures were re-analysed, and it was noticed that an equivalent of dimethyl carbonate (DMC) was being produced for every equivalent of EG. This revealed that the reaction was in fact a transesterification of the EC, not a hydrogenation.

The transesterification of EC with MeOH to give EG and DMC is a well-known reaction but, a catalyst free variant has not been published. As with many transesterifications, basic reagents such as K_2CO_3[12] or KOH[13] are required. Ionic liquids[14] and heterogenous metal catalysts including MgO,[15] ceria[16] and Zn/YO[17] have also been successfully utilised. As discussed above, the transesterification necessitates a breaking of a 5 membered ring, albeit one that is heavily polarised. The strong relationship between EG yield and temperature suggests that simply by performing this reaction at 150 °C or greater there

is enough thermal energy supplied to force the reaction to occur. The pressure is needed to keep the MeOH in the liquid phase so it can react with the EC, which has a boiling point of 240°C well above the reaction temperature.

$$\ln(\frac{P_1}{P_2}) = -L/R \times (\frac{1}{T_1} - \frac{1}{T_2})$$

Equation 4.1. Clausius-Clapeyron relation

Using the Clausius-Clapeyron relation (Equation 4.1) where L is the specific latent heat of MeOH and R is the ideal gas constant it can be calculated that the boiling point of MeOH is greater than 180 °C, the reaction temperature, at approximately 25 bar. When the autoclave pressurised with 20 bar H_2 is fully heated to 180 °C, the actual reaction pressure is around 30 bar so the liquid phase is still thermodynamically favourable for the methanol. This explains why there is no improvement in EG yield on increasing the pressure from 20 bar, once the methanol is entirely liquid additional H_2 makes no impact. At lower pressures, although the gas phase will be thermodynamically favoured, the methanol will not vaporise instantly and there will be an equilibrium between the two phases meaning that there will always be a portion of the methanol still liquid to give some turnover. A test pressurising the reaction autoclave with 20 bar argon instead of hydrogen had no effect on EG yield (Run 6). This strongly suggests that it is purely the pressure within the reaction vessel driving the reaction.

To prevent transesterification, the EC hydrogenation was repeated using THF as the solvent. Unfortunately, this only yielded 5% EG with 10% EC conversion at 30 bar H_2 with 0.25 mol% **3.1**. To counter this an alternative, indirect synthesis was put forward (Scheme 4.11). This consisted of the transesterification with methanol to give EG and DMC followed by a hydrogenation of the DMC to 3 equivalents of MeOH. This would give an indirect EC to EG and MeOH synthesis, with 2 equivalents of MeOH used, but re-produced in the final step. The success of this synthesis hinged on the hydrogenation of DMC. First published by the Milstein group with a (PNN)Ru^{II} complex the hydrogenation of DMC and other organic carbonates has been widely studied.[18,19,20] This DMC

hydrogenation was tested with **3.1** under the same conditions as the EC hydrogenation in THF. This only yielded 7% MeOH, taking into account the 1:3 molar ratio, which improved to 9% after a 20 hour run.

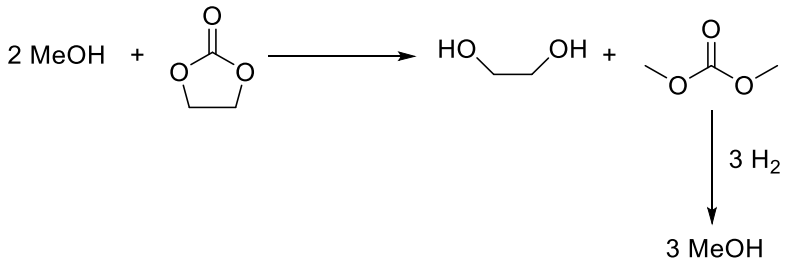

Scheme 4.11. Proposed indirect route to EG and MeOH via DMC

It is disappointing that these ruthenium complexes which were successful for ester hydrogenation do not show catalytic activity for carbonate hydrogenation. Perhaps an explanation can be found in the ligands themselves. The initial Milstein carbonate hydrogenation catalyst features a PNN ligand with a central pyridinyl group. The mechanism for carbonate hydrogenation with this complex was found to involve a strong degree of metal ligand cooperation through an aromatisation-dearomatisation of the pyridine ring. The dearomatised complexes react with dihydrogen and then perform a hydride transfer to the bound unsaturated organic substrate.[18] The other systems reported for EC hydrogenation use MACHO ligands or similar which also play a role in catalysis, usually involving a deprotonation of the central amine to give an imido species. Metal-ligand cooperation with tripod ligands however has not been observed. Their tridentate nature means that they form robust complexes which do not degrade under high temperatures and pressure. Apart from keeping the metal chelated, soluble and in the desired oxidation state they appear to have no other function. Perhaps it is the fact that these ligands do not form an unsaturated moiety to act as a hydrogen acceptor site is the reason why they show no catalytic activity for these carbonate hydrogenations.

4.5 – Summary

A multi-step synthetic route from glycerol to EG was envisaged. The first reaction, a carbonylation of glycerol to GLC proceeded smoothly. The preparation of EC from GLC proved challenging and efforts to perform this transformation directly and indirectly *via* both an aldehyde and carboxylic acid were unsuccessful. The carboxylic acid itself was synthesised but could not be converted to the desired cyclic carbonate target. The hydrogenation of EC to EG was also attempted and while initial results seemed promising, it transpired that the EG was in fact being produced through a transesterification. Despite not being the desired reaction, this is believed to be the first example of this transesterification being performed without a catalyst or other additive. Further tests for the direct hydrogenation of EC were unsuccessful with only low yields obtained.

4.6 – Future Work

There are two main avenues for future work. The first is the transformation of GLC to EC, while the attempts made here were unsuccessful, testing a wider range of organic reactions may yield some success. With the carboxylic acid derivative of GLC prepared one such route could be a Barton decarboxylation (Scheme 4.12).

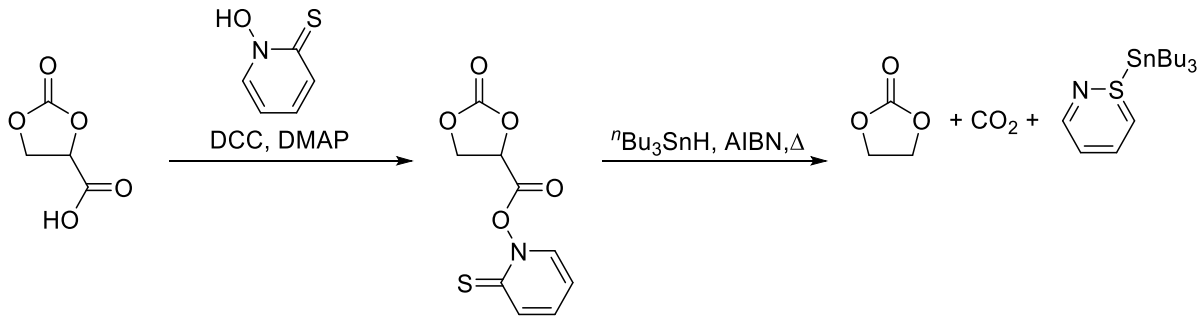

Scheme 4.12. Potential Barton decarboxylation of GLC

A thiohydroximate ester is formed from the carboxylic acid. This is then reacted with a radical initiator AIBN and a hydrogen donor $^{n}Bu_3SnH$ which produces the decarboxylated product, CO_2 and a thiopyridine by-product. A potential problem with this reaction is that the radical step, especially at

temperature, may perform an undesired side reaction with the cyclic carbonate breaking it apart. Once initiated, radical reactions are often difficult to control and, as discussed above, the cyclic carbonate is a relatively fragile functional group.

Another source of future work is in the hydrogenation of EC to EG. While unsuccessful with the ruthenium-tripod systems featured here carbonate, including cyclic carbonate, hydrogenation is a very active area of research. This is largely due to its potential as a method for CO_2 capture and utilisation. Most of the current systems are based around PNN or PNP ligand systems as highlighted above. First row transition metals, Mn and Co, have been the subject of much study in recent years and although they have shown come promise, a number of caveats still exist; long reaction times, high H_2 pressures, high loadings and the use of substantial quantities of bases such as metal alkoxides or hydrides. There is plenty of room for improvement in these systems focussing on ligand and catalyst design to develop systems that rival those of the ruthenium-based forerunners.

4.7 – References

1. S. H. Pyo and R. Hatti-Kaul, *Adv. Synth. Catal.*, 2016, **358**, 834–839.
2. E. P. K. Olsen, T. Singh, P. Harris, P. G. Andersson, and R. Madsen, *J. Am. Chem. Soc.*, 2015, **137**, 834–842.
3. J. M. Hoover and S. S. Stahl, *J. Am. Chem. Soc.*, 2011, **133**, 16901–16910.
4. A. J. Mancuso and D. Swern, *Synthesis*, 2003, **1981**, 165–185.
5. H. Woelfle, B. Walther, M. Kohler, and S. Putzien, 2013, WO2013092011A1.
6. L. De Luca, G. Giacomelli, S. Masala, and A. Porcheddu, *J. Org. Chem.*, 2003, **68**, 4999–5001.
7. Z. Han, L. Rong, J. Wu, L. Zhang, Z. Wang, and K. Ding, *Angew. Chem. Int. Ed.*, 2012, **51**, 13041–13045.
8. S. H. Kim and S. H. Hong, *ACS Catal.*, 2014, **4**, 3630–3636.

9. A. Kaithal, M. Hölscher, and W. Leitner, *Angew. Chem. Int. Ed.*, 2018, **57**, 13449–13453.

10. V. Zubar, Y. Lebedev, L. M. Azofra, L. Cavallo, O. El-Sepelgy, and M. Rueping, *Angew. Chem. Int. Ed.*, 2018, **57**, 13439–13443.

11. F. Ferretti, F. K. Scharnagl, A. Dall'Anese, R. Jackstell, S. Dastgir, and M. Beller, *Catal. Sci. Technol.*, 2019, **9**, 3548–3553.

12. J. Q. Wang, J. Sun, C. Y. Shi, W. G. Cheng, X. P. Zhang, and S. J. Zhang, *Green Chem.*, 2011, **13**, 3213–3217.

13. M. Tojo and H. Miyaji, 2005, WO2005123638.

14. V. B. Saptal and B. M. Bhanage, *ChemCatChem*, 2016, **8**, 244–250.

15. B. M. Bhanage, S. I. Fujita, Y. Ikushima, K. Torii, and M. Arai, *Green Chem.*, 2003, **5**, 71–75.

16. J. Xu, K. Z. Long, F. Wu, B. Xue, Y. X. Li, and Y. Cao, *Appl. Catal. A Gen.*, 2014, **484**, 1–7.

17. L. Wang, Y. Wang, S. Liu, L. Lu, X. Ma, and Y. Deng, *Catal. Commun.*, 2011, **16**, 45–49.

18. E. Balaraman, C. Gunanathan, J. Zhang, L. J. W. Shimon, and D. Milstein, *Nat. Chem.*, 2011, **3**, 609–614.

19. J. Chen, H. Zhu, J. Chen, Z. G. Le, and T. Tu, *Chem. Asian J.*, 2017, **12**, 2809–2812.

20. A. Kumar, T. Janes, N. A. Espinosa-Jalapa, and D. Milstein, *Angew. Chem. Int. Ed.*, 2018, **57**, 12076–12080.

Chapter 5 - Catalysis with Ruthenium Tridentate Phosphine Complexes

5.1 – Introduction

The range of ruthenium complexes with tridentate phosphorus ligands synthesised in Chapter 3 were tested for other reactions of interest. These reactions could be used for the preparation of industrially relevant products, some based on existing areas of research in the Wass group while others have been previously performed with similar ruthenium complexes.

5.2 – Methanol and Ethanol to *Iso*Butanol Catalysis

5.2.1 – Introduction

As discussed in Section 1.3, there is a growing need to move away from fossil fuel derived chemicals. Liquid fuels for transport are substantial consumers of petrochemicals worldwide and many efforts have been made to replace these with renewable alternatives. (Bio)ethanol has emerged as a popular replacement but, it does have some drawbacks including a lower energy density, 70% of that of gasoline, it is corrosive to engine parts and fuel systems and it absorbs water creating issues around dilution. These problems mean that (bio)ethanol is only widely used in blends with existing fuels rather than as a drop-in alternative to gasoline.

Butanol has much more advantageous properties; it has a higher energy density, 90% of gasoline, is non-corrosive and immiscible with water. This has led to it being dubbed an "advanced biofuel" and it is viewed as a potential direct replacement for petrochemical liquid fuels.[1,2] An attractive synthetic route to butanol is the catalytic upgrading of bio(ethanol), which would make use of the existing bio(ethanol) infrastructure. Initial homogeneous catalytic routes focussed on the synthesis of *n*-butanol from ethanol homocoupling *via* the Guerbet reaction.[3] In recent years, this reaction has been modified to produce the branched isomer, *iso*butanol which has superior fuel properties (Scheme 5.1).[4] Previous work in the Wass group has identified a number of active catalysts for this transformation, including the $[RuCl_2(dppm)_2]$ complex which gives exceptionally high selectivity (>99%) at high yield (75%)(See Section 5.1.1).[5]

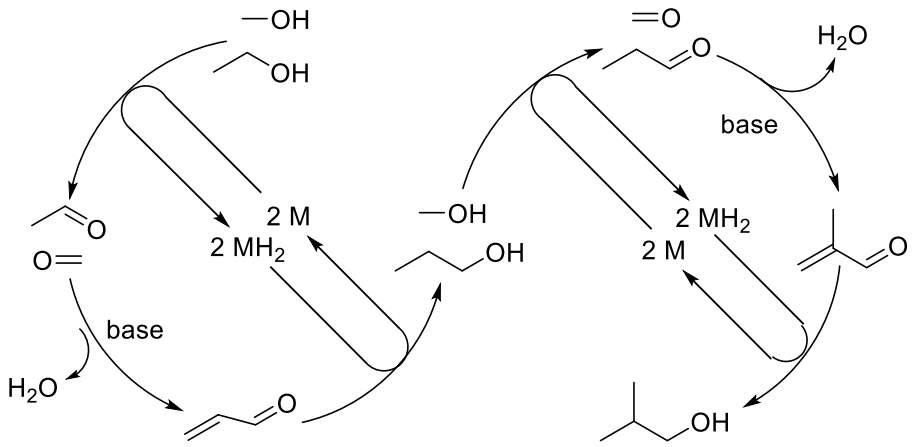

Scheme 5.1. Guerbet mechanism for EtOH/MeOH heterocoupling to ^{i}BuOH

Ethanol and methanol are dehydrogenated to acetaldehyde and formaldehyde respectively. These then undergo a base catalysed aldol condensation and a hydrogenation step to *n*-propanol. The reaction is an example of borrowed hydrogen chemistry as the hydrogen released from the dehydrogenation of the substrates is stored by the metal catalyst as a dihydride complex which then performs the hydrogenation. The second part of the mechanism is a repeat of the first; the newly formed *n*-propanol and more methanol are dehydrogenated before the aldol coupling and the product is hydrogenated to give *iso*butanol.

5.2.2 – Initial Tests

Some of the work in this section, the initial benchmarking and reaction conditions screen was performed by MSci student Matthew Shaw.

The ruthenium complexes prepared in Chapter 3 were tested for methanol and ethanol coupling to *iso*butanol (^{i}BuOH). Previous work in the Wass group had found these complexes to show poor activity for ethanol homocoupling to *n*-butanol. Under the harsher conditions used for heterocoupling (180 °C and 200 mol% NaOMe base vs 150 °C and 5 mol% NaOEt) the stability of the Ru/tridentate phosphine species may be beneficial. Both the Tripod (**3.1**), N-Tripod (**3.3**) and Triphos (**3.9**) complexes were tested at conditions previously optimised for the current best performing catalyst, a *bis*-chelate ruthenium dichloride complex with the small bite angle bidentate phosphine ligand dppm (Table 5.1).[6]

*Table 5.1. Conditions test of **3.1**, **3.3** and **3.9** for ^{i}BuOH catalysis*

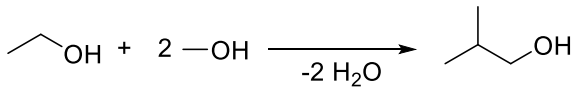

Run[a]	Catalyst	% Yield ^{i}BuOH	% Select.^{i}BuOH
1	**3.1**	5	80
2	**3.3**	13	87
3	**3.9**	5	92
4	$RuCl_2(dppm)_2$	62	97
5	none	0.2	9

[a]conditions: 0.1 mol% Ru catalyst, 200 mol% NaOMe, 10 mL MeOH, 1 mL EtOH, 180 °C, 2 h (mol % relative to EtOH)

While still catalytically active, the tridentate complexes show poor performance for ^{i}BuOH synthesis compared to the best catalyst (Run 4). Although **3.3** (Run 2) with the N-centred ligand performs significantly better than **3.1** and **3.9** (Runs 1 and 3) giving a 13% yield over 2 hours. Ongoing work in the Wass group has suggested that dppm gives "ligand assisted" reaction pathways, in which the acidic backbone C-H of this ligand is either fully deprotonated or assists in catalytic performance by hydrogen bonding to substrates or catalytic intermediates. Consistent with this hypothesis, if the carbon is disubstituted removing both these protons then the activity of the resulting complex in catalysis is significantly inferior.[7] The improved performance of **3.3** could be due to the increased electron withdrawing nature of the apical N atom making the protons in the alkyl arms of the ligand more acidic compared to those in **3.1** and **3.9**.

It was decided that increasing the total reaction time could improve the overall ^{i}BuOH yield. The tridentate complexes were originally investigated because of their stability to the reaction conditions. Perhaps this stability is slowing the rate of reaction for these compounds so a longer time might allow for increased turnover? The initial tests with **3.1**, **3.3** and **3.9** showed that this was indeed the case

with the yields vastly improved over 20 hours. Therefore, a full screen with the tridentate phosphorus catalysts prepared in Chapter 3 was performed (Table 5.2).

Table 5.2 – EtOH/MeOH heterocoupling to ^{i}BuOH with Ru/phosphorus complexes

Run[a]	Catalyst	% Conv EtOH	% Yield ^{i}BuOH	% Select. ^{i}BuOH	% Yield ^{n}Propanol
1	**3.1**	97	51	99	<1
2	**3.2**	99	24	66	13
3	**3.3**	94	45	97	<1
4	**3.4**	95	11	96	<1
5	**3.5**	84	19	90	2
6	**3.6**	97	18	98	<1
7	**3.7**	97	22	99	<1
8	**3.8**	94	48	98	1
9	**3.9**	91	38	96	1
10	**3.10**	91	32	98	1
11	**3.12**	96	15	98	<1
12	**3.13**	89	22	93	2
13	**3.14**	98	2	92	<1
14	$RuCl_2(dppm)_2$[6]	75	75	>99	<1

[a]conditions: 0.1 mol% Ru catalyst, 200 mol% NaOMe, 10 mL MeOH, 1 mL EtOH, 180 °C, 20 h

There was a large variation in catalyst performance even between complexes with very similar structures. The highest activity was seen with **3.1**, **3.3** and **3.8** (Runs 1, 3 and 8), not dissimilar to the ester hydrogenation reactions in Chapter 3. As with the ester hydrogenation reactions it seems that increased steric bulk may hinder the catalytic activity. **3.5** and **3.6** with cyclohexyl and *ortho*-tolyl substituents respectively (Runs 5 and 6) gave significantly lower yields than their phenyl counterpart **3.3**. However, all three of the complexes with ethyl substituted ligands **3.2**, **3.4** and **3.10** (Runs 2, 4

and 10) also gave lower turnovers than their phenyl-based analogues. **3.2** showed the lowest selectivity to *iso*butanol and was the only catalyst to produce a significant quantity of *n*-propanol, the product of the first Guerbet reaction between EtOH and MeOH. The reaction mechanism is shown above (Scheme 5.1). The phosphinite complex, **3.14** (Run 14), only gave a trace of *iso*butanol. Catalyst decomposition is likely in this case since such ligands are known to be prone to cleavage of the P-O bond by hydrolysis, two equivalents of water being generated by each Guerbet cycle. As well as large amounts of organic solids, discussed below (Section 5.1.2), a black, metallic residue was also observed in the post-reaction mixture when **3.14** was used.

The reaction is conducted using 1 mL of EtOH in 10 mL of MeOH to prevent unwanted EtOH homocoupling to *n*-butanol and dehydrogenative coupling to ethyl acetate. As the reaction progresses the EtOH concentration drops and the water concentration increases so more side reactions involving this water, the NaOMe base and methanol occur. This limits the total yield of ^{i}BuOH; there is only a small increase in yield from 2 hr to 20hr with the best performing [Ru(dppm)$_2$Cl$_2$] catalyst (Compare Run 4, Table 5.1 and Run 14, Table 5.2). Some of the catalysts previously tested are not stable to the high concentrations of base required or the water produced and decompose to give low turnover or are active at the start of the reaction but decompose over time as the water content increases. This decomposition is normally accompanied by the formation of a black metallic solid indicating metal or Ru(0) nanoparticles have been formed. The tridentate complexes above gave no such metallic solids, apart from **3.14** as discussed. Analysis of the post reaction solutions of **3.1** and **3.3** showed the same peaks as the dimer starting complexes in the ^{31}P{^{1}H} NMR spectrum. This coupled with the fact that the ^{i}BuOH yields greatly improved from 2 to 20 hrs suggests that these complexes are robust to the reaction conditions.

The results above were generated by GC analysis from the components in the post-reaction liquid phase. Many of the reactions also produced large quantities of solid products. It is this discrepancy between solid and liquid products that gives the high ethanol conversion and *iso*butanol selectivities

(which are calculated in the liquid phase), but low *iso*butanol yields. The amount of solid produced seemed to vary drastically between catalysts even those with a similar structure. For example, **3.7** and **3.8**, the *para*-tolyl and *para*-anisole N-Tripod complexes which have near identical structures produced 1.20 g and 0.11 g of solid products respectively.

5.2.3 – Solid Analysis

The solid products from a catalytic test with **3.1** were analysed by ^{1}H and ^{13}C NMR spectroscopy in D_2O. The proton spectrum showed the presence of formate with a sharp singlet at 8.38 ppm (Figure 5.1). No acetate peaks (typically around 1.9 ppm in the ^{1}H NMR spectrum) were observed. This is unusual, as many of the literature examples of ^{i}BuOH formation *via* Guerbet chemistry including those performed in the Wass group cite acetate salts as a substantial solid by-product.[8] The ^{13}C NMR spectrum (Figure 5.2) confirmed the presence of formate with a peak at 171 ppm; a peak at 168 ppm indicated that carbonate had been formed.

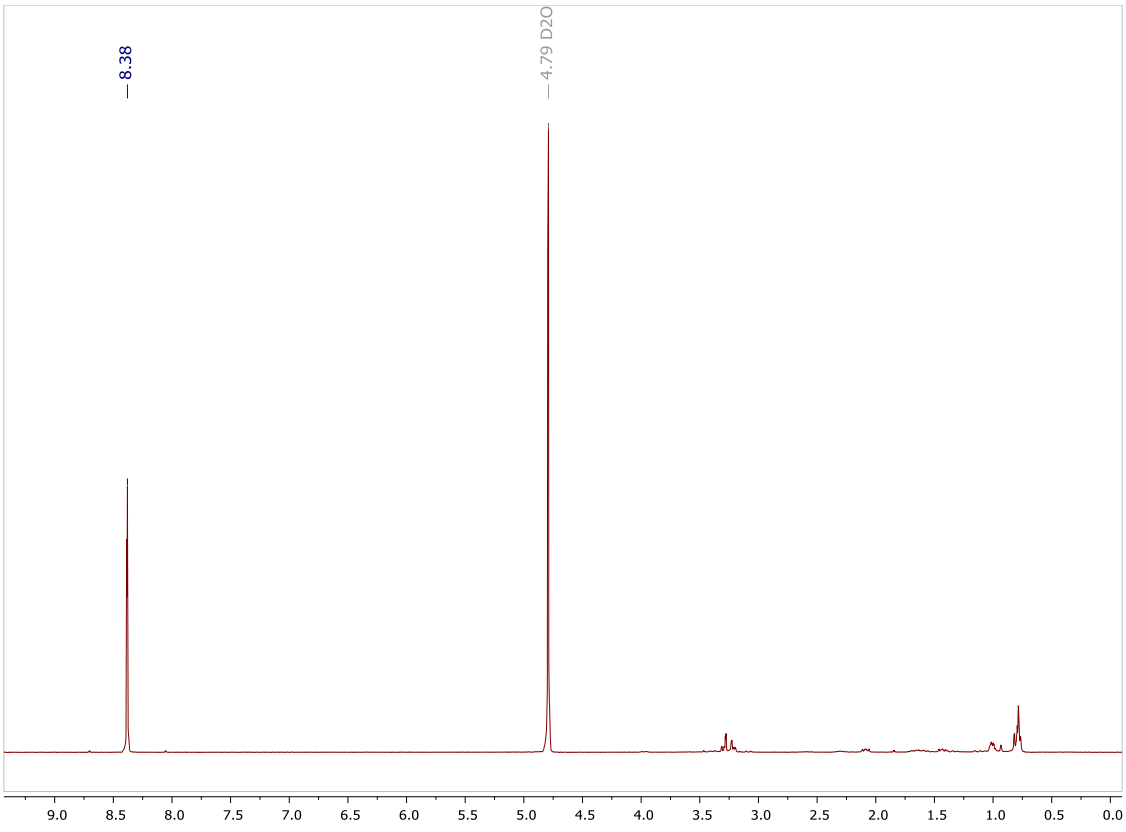

Figure 5.1. ^{1}H NMR (300 MHz, D_2O) spectrum of solid products

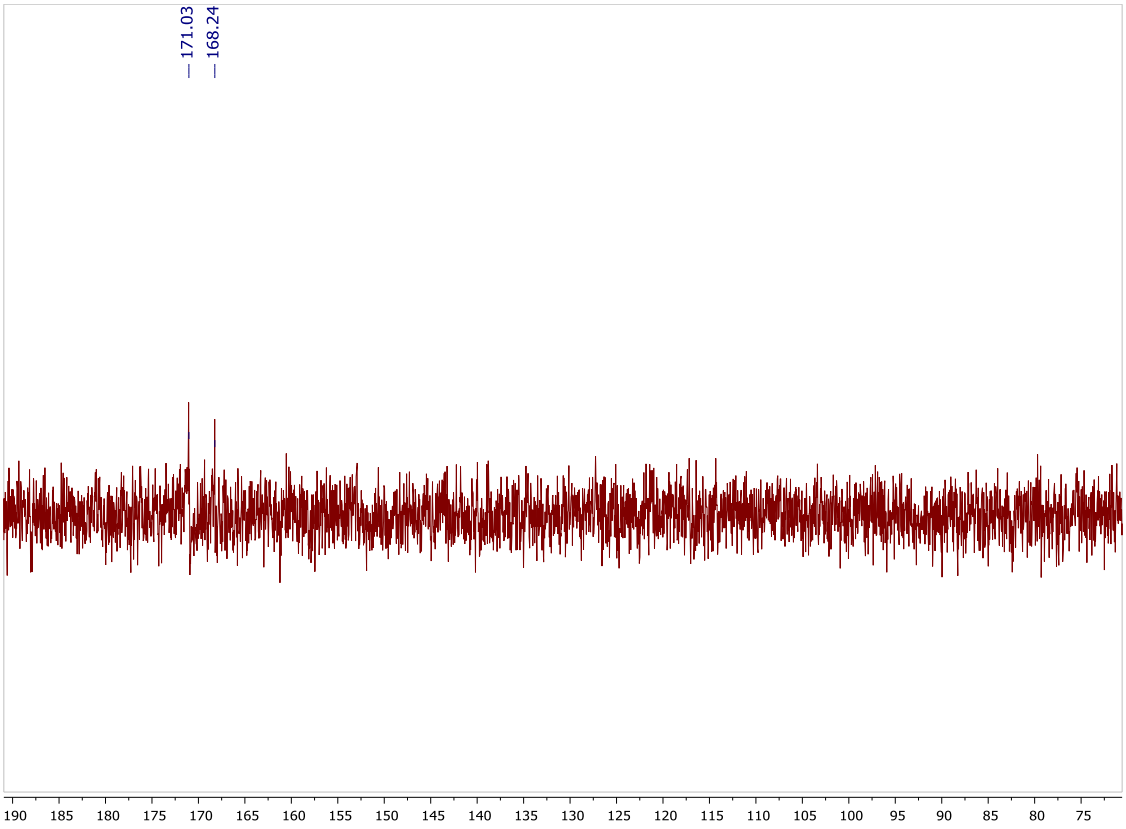

Figure 5.2. ^{13}C NMR (300 MHz, D_2O) spectrum of solid products

A quantitative ^{1}H NMR experiment using DMSO-d_6 as a standard with a 10 mg solid sample gave 0.039 mmol formate, which if assumed to be sodium formate has a mass of 2.6 mg. The remaining 7.4 mg can be attributed to sodium carbonate. The entire solid mass obtained from the reaction was 0.781 g, which gives sodium formate (3.04 mmol, 0.206 g) and sodium carbonate (5.41 mmol, 0.574 g) based on the NMR sample. Sodium carbonate forms several hydrated complexes which are likely to have formed in the ^{1}H NMR sample in the D_2O solvent. No other deuterated NMR solvents were able to dissolve the solid by-products. The above sodium carbonate yield may therefore be an overestimate of the total number of moles.

The sodium formate is likely produced by the Cannizzaro reaction (Scheme 5.2). As the Guerbet reaction proceeds the water produced reacts with the sodium methoxide base to form sodium hydroxide. This can react with formaldehyde, formed by the dehydrogenation of methanol, to give formic acid and methanol. In the basic environment of the reaction the formic acid instantly reacts

with the methoxide base to produce sodium formate and methanol. The dehydrogenation of methanol to formaldehyde has been reported with Ru-PNP pincer compounds in the presence of base.[9]

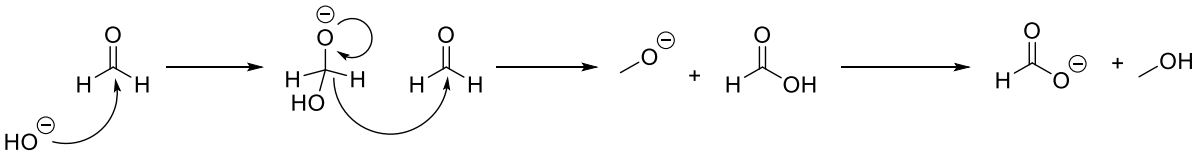

Scheme 5.2. Formation of formate by the Cannizzaro reaction

This formate produced can also be dehydrogenated by the catalyst to give carbon dioxide.[9] This can react with the hydroxide base formed *in situ* to produce carbonate (Scheme 5.3). The solid analysis showed that an excess of carbonate was given by the reaction suggesting that the dehydrogenation of formate is relatively facile under these reaction conditions.

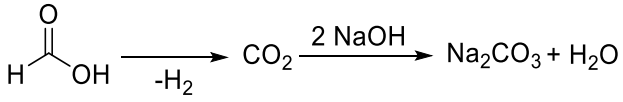

Scheme 5.3. Formation of sodium carbonate by formate dehydrogenation

5.2.4 – Mechanistic Insights

The role of the potential catalyst intermediate complexes during the reaction was investigated to give an insight into the mechanism. The Tripod and N-Tripod complexes **3.1** and **3.3** were reacted with NaOMe to see if any other Ru complexes were formed, other than the initial dimer complexes. When **3.1** was heated to reflux in MeOH with an excess of base over 20 hours most of the ruthenium complex remained in solution with the $^{31}P\{^{1}H\}$ NMR spectrum showing the usual dimer peak at 36 ppm. However, some yellow solid also precipitated out of the solution which was isolated and analysed. The resulting $^{31}P\{^{1}H\}$ NMR spectrum featured a doublet at 28 ppm and a triplet at -8 ppm (Figure 5.3). The ESI-MS analysis gave a molecular ion peak at 817 m/z which corresponds to a monometallic complex with Ru bonded to the three phosphine atoms from the ligand with two carbon monoxide ligands and

one chloride (Scheme 5.4). The CO ligands are highlighted by two other large peaks at 789 and 761 each showing a difference of 28 mass units. This species is a 6 coordinate, octahedral Ru(II) complex with a positive charge balanced with a chloride anion which dissociated during the ESI ionisation. The large difference in chemical shift values in the ^{31}P NMR signals, -8 and 28 ppm, must be caused by one of the phosphine atoms being trans to the electron rich, π-donor chloride ligand giving a significant upfield shift. The fact that the complex has two CO ligands means that it has performed a decarbonylation of the methanol solvent producing CO and 2 equivalents of H_2. These Ru carbonyls are believed to be off-cycle complexes which are inactive for Guerbet-type catalysis. One reason for using a large excess of base is for the methoxide to react with these ruthenium carbonyl complexes to regenerate an active catalyst. It is worth reiterating that the majority of the **3.1** precursor used remained unaltered in solution. This solid product only represents around 20 mol% of the catalyst studied.

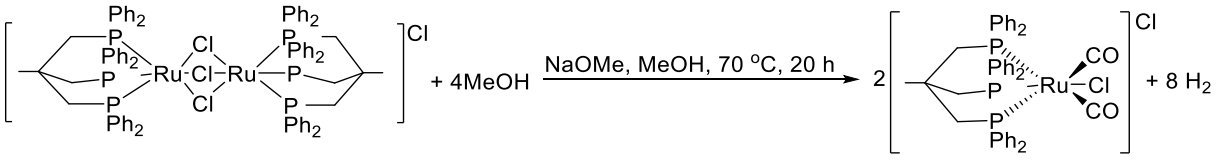

Scheme 5.4. Proposed structure and formation of bidentate ruthenium carbonyl complex with NaOMe

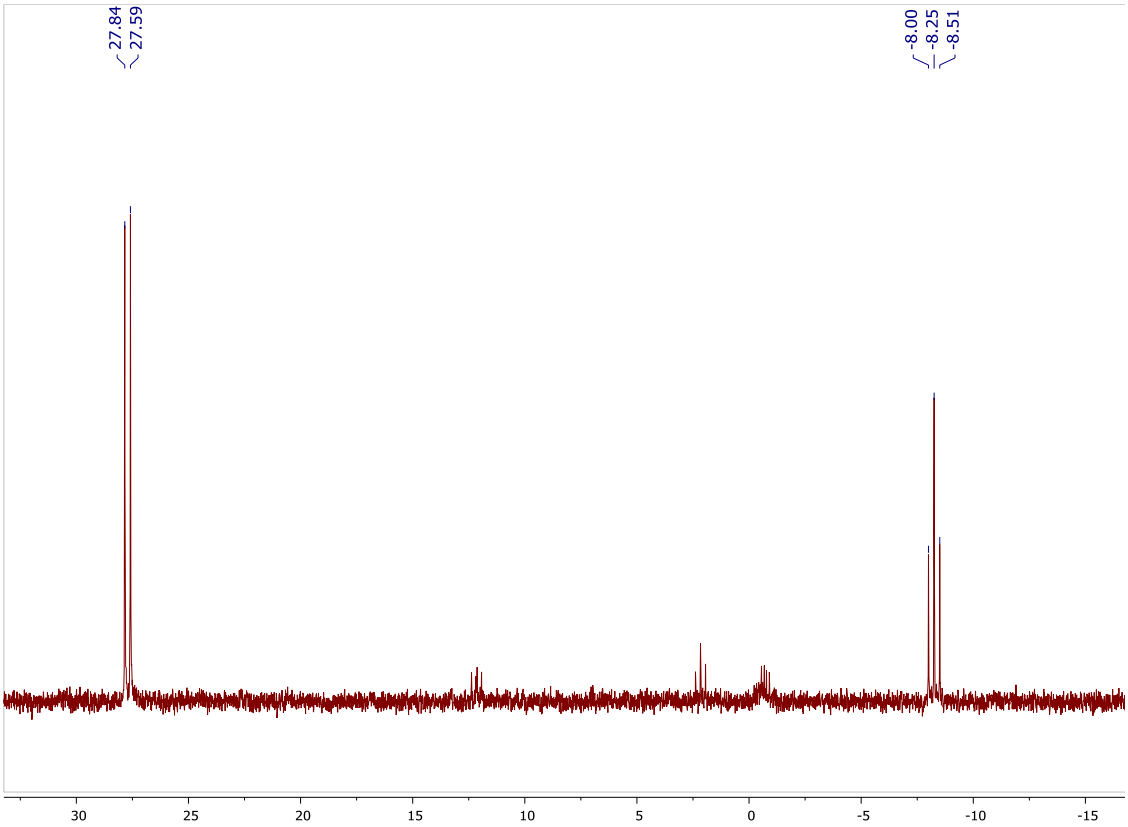

Figure 5.3. $^{31}P\{^{1}H\}$ NMR (162 MHz, $CDCl_3$) spectrum of solid product

The experiment above was performed in an open system which is quite different to the actual conditions the catalysts are subjected to for ^{i}BuOH synthesis. A sealed autoclave is used for two main reasons; firstly, to retain the hydrogen formed in the first step of the reaction to be used in the final hydrogenation step of the borrowed hydrogen cycle and secondly, to withstand any pressure generated by solvent vapour at high temperature. To see if the catalyst reacted differently under these more realistic conditions the previous experiment was repeated in a sealed autoclave at 180 °C. As with the open system, an orange solution had formed with a small quantity of yellow solid also produced. Analysis of the solution showed a peak at 36 ppm in the $^{31}P\{^{1}H\}$ NMR caused by **3.1**. However, the solid formed was completely different to that prepared in the open vessel test. The $^{31}P\{^{1}H\}$ NMR showed two peaks a triplet at 34.2 ppm and a doublet at 26.6 ppm illustrating two different phosphorus environments, but both still bound to Ru (Figure 5.4). Both signals showed the same $^{2}J_{PP}$ coupling constant of 31.6 Hz. Unbound phosphine resonances are observed at around -10 ppm.

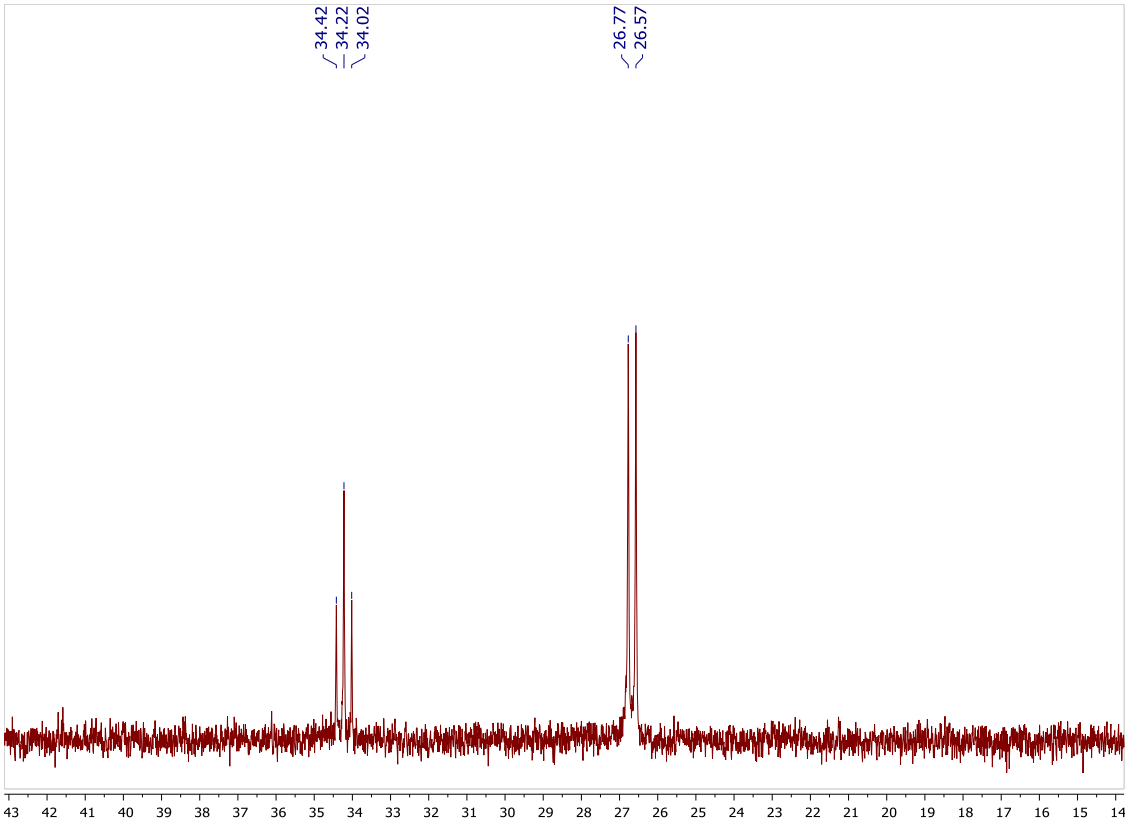

Figure 5.4. $^{31}P\{^{1}H\}$ NMR (162 MHz, $CDCl_3$) of closed system solid product

The ^{1}H NMR shows a signal at -7.4 ppm revealing that a hydride complex has been made (Figure 5.6). The signal appears to be a doublet of doublets suggesting that the hydridic hydrogen atom is coupling to two of the phosphorus atoms from the ligand, perhaps those trans to the hydride. It is unclear why coupling to the third, cis phosphorus atom is not occurring or is not visible in the $^{31}P\{^{1}H\}$ NMR spectrum. It might also be possible that a dihydride complex has been formed and that the signal in the NMR spectrum consists of two doublets. Performing a $^{1}H\{^{31}P\}$ NMR experiment would remove any H-P coupling and indicate how many hydrides are present. The ESI-MS shows a molecular ion peak at 881 with a much larger peak at 853, which has a difference of 28 indicating the loss of CO. A large peak at 755 m/z units corresponds to the tripod ligand bound to Ru with one carbonyl and one hydride ligand. The chloride complex is perhaps the most likely structure as it preserves the Ru(II) oxidation state and is coordinatively saturated (Figure 5.5). These tests prove that having a sealed system which contains the hydrogen atmosphere produced leads to a completely different Ru complex being formed. A hydride complex could play a more significant role in Guerbet catalysis as an aldehyde

formed by the alcohol dehydrogenation step could insert into the Ru-H bond. As with the open system only a fraction of the Ru complex **3.1** used for this test, again approximately 20 mol%, went on to form this hydride species, most stayed as a dimer in the methanol solution.

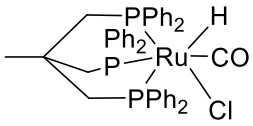

*Figure 5.5. Proposed structure from **3.1** closed autoclave experiment*

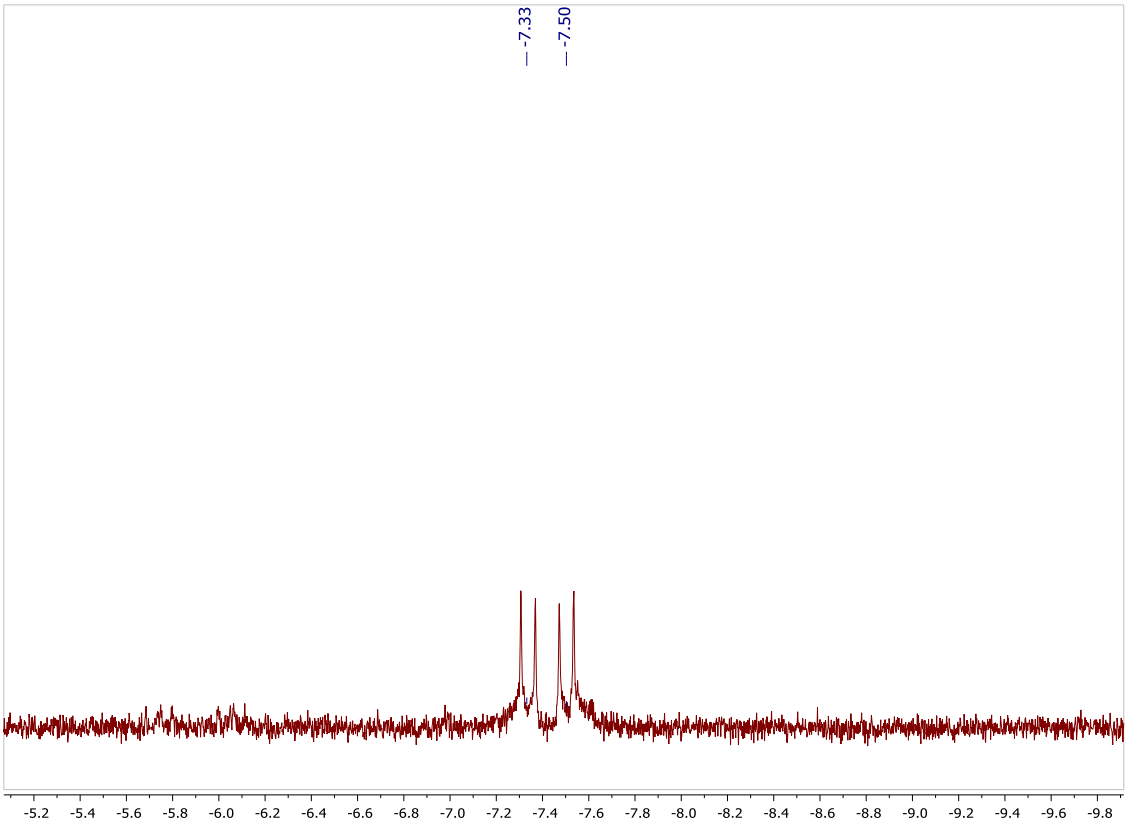

Figure 5.6. ^{1}H NMR (300 MHz, $CDCl_3$) hydride region of solid product

The same experiments were repeated with the N-Tripod dimer **3.3**. The sealed autoclave experiment yielded no solid product with the $^{31}P\{^{1}H\}$ NMR suggesting that only the initial dimer complex was present. The open vessel reaction yielded a small amount (<10 mg) of yellow solid. Unfortunately, the NMR signals from this sample were too weak for analysis, but ESI-MS data was obtained. The molecular ion peak is seen at 1024 m/z units which suggests an unusual structure (Figure 5.7) which features bridging carbonyl ligands in between two Ru centres only one of which is capped with the

phosphine ligand. It is possible that this complex was formed in the ESI experiment itself rather than during the NaOMe test. Two large peaks at 996 and 968 are observed with the differences of 28 caused by the loss of the terminal CO ligands. A peak at 783 is present which matches with a monometallic dichloride complex with the N-Tripod ligand. Furthermore, a large peak at 742 m/z units could be due to the presence of a N-Tripod-Ru-CO fragment.

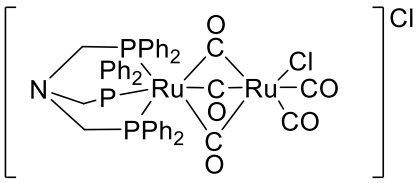

*Fig 5.7. Proposed structure from **3.3** open vessel experiment*

5.3 – Dehydrogenative Coupling of Ethanol to Ethyl Acetate

Ethyl acetate is an important commodity chemical widely used as a solvent, food additive and in cosmetics and fragrances.[10] The current procedures for synthesising ethyl acetate are centred on fossil fuel substrates. The three widely performed routes are 1) the Fisher esterification of acetic acid, 2) the coupling of acetaldehyde *via* the Tishchenko reaction and 3) the reaction of acetic acid with ethylene.[11] As mentioned previously, biomass can give a renewable source of bioethanol which offers a greener route to ethyl acetate. Work published by Beller,[10] Gusev[12] and Leitner[13] uses a range of tridentate PNP and PNN ligands on Ru for the acceptorless dehydrogenative coupling of two ethanol molecules to ethyl acetate, liberating two equivalents of hydrogen gas.

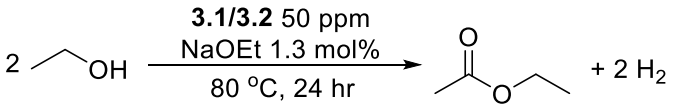

Scheme 5.5. Acceptorless dehydrogenative coupling of ethanol to ethyl acetate

Complexes **3.1** and **3.2**, which had produced a large quantity of solid product during the Guerbet catalysis, were tested using the conditions reported by Beller,[10] (Scheme 5.5) the best performing of the three published systems. This uses a low Ru loading (50 ppm) with NaOEt base. An open vessel is

used, unlike in Guerbet catalysis, as allowing the hydrogen gas produced to leave the reaction vessel helps to pull the reaction equilibrium to the products side in accordance with Le Chatelier's principle. Aliquots from both reactions were taken after 16 and 24 hours and examined by ^{1}H NMR spectroscopy. Neither of the catalysts showed any turnover to ethyl acetate, a result which was confirmed by GC analysis. As no acetates were found in the solid analysis from the ^{i}BuOH catalysis discussed above (Section 5.1.2) it can be suggested that these tripod complexes catalyse neither the acceptorless dehydrogenative coupling of ethanol nor the Tishchenko reaction to produce sodium acetate. Tishchenko chemistry concerns the reaction of an aldehyde with a basic alkoxide to give an ester. In this case acetaldehyde with sodium ethoxide to give ethyl acetate (Scheme 5.6). The acetaldehyde could be formed by the ruthenium catalyst dehydrogenating ethanol as in the first step of the Guerbet mechanism. The formation of acetates through this reaction has been observed with other ruthenium catalysts in EtOH/MeOH heterecoupling,[8] but has not been noted with these tripod complexes.

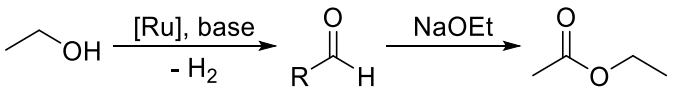

Scheme 5.6. Tishchenko route to ethyl acetate from ethanol and sodium ethoxide

5.4 – Hydrogenation of C3 diesters

With some of the Ru complexes prepared in Chapter 3, particularly **3.1** and **3.3**, being effective catalysts for the hydrogenation of C2 esters to EG their efficacy for the hydrogenation of linear C3 esters to 1,3-propandiol (PDO) was examined.

PDO is used as a co-monomer for polymers, most notably polytrimethylene terephthalate (PTT) as well as other niche uses such as coatings and adhesives.[14] PTT is used in similar products to PET, especially in fibres, but is of interest as it is potentially more biodegradable. The larger scale production of PTT is somewhat hindered by the lack of a cost-effective synthesis of PDO. The most widely used method is the hydration of acrolein.[15] A hydroformylation of ethylene oxide developed

by Shell has also been used on a large scale. Bacterial synthesis and the hydrogenolysis of glycerol are also used to a much smaller extent.[16]

Dimethyl malonate (DMM) was chosen as a substrate; it is the simplest C3 diester and mirrors the C2 substrate DMO used previously. It can be prepared from syngas and methanol *via* dimethyoxymethane or from a Claisen condensation with methyl carbonate and dimethyl carbonate, as well as other petrochemical based reactions.[17] The only example of DMM hydrogenation to PDO reported in the literature was conducted with a heterogeneous Cu/SiO_2 catalyst.[18] This gives the mono-ester, methyl 3-hydroxypropionate (MHP), produced after one hydrogenation as the main product with the double hydrogenated PDO also formed, but only in small quantities (<10 %).

The hydrogenation of DMM was attempted using the same conditions optimised for DMO hydrogenation with both **3.1** and **3.3** tested as catalysts. Separation of MHP and PDO was not possible by GC methods so the yield was calculated by ^{1}H NMR using mesitylene as a standard (Table 5.3). All three compounds have a proton environment distinct from any other signals (and the methyl singlet for mesitylene at 2.20 ppm) to use as a handle for the calculations (Figure 5.8).

*Table 5.3 Hydrogenation of DMO to MHP and PDO with **3.1** and **3.3***

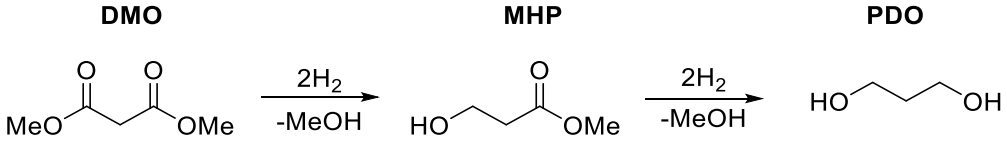

Run[a]	Catalyst	%Yield MHP	%Yield PDO	%Conv DMM
1	**3.1**	38	2	44
2[b]	**3.1**	55	3	69
3	**3.3**	48	3	60
4[b]	**3.3**	53	9	92

[a]conditions: 5 mmol DMM, 0.25 mol% Ru catalyst, 10 mL MeOH, 30 bar H_2, 180°C, 3 hr [b] 20 hr

The results above show that only a very small yield of PDO is given over 3 hours with the major product being the MHP ester (Runs 1 and 3). To try to improve these yields the reaction time was lengthened to 20 hours which gave an improvement from 3% to 9% with **3.3** (Run 4) but made no change with **3.1** (Run 3) regarding PDO yield. The MHP yield and overall DMM conversion both increased. The presence of PDO was confirmed by ^{13}C NMR spectroscopy with the two expected signals at 61 and 34 ppm present in the spectra. The diacid, malonic acid, was tested as a substrate with the idea that it might undergo an autocatalytic esterification to DMM in the same way that GA forms MG, see Chapter 3 (Section 3.3). This was unsuccessful and analysis of the product solution showed the full yield of unreacted malonic acid.

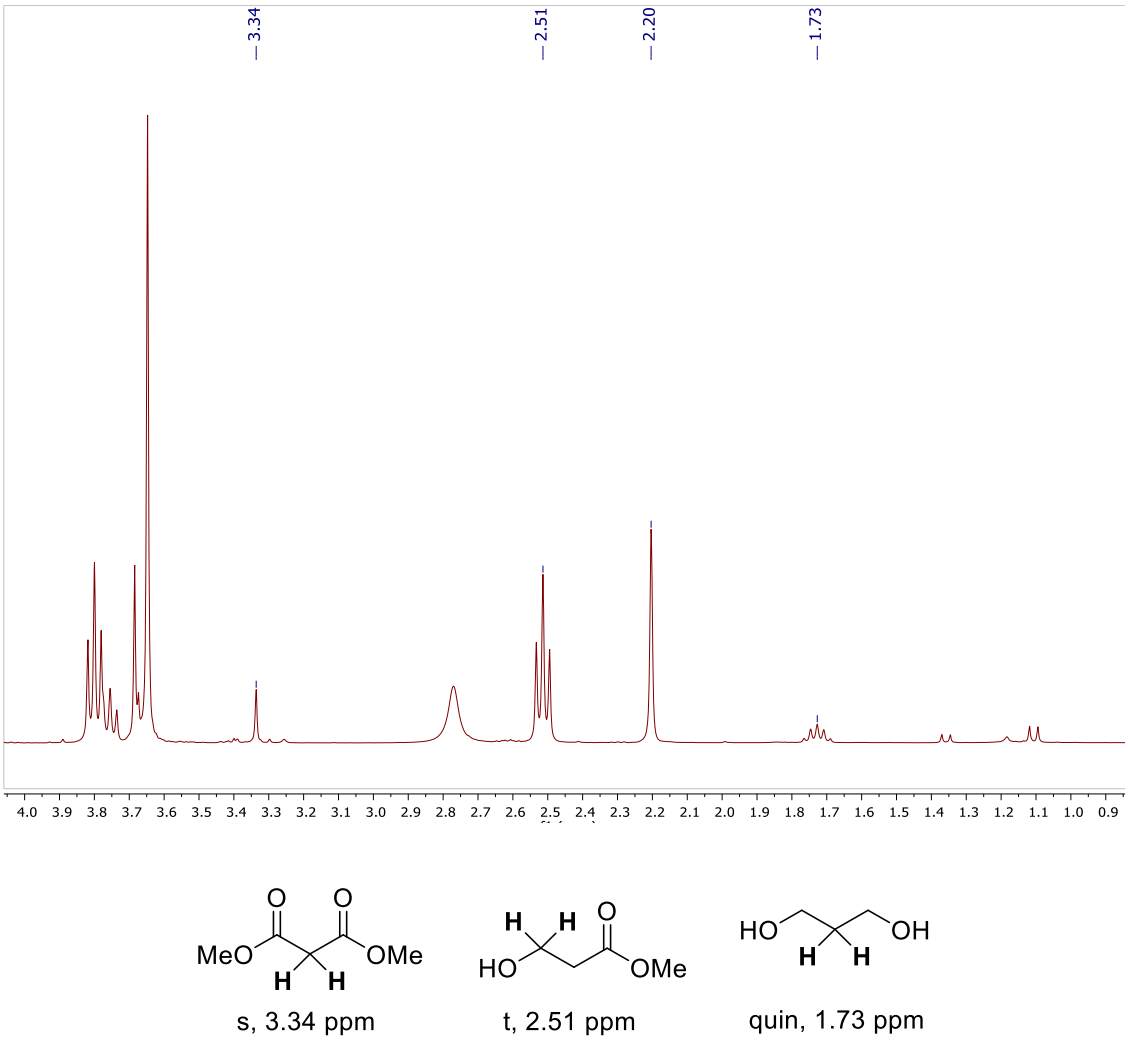

Fig 5.8. ^{1}H NMR Spectrum (300 MHz, $CDCl_3$) and proton environments used for ^{1}H NMR yield calculations

5.5 – Amide Hydrogenation

The hydrogenation of amides to amines is a very important process in the chemical industry, especially in pharmaceuticals where many drug molecules feature an amine group. However, amides are the most thermodynamically stable of the carboxylic acid derivatives and the most resistant to hydrogenation.[19] This is largely because the lone pair of electrons on the N atom are able to delocalize, forming a partial double bond between the nitrogen and carbonyl carbon atoms. Historically, amide hydrogenations have been performed using stoichiometric hydride reagents including $LiAlH_4$, DIBAL, boranes and silanes, which react with low atom economy and create a large amount of waste products. A catalytic hydrogenation of amides using H_2 is much greener and alleviates some of the concerns around by-product formation. The first reported, amide hydrogenation with a homogeneous catalyst was reported by Crabtree *et al.* using a $Ru(acac)_3$/Tripod system, similar to those used for ester hydrogenation, discussed in Chapter 3.[20] A more selective system with milder conditions, again using $Ru(acac)_3$/Tripod, for the hydrogenation of butanamide to its secondary amine was later reported by Cole-Hamilton *et al.*[21]

Hydrogenation of an amide can go through two possible routes (Scheme 5.7). The amide is first hydrogenated to a hemiaminal which can then either form an aldehyde by the elimination of the primary amine or form an imine through the elimination of water. The aldehyde or imine are then hydrogenated to the alcohol or secondary amine respectively.[22]

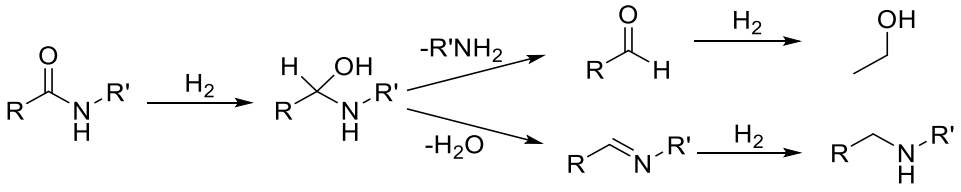

Scheme 5.7. Two pathways for amide hydrogenation

The Tripod and N-Tripod Ru dimers, **3.1** and **3.3**, discussed in Chapter 3, were tested for a number of amide hydrogenations using the same conditions as with the C2 oxalates. The first substrate was *N*-

phenyl-2-hydroxyacetamide which was prepared by the reaction of ethylene glycol with aniline (Scheme 5.8).[23]

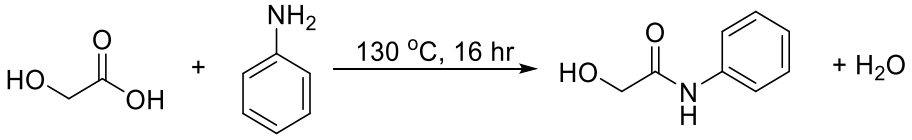

Scheme 5.8. Synthesis of N-phenyl-2-hydroxyacetamide

The attempted hydrogenation reaction cleaved the C-N bond (top pathway Scheme 5.6) giving a mixture of the primary alcohol EG and the primary amine aniline. None of the secondary amine, formed by C-O cleavage, was observed in the ^{1}H or ^{13}C NMR spectra of the product mixture. Quantitative analysis was performed by GC for the alcohol and ^{1}H NMR with mesitylene as a standard for the amine and amide. **3.1** and **3.3** both gave near identical yields of EG and aniline with the two produced in the expected 1:1 ratio (Table 5.4, Runs 1 and 2). Most of the amide remained unconverted with no other major side products observed.

Table 5.4 Hydrogenation of amides to alcohols and primary amines

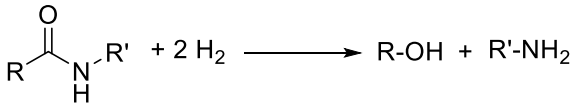

Amide	Run[a]	Catalyst	% Yield Alcohol	% Yield Amine	% Conv. Amide
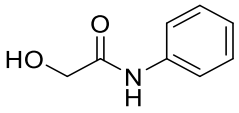	1	**3.1**	38	33	40
	2	**3.3**	34	32	39
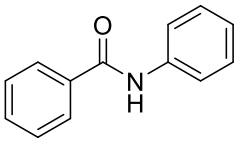	3	**3.1**	2	0	2
	4	**3.3**	2	0	2
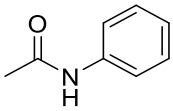	5	**3.1**	0	0	0
	6	**3.3**	0	0	0
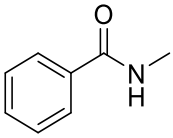	7	**3.1**	2	0	2
	8	**3.3**	2	0	2

[a]conditions 5 mmol DMM, 0.25 mol% Ru catalyst, 10 mL MeOH, 30 bar H_2, 180°C, 3 hr

After some success with *N*-methyl-2-hydroxyacetamide, three other commercially available amides were tested for hydrogenative cleavage of the C-N bond (Table 5.4). Unfortunately, these were unsuccessful producing trace amounts of the alcohol with none of the corresponding primary amine observed (Runs 3-8). The low concentrations may not have been detected in the GC analysis. No evidence of the secondary amine products was obtained either. One reason for this could be that *N*-phenyl-2-hydroxyacetamide features a hydroxy group situated two bonds away from the carbonyl of the amide. This could potentially withdraw electron density from the delocalised system around the amide making the C-N bond weaker. The other amides tested do not feature such an electron withdrawing group so may contain stronger C-N bonds increasing the thermodynamic barrier to hydrogenation.

5.6 – Transfer Hydrogenation with Ammonium Formate

The following work was conducted during a visit to BP at the Centre of Expertise for Applied Chemistry and Physics, Saltend HRTC, Hull under the supervision of industrial supervisor Prof. Glenn Sunley and Dr Greg Price.

The hydrogenation reactions attempted above use hydrogen gas as the hydrogenation agent. While this gives excellent atom economy there are several practical issues. Using pressurised gas of any kind carries an explosion risk while hydrogen itself is flammable and when used at the high temperatures required in the above reactions creates a severe fire hazard. The equipment needed for these reactions is expensive and the apparatus must be checked and replaced regularly and only used by trained personnel. A way of circumventing these issues is to perform a transfer hydrogenation. These reactions involve generating H_2 *in situ* from another reagent, avoiding the use of hydrogen gas. Ruthenium complexes have been used for transfer hydrogenation since the work of Sasson and Blum who successfully hydrogenated acetophenone with isopropanol using a $RuCl_2(PPh_3)_3$ catalyst.[24] Further developments have been made since, particularly by Noyori who developed a series of ruthenium catalysts for asymmetric transfer hydrogenation during the 1990s.[25] These reactions all use *iso*propanol as the transfer hydrogenation agent. This is dehydrogenated by the catalyst to give H_2 and acetone and has been the most widely used transfer hydrogenation agent. Another source of hydrogen is ammonium formate which has been used for alkene reductions with palladium catalysts.[26] When reacted with an appropriate catalyst ammonium formate produces H_2, CO_2 and NH_3. This gives a source of hydrogen while the by-products can be easily removed from the reaction mixture.

A transfer hydrogenation was attempted using complex **3.1** with ammonium formate as the hydrogen source. It was unlikely that an ester would be hydrogenated by this method so the aldehyde 2-ethylhexanal was chosen as a model substrate (Scheme 5.9). The results were analysed by GC-MS with approximate quantitative values obtained (Table 5.5)

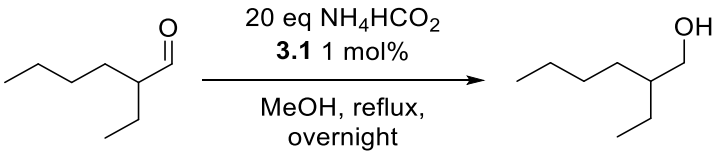

*Scheme 5.9 Transfer hydrogenation of 2-ethylhexanal with **3.1***

*Table 5.5 – Products obtained from transfer hydrogenation with **3.1***

Product	% Yield (estimate from GC-MS)
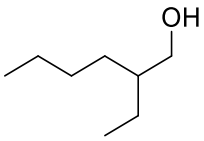	1
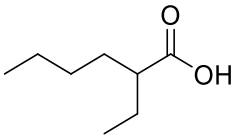	2
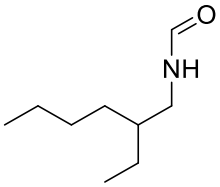	11
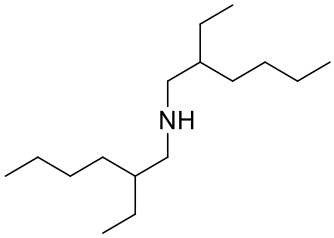	5
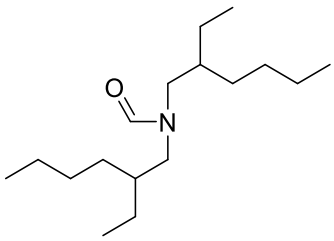	2
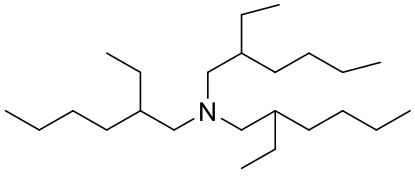	1
Unidentified products (N containing)	2

Conditions: 7.80 mmol 2-ethylhexanal, 156 mmol NH_4HCO_2 (20 eq), 0.078 mmol $[Ru(Tripod)Cl_{1.5}]_2Cl$ (1 mol%), 10 mL MeOH, 75 °C, overnight

As well as a small quantity of the desired alcohol, a range of other products had been formed. A condensation between the aldehyde and ammonia formed *in situ* has formed the corresponding

amine which has been further substituted to the di-and tri-substituted analogues. Formamides have also been produced, due to a dehydrogenation of the methanol solvent to formaldehyde. A small quantity of the carboxylic acid was also detected, but this was later found to be present in the starting material as an impurity. To determine whether this reactivity was inherent to the tripod complex **3.1**, the experiment was repeated using the common precursor [Ru(*p*-cymene)Cl_2]$_2$ complex (Table 5.6).

Table 5.6 – Products obtained from transfer hydrogenation with [Ru(p-cymene)Cl_2]$_2$

Product	% Yield
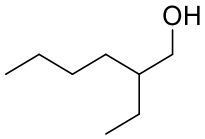	1
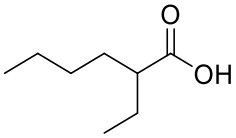	1
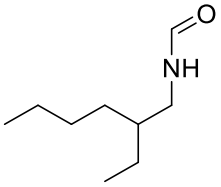	5
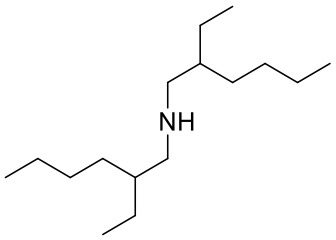	42
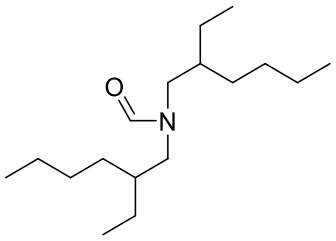	2
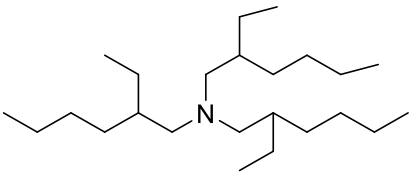	4
Unidentified products (N containing)	6

Conditions: 7.80 mmol 2-ethylhexanal, 156 mmol NH_4HCO_2 (20 eq), 0.078 mmol [Ru(*p*-cymene)Cl_2]$_2$ (1 mol%), 10 mL MeOH, 75 °C, overnight

The same range of products were seen although with a much higher quantity of the di-substituted amine which was clearly the major product. As with the **3.1** experiment, two formamide compounds were formed. To see if this could be controlled the **3.1** test was repeated using ^{t}BuOH as the solvent which cannot be dehydrogenated to an aldehyde (Table 5.7).

*Table 5.7 – Products obtained from transfer hydrogenation with **3.1** in ^{t}BuOH*

Product	% Yield
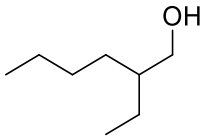	26
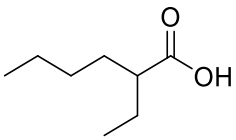	1
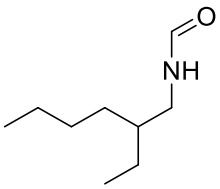	1
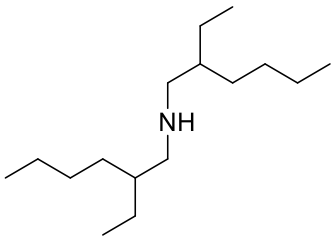	60
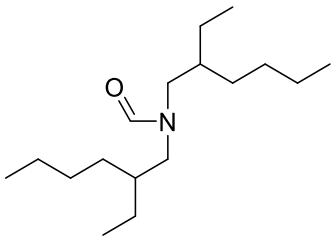	<1
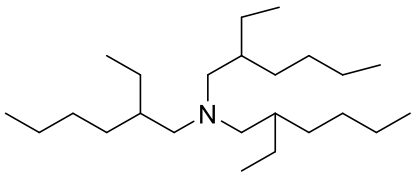	1
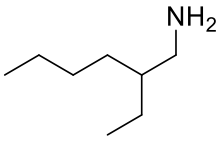	1
Unidentified products (N containing)	1

Conditions: 7.80 mmol 2-ethylhexanal, 156 mmol NH_4HCO_2 (20 eq), 0.078 mmol $[Ru(Tripod)Cl_{1.5}]_2Cl$ (1 mol%), 7.75 g ^{t}BuOH, 85 °C, overnight

The reaction produced almost exclusively the alcohol hydrogenation product (26%) and the disubstituted amine (60%) with around 90% total conversion of the 2-ethylhexanal substrate. This unexpected reactivity could open up a route to the synthesis of useful secondary amines. As mentioned above (Section 5.4), these are a class of compound with relevance to the pharmaceutical industry. Their synthesis is currently being studied by amide hydrogenation, which uses pressurised H_2, high temperature and often strong bases. The results shown here could potentially offer a milder route to the synthesis of these target molecules.

5.7 – Summary

The Ru/tridentate complexes introduced in Chapter 3 were trialled for the synthesis of *iso*butanol from the heterocoupling of methanol and ethanol. All the catalysts showed some activity, with the tripod dimer **3.1** giving the best performance. However, there was no clear structure activity relationship across the catalysts. All the reactions produced a significant quantity of solid, which was found to be carbonate and formate in the case of **3.1**. No acetate production was observed and attempts to use **3.1** for the acceptorless dehydrogenative coupling of ethanol to ethyl acetate were unsuccessful. Catalyst studies revealed the structure of different complexes formed during the reaction, most notably a monometallic carbonyl dihydride complex formed in an autoclave under reaction conditions.

3.1 and **3.3** were also tested for the hydrogenation of DMM to PDO, while giving low conversion of PDO they showed significant turnover to the intermediate MHP. Furthermore, these two catalysts were tested for the hydrogenation of a series of amides, which was largely unsuccessful with only the amide featuring an electron withdrawing alcohol group showing any conversion.

5.8 – Future Work

A clear next step for the *iso*butanol catalysis is to investigate the nature of the catalyst. The initial organometallic studies here have identified complexes of interest in the ethanol/methanol heterocoupling. The dihydride carbonyl complex produced in the closed system (Figure 5.5, Section 5.1.3) most similar to actual reaction conditions, could be reacted in stoichiometric quantities with ethanol (Scheme 5.10). As the dehydrogenation of ethanol is the first step of the catalytic cycle a bound ethoxide complex, or even bound acetaldehyde could be observed using ^{1}H NMR analysis. This would indicate that the monometallic hydride complex is the true active catalyst and would give a starting point for further mechanistic investigations. If no such interaction is seen it may be that the complex is simply an off-cycle resting state or deactivated form of the true catalyst.

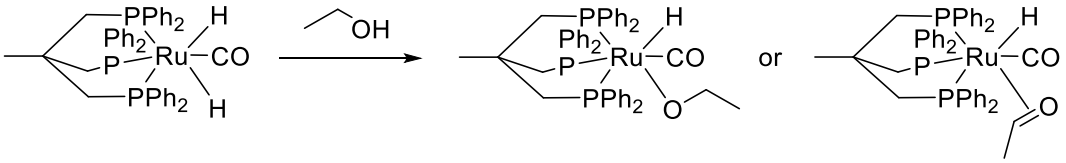

*Scheme 5.10. Potential structures from the reaction of **3.1** NaOMe study complex and ethanol*

In the case of the hydrogenation of DMM to PDO, the lack of desired product could be due to the MHP, or perhaps more likely PDO, produced binding to the catalyst rendering it inactive (Figure 5.9). These chelated complexes would feature a thermodynamically stable 6-membered ring which would require forcing conditions to be removed from the Ru centre. Experiments to examine the formation of these species, both with MHP and PDO, could be conducted and analysed by ^{31}P{^{1}H], ^{1}H NMR and ESI-MS. If isolated, their subsequent hydrogenation to free PDO under a range of conditions could also be investigated.

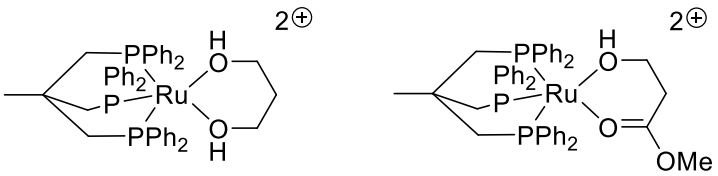

Fig 5.9. Potential complexes formed in situ from DMM hydrogenation

Longer chain diesters e.g. a dimethyl succinate or dimethyl adipate, which would be hydrogenated to 1,4-butanediol and 1,6-hexanediol respectively, could be trialled as other substrates (Scheme 5.11). Neither the product diols nor intermediate monoesters can form stable 5 or 6 membered ring structures with the ruthenium centre. This could suggest how significant an impact chelation of the organic products has on hydrogenation catalysis. These reactions could also be useful for exploring the tripodal catalysts' ability to hydrogenate a wider range of esters and diesters.

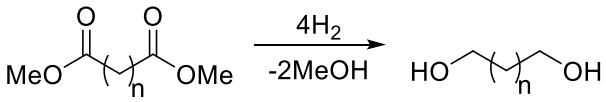

n = 2, dimethyl succinate
n = 4, dimethyl adipate

Scheme 5.11. Hydrogenation of dimethyl succinate and dimethyl adipate

As mentioned previously, a range of amides activated with more electron withdrawing groups could be used as substrates for the hydrogenation to alcohols and primary amines. Changing the reaction conditions and potentially using a Lewis acidic promoter to activate the C=O bond could also be tested to alter the selectivity from the hydrogenation to alcohol and primary amine to water and the secondary amine. This is the more useful pathway for the synthesis of commercially relevant molecules.

The unexpected synthesis of secondary amines from aldehydes and ammonium formate with a ruthenium complex could be explored further. Adjusting reaction conditions and the catalyst itself could improve selectivity to the amine product. The initial transfer hydrogenation from an aldehyde to alcohol also showed some promise and could also be examined. Using two different aldehydes to produce a hetero-disubstituted amine could be attempted (Scheme 5.12). This would likely require significant catalyst development and reaction optimisation to achieve a good selectivity for this product over the two homo-disubstituted amines.

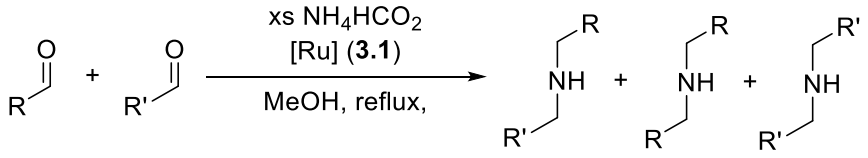

Scheme 5.12. Potential synthesis of secondary amines from aldehydes with ammonium formate

5.9 - References

1. S. Atsumi, A. F. Cann, M. R. Connor, C. R. Shen, K. M. Smith, M. P. Brynildsen, K. J. Y. Chou, T. Hanai, and J. C. Liao, *Metab. Eng.*, 2008, **10**, 305–311.

2. B. G. Harvey and H. A. Meylemans, *J. Chem. Technol. Biotechnol.*, 2011, **86**, 2–9.

3. H. Aitchison, R. L. Wingad, and D. F. Wass, *ACS Catal.*, 2016, **6**, 7125–7132.

4. A. M. Brownstein, *Renewable Motor Fuels: The Past, the Present and the Uncertain Future*, Elsevier Inc., 2014.

5. R. L. Wingad, E. J. E. Bergström, M. Everett, K. J. Pellow, and D. F. Wass, *Chem. Commun.*, 2016, **52**, 5202–5204.

6. R. L. Wingad, E. J. E. Bergström, M. Everett, K. J. Pellow, and D. F. Wass, *Chem. Commun.*, 2016, **52**, 5202–5204.

7. H. Aitchison, R. Wingad, and D. F. Wass, *Manuscript in Preparation*, .

8. K. J. Pellow, R. L. Wingad, and D. F. Wass, *Catal. Sci. Technol.*, 2017, **7**, 5128-5134.

9. M. Nielsen, E. Alberico, W. Baumann, H. J. Drexler, H. Junge, S. Gladiali, and M. Beller, *Nature*, 2013, **495**, 85-89.

10. M. Nielsen, H. Junge, A. Kammer, and M. Beller, *Angew. Chem. Int. Ed.*, 2012, **51**, 5711–5713.

11. N. Armaroli and V. Balzani, *Chem. An Asian J.*, 2011, **6**, 768–784.

12. D. Spasyuk and D. G. Gusev, *Organometallics*, 2012, **31**, 5239–5242.

13. M. H. G. Prechtl, K. Wobser, N. Theyssen, Y. Ben-David, D. Milstein, and W. Leitner, *Catal. Sci. Technol.*, 2012, **2**, 2039–2042.

14. J. V. Kurian, *J. Polym. Environ.*, 2005, **13**, 159–167.

15. C. J. Sullivan, A. Kuenz, and K.-D. Vorlop, in *Ullmann's Encyclopedia of Industrial Chemistry*, 2018, pp. 1–15.

16. R. K. Saxena, P. Anand, S. Saran, and J. Isar, *Biotechnol. Adv.*, 2009, 27, 895–913.

17. R. A. Sheldon, *Chemicals from Synthesis Gas*, Springer Netherlands, Dordrecht, 1983, vol. 3.

18. S. Zheng, K. Zhu, W. Li, and Y. Ji, *New J. Chem.*, 2017, **41**, 5752–5763.

19. A. J. McAlees and R. McCrindle, *J. Chem. Soc. C Org.*, 1969, 2425–2435.

20. M. Kilner, D. V. Tyers, S. P. Crabtree, and M. A. Wood, 2003, US9636671B2.

21. A. A. Núñez Magro, G. R. Eastham, and D. J. Cole-Hamilton, *Chem. Commun.*, 2007, 3154–3156.

22. S. Werkmeister, K. Junge, and M. Beller, *Org. Process Res. Dev.*, 2014, 18, 289–302.

23. J. M. Hung, H. J. Arabshahi, E. Leung, J. Reynisson, and D. Barker, *Eur. J. Med. Chem.*, 2014, **86**, 420–437.

24. Y. Sasson and J. Blum, *Tetrahedron Lett.*, 1971, **12**, 2167–2170.

25. M. Kitamura, M. Tokunaga, and R. Noyori, *J. Am. Chem. Soc.*, 1995, **117**, 2931–2932.

26. Z. Paryzek, H. Koenig, and B. Tabaczka, *Synthesis*, 2003, 2023–2026.

Chapter 6 – Experimental

6.1 – General Considerations

Unless otherwise stated, all procedures were carried out under an inert atmosphere (N_2) using Schlenk line techniques or in a glovebox under an argon atmosphere. All glassware was oven dried at 200 °C for at least one hour before use. CH_3CN, CH_2Cl_2, Et_2O, hexane, THF and toluene were obtained from a Grubbs type solvent purification system and degassed before use. Anhydrous MeOH and EtOH were bought from Acros Organics and were kept over 4Å molecular sieves and degassed before use. Deuterated solvents were purchased from Sigma Aldrich and were dried over 4Å molecular sieves and degassed before use. All other chemicals were purchased from Sigma-Aldrich, Alfa Aesar or Fisher and used without further purification, unless stated. Reagent gases (H_2/CO 2:1 blend, H_2 and CO) were purchased from BOC gases and used without further purification. NMR spectra were recorded on Jeol ECS300, Jeol ECS400, Bruker Fourier 300 MHz, Bruker DPX 400 MHz or Bruker Avance 500 MHz spectrometers. ESI-MS analysis was conducted using a Bruker Daltonics MicrOTOF II or Waters QTOF micro. Catalytic results were analysed by GC-FID using an Agilent 7820A GC.

6.2 – Experimental Procedures

Chapter 2

The phosphinoamide ligand[1], **2.1**,[2] **2.2**, **2.4**,[3] **2.3,**[4] $[PPh_4][Co(CO)_4]$,[5] $HCo(CO)_4$,[6] 2.5, 2.6, 2.7,[7] and 2.8[8] were prepared as reported in the literature.

Example of Reductive Hydroformylation of Paraformaldehyde with Co/PPh_3 (Section 2.2.1)

Paraformaldehyde (152 mg, 5 mmol) and PPh_3 (561 mg, 2 mmol, 40 mol%) were added to a clean oven-dried PTFE insert. The insert and a Parr 100 mL stainless steel autoclave were then taken inside the glovebox where $[Co_2(CO)_8]$ (175.3 mg, 0.5 mmol, 10 mol%) was added. The autoclave was sealed inside the glovebox then put under an inert nitrogen atmosphere. CH_3CN (7 mL) was injected into the autoclave through an inlet against a positive flow of nitrogen. The autoclave was pressurised with 40

bar syngas (2:1 H_2/CO), sealed and placed in a pre-heated aluminium mantle (180 ^oC) for 3 hours. The autoclave was then cooled to room temperature in an ice/water bath and vented to remove any gas. A liquid sample was removed, filtered and analysed by GC (300 µL of sample, 25 µL of *n*-pentanol standard, 1 mL CH_3CN).

GC-FID DB-Wax capillary column 30 m x 0.32 mm, I.D. 0.25 µm. Method: starting oven temp 35 °C, hold at 35 °C for 5 min, heat to 250 °C at 50 °C min^{-1}, hold at 250 °C for 5 min.

Catalyst Pre-form Test (Section 2.2.1)

PPh_3 (561 mg, 2 mmol, 40 mol%) was added to a clean oven-dried PTFE insert. The insert and the autoclave were then taken inside the glovebox where [$Co_2(CO)_8$] (175 mg, 0.5 mmol, 10 mol%) was added. The autoclave was sealed inside the glovebox then removed. CH_3CN (7 mL) was injected into the autoclave through an inlet against a positive flow of nitrogen. The autoclave was pressurised with 40 bar syngas (2:1 H_2/CO), sealed and placed in the pre-heated aluminium heating mantle (180 ^oC) for 1 hour. The autoclave was then cooled to room temperature in an ice/water bath. The autoclave was connected to a Schlenk line, any residual gas vented and the autoclave was placed under a flow of nitrogen. An aliquot of the reaction mixture (0.7 mL) was transferred to a J. Youngs NMR tube and was analysed by $^{31}P\{^1H\}$ NMR.

Cleavage of Glycolaldehyde Dimer (Section 2.2.2)

Glycolaldehyde dimer (100 mg, 0.83 mmol) was dissolved in MeOH (10 mL) to give a colourless solution. Against a flow of N_2, HCl (2.0 M in Et_2O, 0.42 mL, 0.83 mmol) was added dropwise over a few minutes. The mixture was then left to stir overnight at room temperature. An aliquot (1 mL) was then taken for GC-MS analysis.

***m*-Anisaldehyde Model Reaction (Section 2.4.5)**

2.4 (0.219 g, 0.25 mmol), was weighed out into an oven-dried PTFE insert inside a glovebox. The insert was placed in a Parr 100ml stainless steel autoclave which was then sealed and placed under an inert

nitrogen atmosphere. *m*-anisaldehyde (0.61 mL, 5 mmol) and THF (10 mL) were added against a flow of N_2. The autoclave was then pressurised with 40 bar syngas (2:1 H_2:CO), placed into a pre-heated aluminium mantle (180 °C) and left stirring for 20 hours at 700 rpm. The autoclave was then cooled to room temperature in an ice/water bath for 30 minutes. Any residual gas was vented, and the reaction contents collected. An aliquot of the reaction solution (0.7 mL) was used for ^{1}H NMR analysis with mesitylene (14 µL, 0.1 mmol) used as a standard.

Chapter 3

L1 and **L10** were purchased from Sigma Aldrich and used without further purification. $RuCl_2(DMSO)_4$,[9] **3.1,**[10] **L2,**[11] **L3,**[12] **L4,**[13] **L11,**[14] **L13,**[15] **L14,**[16] **L15**, **3.14,**[9] **3.16, 3.17,**[17] PNP ligands,[18] ^{NH}PNP ligands,[19] **3.18,**[20] **3.19,**[21] **3.20,**[22] **3.21,**[23] and **3.22**[24] were synthesised according to literature procedures.

Synthesis of 3.2 $[Ru_2Cl_3(L2)_2]Cl$ (Section 3.2.2)

L2 (0.310 g, 0.5 mmol) and $[RuCl_2(DMSO)_4]$ (0.242 g, 0.5 mmol) were added to a Schlenk flask and toluene (10 mL) was added to give a yellow suspension. The mixture was heated under reflux for 90 hours. The solvent was removed under vacuum to give a yellow residue which was washed with hexane (6 x 5 mL) and dried under vacuum to give a yellow solid (0.090 g, 0.09 mmol, 36%)

^{1}H NMR (400 MHz, $CDCl_3$) δ: 1.18(m, 9H, -CH_2CH_3), 1.75 (m, 6H, -CH_2CH_3), 2.19 (br s, 6H, NCH_2-) ppm $^{31}P\{^1H\}$ NMR (400 MHz, $CDCl_3$) δ: 44.2 (s) ppm High Res ESI-MS 981.1680 $[M-Cl]^+$

Synthesis of 3.3 $[Ru_2Cl_3(L3)_2]Cl$ (Section 3.2.3)

L3 (306 mg, 0.5 mmol) and $RuCl_2(DMSO)_4$ (242 mg, 0.5 mmol) were added to a Schlenk flask and toluene (20 mL) was added giving a yellow suspension which was heated to reflux. Upon heating the solids dissolved to give an orange solution which was heated under reflux for 16 hours. The resulting yellow precipitate was isolated *via* cannula filtration, washed with ether (3 x 8 mL) and dried under vacuum to give a yellow solid. (196 mg, 0.13 mmol, 52%)

^{1}H NMR (300 MHz, $CDCl_3$) δ: 4.06 (bs, CH_2), 6.85 (t, 12H, *o*-Ph), 7.17 (t, 6H, *p*-Ph), 7.32 (bm, 12H, *m*-Ph) ppm $^{31}P\{^{1}H\}$ NMR (300 MHz, $CDCl_3$) δ: 19.1 (s) ppm High Res ESI-MS m/z: 1531.1274$[M\text{-}Cl]^+$

Synthesis of 3.4 $[Ru_2Cl_3(L4)_2]Cl$ (Section 3.2.3)

L4 (0.400 g, 0.50 mmol) and $RuCl_2(DMSO)_4$ (0.242 g, 0.50 mmol) were added to a Schlenk flask and toluene (10 mL) was added to give a yellow suspension. The mixture was heated under reflux for 16 hours. The resulting red precipitate was isolated *via* cannula filtration, washed with ether (3 x 10 mL) and dried under vacuum to give an orange solid. (0.351 g, 0.18 mmol, 73%)

^{1}H NMR (400 MHz, $CDCl_3$) δ: 3.33 (m, 18H, CH_2CH_3), 3.52 (m, 12H, CH_2CH_3), 3.55(bs, 12 H, NCH_2) ppm $^{31}P\{^{1}H\}$ NMR (400 MHz, $CDCl_3$) δ: 55.5 ppm High Res ESI-MS m/z 1701.3 $[M\text{-}Cl]^+$

Synthesis of L5 (Section 3.2.3)

$LiAlH_4$ (0.331 g, 8.70 mmol) was weighed into a 100 mL round bottom Schlenk flask equipped with a magnetic stirrer bar in a glovebox before being transferred to an ice/water bath. Et_2O (30 mL) was then added to give a dark grey suspension. Chlorodicyclohexylphosphine (1.90 mL, 8.60 mmol) was added dropwise over 5 minutes. The flask was left in the ice/water bath for 10 minutes then allowed to heat up to room temperature under a flow of N_2 overnight. The colourless solution was collected *via* filter cannula with the receiving flask placed in an ice/water bath. Against a flow of N_2, degassed H_2O (30 mL) was added, very slowly at first, causing significant effervescence. The ether layer was collected, and the aqueous fraction washed with Et_2O (2 x 10 mL). The ether washings were combined and dried over $MgSO_4$ with the solvent removed under vacuum to give a dicyclohexylphosphine as a colourless liquid (1.40 g).

Aqueous formaldehyde solution (1 mL, 40 wt%) and aqueous hydrochloric acid (0.5 mL, 37 wt%) were added to the dicyclohexylphosphine (1.40 g, 1.54 mL, 7.06 mmol) in a Schlenk flask. The mixture formed a white suspension and the flask became hot. On cooling a white crystalline solid precipitated which was collected and dried (1.782 g).

The crude hydroxonium salt (1.601 g) was dissolved in methanol (10 mL) to give a colourless solution. Triethylamine (2.40 mL, 17.21 mmol) was then added and the solution left to stir for one hour. Ammonia solution (1.00 mL, 2M in methanol) was then added causing the formation of a white solid. The mixture then then heated to reflux and left for two hours. The white solid formed was isolated *via* cannula filtration, washed with methanol (3 x 5 mL) and dried under vacuum to give a powdery, white solid. (0.733 g, 1.13 mmol, 62%)

^{1}H NMR (400 MHz, $CDCl_3$) δ: 1.05-1.55 (br m, 18H, *m*-Cy + *p*-Cy), 1.60 – 2.10 (br, m, 12 H, *o*-Cy), 2.80 (bs, 6H -C*H*$_2$-) ppm ^{13}C{^{1}H} NMR (400 MHz, $CDCl_3$)δ: 25.6 (-*C*H_2-), 26.4 (*p*-Cy), 28.8 (*m*-Cy), 31.7 (*o*-Cy) ppm ^{31}P{^{1}H} NMR (400 MHz, $CDCl_3$) δ: -17.0 (s) ppm ESI-MS: 680.46 $[M+Na]^+$, 482.31 $[M-2xCy]^+$

Synthesis of 3.5 $[Ru_2Cl_3(L5)_2]Cl$ (Section 3.2.3)

L5 (324 mg, 0.5 mmol) and $RuCl_2(DMSO)_4$ (242 mg, 0.5 mmol) were weighed out into a Schlenk flask. Toluene (10 mL) was added to give a pale yellow suspension which was heated under reflux. Upon heating a yellow solution was formed and the reaction was left for three hours during which an orange precipitate formed. This was collected *via* cannula filtration, washed with ether (3 x 10 mL) and dried under vacuum to give a yellow solid (204 mg, 0.12 mmol, 48%)

^{1}H NMR (400 MHz, $CDCl_3$) δ: 1.18-1.25 (m, 42H, Cy), 2.29 (br s, NC*H*$_2$, 12H) ppm ^{31}P{^{1}H} (400 MHz, $CDCl_3$) δ: 48.9 (s), 50.2 (s) ppm High Res ESI-MS accurate mass m/z: 1603.6908 $[M-Cl]^+$

Synthesis of L6 (Section 3.2.3)

Chlorodiorthotolylphosphine (0.86 mL, 4.02 mmol) was weighed into a Schlenk flask and dissolved in Et_2O (10 mL). $LiAlH_4$ (0.150 g, 4.02 mmol) was slurried in Et_2O (10 mL) and cooled in an ice/water bath. The chlorophosphine solution was added dropwise to the cooled $LiAlH_4$ slurry over ten minutes. The mixture was then removed from the ice/water bath and left stirring at room temperature overnight. The colourless solution was isolated *via* cannula filtration and degassed water (20 mL) was slowly added causing some effervescence. The organic layer was collected, and the aqueous layer washed

with Et_2O (2 x 5 mL). The combined ether washings were dried over $MgSO_4$ and the solvent removed under vacuum to give a white solid. $^{31}P\{^1H\}$NMR (300MHz) δ: -57 ppm

The solid was dissolved in toluene (2 mL) to give a colourless solution. Aqueous formaldehyde solution (0.67 mL, 40 wt%) and aqueous hydrochloric acid (0.37 mL, 37wt%) were added forming a cloudy suspension which was left overnight. The solvent was then removed under vacuum to give a white solid. This was dissolved in MeOH (3 mL) and then dried under vacuum three times to give a white crystalline solid. (0.60 g, 1.92 mmol, 48%)

The salt was dissolved in MeOH (10 mL) and triethylamine (0.45 mL, 10 mmol) was added. The solution was stirred for one hour then ammonia solution (0.96 mL, 2M in methanol, 1.92 mmol) was added and the solution heated to reflux for three hours. The solvent was removed under vacuum to give a white solid which was washed with MeOH (3 x 5 mL) and dried under vacuum to give a white solid. (0.226 g, 0.32 mmol, 17%)(8% from chlorophosphine)

^1H NMR (400 MHz, $CDCl_3$) δ: 2.31, 2.35 (2 x s, 6H + 12H, *o*-tolyl), 3.52-3.60 (m, -CH_2-), 6.74 (t, 6H, *p*-Ph) 6.92-7.20 (m, 18H, *m*-Ph) ppm $^{31}P\{^1H\}$ NMR (400 MHz, $CDCl_3$) δ: -45.0 (s), -46.2 (s) ppm

Synthesis of L7 (Section 3.2.3)

Mg powder (1.720 g, 72 mmol, 1.2 eq) and iodine (a few crystals) were added to THF (100 mL) in a round bottom flask with condenser attached. 4-Bromotoluene (7.38 mL, 60 mmol, 1 eq) was added over 10 minutes while the flask was heated using a heat gun. Formation of the Grignard reagent was indicated by the Mg powder dissolving to form a yellow solution. The flask was lowered into a heating block and left at reflux (70 °C) for three hours. The flask was then placed into an ice/water bath and diethyl phosphite (2.58 mL, 20 mmol) was added over fifteen minutes. The mixture was left to stir at room temperature for four hours. The flask was placed in an ice/water bath and water (30 mL) was added slowly to quench any Grignard residues. The solution was transferred to a separating funnel and the organic components were extracted with EtOAc (3 x 40 mL), washed with brine (2 x 20 mL)

and dried over $MgSO_4$. The solvent was removed under reduced pressure to give the crude product which was recrystallised from EtOAc and heptane to give the secondary phosphine oxide as a white crystalline solid. (2.611 g, 11.3 mmol, 19%)

The phosphine oxide (2.611 g, 11.3 mmol) was suspended in THF (30 mL) in a large Schlenk flask. DIBAL-H solution (1M in DCM, 30 mL, 30 mmol, 2.7 eq) was added dropwise over 15 minutes. During the addition, the solid dissolved to give a pale yellow solution and substantial effervescence was observed. The solution was then left to stir at room temperature for three hours. Et_2O (30 mL) was added and the flask cooled in an ice/water bath. Sodium hydroxide solution (2M aq, 30 ml, xs) was then added dropwise, very slowly to the flask causing severe gas evolution. The organic layer was transferred to a clean flask *via* cannula filtration and the aqueous fraction was extracted with Et_2O (20 mL). The combined ether fractions were dried over $MgSO_4$ and the solvent removed under vacuum to give the crude secondary phosphine as a colourless oil (0.920 g, 4.23mmol, 38%).

The oil (0.920 g, 4.27 mmol) was weighed into a Schlenk flask. Aqueous formaldehyde solution (40wt%, 0.7 mL) and aqueous hydrochloric acid (37wt%, 0.4 mL) were added to give a cloudy white suspension that was left overnight. The solvent was then removed under vacuum to give a sticky, cream solid. This was re-dissolved in MeOH (2 mL) and dried under vacuum to give a white, crystalline solid (0.997 g, 3.21 mmol, 76%).

The white solid (0.997 g) was weighed into a Schlenk flask and methanol (10 mL) was added to give a cloudy solution. Triethylamine (1.34 mL, 9.60 mmol) was added and the solution stirred for one hour. Ammonia solution (2M in methanol, 0.60 mL, 1.20 mmol) was then added and the solution heated to reflux for two hours. The white precipitate formed was isolated *via* cannula filtration washed with MeOH (3 x 10 mL) and dried under vacuum to give the ligand as a white solid. (0.364 g, 0.52 mmol, 16%) (0.9% from 4-bromotoluene)

^{1}H NMR (400 MHz, $CDCl_3$) δ: 2.30 (s, 9H, *p*-CH_3), 3.71 (bs, -CH_2-) 7.02 (d, 12H, *m*-Ph), 7.22 (t, 12H, *o*-Ph) ^{13}C NMR (400 MHz, $CDCl_3$) δ: 14.2 (-*C*H_2-), 20.2 (*p*-*C*H_3), 127.9 (*p*-Ph), 132.0 (*m*-Ph), 132.2 (*o*-Ph) ppm ^{31}P{^{1}H} NMR (300 MHz, $CDCl_3$) δ: -29.5 (s) ppm

Synthesis of L8 (Section 3.2.3)

Mg powder (1.721 g, 72 mmol, 1.2 eq) and iodine (a few crystals) were added to THF (100 mL) in a round bottom flask with condenser attached. 4-Bromoanisole (7.51 mL, 60 mmol, 1 eq) was added over 10 minutes while the flask was heated using a heat gun. Formation of the Grignard reagent was indicated by the Mg powder dissolving to form a yellow solution. The flask was lowered into a heating block and left at reflux (70 °C) for three hours. The flask was then placed into an ice/water bath and diethyl phosphite (2.58 mL, 20 mmol) was added over fifteen minutes. The mixture was left to stir at room temperature for four hours. The flask was placed in an ice/water bath and water (30 mL) was added slowly to quench any Grignard residues. The solution was transferred to a separating funnel and the organic components were extracted with EtOAc (3 x 40 mL), washed with brine (2 x 20 mL) and dried over $MgSO_4$. The solvent was removed under reduced pressure to give the crude product which was recrystallised from EtOAc and heptane to give the secondary phosphine oxide as a white crystalline solid. (2.502 g, 9.55 mmol, 16%)

The phosphine oxide was suspended in THF (30 mL) in a large Schlenk flask. DIBAL-H solution (1M in DCM, 34 mL, 34 mmol, 3.5 eq) was added dropwise over 15 minutes. During the addition, the solid dissolved to give a pale yellow solution and substantial effervescence was observed. The solution was then left to stir at room temperature for three hours. Et_2O (30 mL) was added and the flask cooled in an ice/water bath. Sodium hydroxide solution (2M aq, 30 ml, xs) was then added dropwise, very slowly to the flask causing severe gas evolution. The organic layer was transferred to a clean flask *via* cannula filtration and the aqueous fraction was extracted with Et_2O (20 mL). The combined ether fractions were dried over $MgSO_4$ and the solvent removed under vacuum to give the crude secondary phosphine as a pale yellow solid (1.052 g, 4.27 mmol, 45%).

The yellow solid (1.052 g, 4.27 mmol) was weighed into a Schlenk flask. Aqueous formaldehyde solution (40wt%, 0.7 mL) and aqueous hydrochloric acid (37wt%, 0.4 mL) were added to give a pale yellow solution that was left overnight. The solvent was then removed under vacuum to give a sticky, cream solid. This was re-dissolved in MeOH (2 mL) and dried under vacuum to give a white, crystalline solid (1.294 g, 3.77 mmol, 88%).

The white solid (1.294 g) was weighed into a Schlenk flask and MeOH (10 mL) was added to give a cloudy solution. Triethylamine (1.53 mL, 11 mmol) was added and the solution stirred for one hour. Ammonia solution (2M in methanol, 0.65 mL, 1.3 mmol) was then added and the solution heated to reflux for two hours. The white precipitate formed was isolated *via* cannula filtration washed with MeOH (3 x 10 mL) and dried under vacuum to give the ligand as a white solid. (0.575 g, 0.73 mmol, 19%) (1.2% from 4-bromoanisole)

^{1}H NMR (300 MHz, $CDCl_3$) δ: 3.66 (bs, 6H, -CH_2-), 3.75 (s, 18H, OMe), 6.70-6.75(m, 12H, *o*-Ph), 7.23-7.27 (m, 12H, *m*-Ph) ^{13}C{^{1}H} NMR (300 MHz, $CDCl_3$) δ: 15.3 (-CH_2-), 55.2 (*p*-OMe), 131.2 (*p*-Ph) , 134.5 (*m*-Ph), 134.7 (*o*-Ph) ppm ^{31}P{^{1}H} NMR (300 MHz, $CDCl_3$) δ: -31.3 (s) ppm ESI-MS: 793.1 $[M+H]^+$

Synthesis of 3.6 $[Ru_2Cl_3(L6)_2]Cl$ (Section 3.2.3)

L6 (0.226 g, 0.32 mmol) and $[RuCl_2(DMSO)_4]$ (0.157 g, 0.32 mmol) were added to a Schlenk flask and toluene (10 mL) was added to give a yellow suspension. The mixture was heated under reflux for 16 hours. The resulting red precipitate was isolated *via* cannula filtration, washed with Et_2O (3 x 10 mL) and MeOH (3 x 3 mL) and dried under vacuum to give a red solid. (0.171 g, 0.10 mmol, 64%)

^{1}H NMR (400 MHz, $CDCl_3$) δ: 2.56 (s, 36H, *o*-tolyl), 3.50 (bs, 12H, -CH_2-), 6.81 (m, Ph) 6.93 (m, Ph), 7.10 (m, Ph) ppm ^{31}P{^{1}H} NMR (400 MHz, $CDCl_3$) δ: 31.9 (br s) ppm High Res ESI-MS m/z 1699.3171 $[M-Cl]^+$

Synthesis of 3.7 $[Ru_2Cl_3(L7)_2]Cl$ (Section 3.2.3)

L7 (0.21 g, 0.3 mmol) and $[RuCl_2(DMSO)_4]$ (0.15 g, 0.3 mmol) were added to a Schlenk flask and toluene (10 mL) was added to give a yellow suspension. The mixture was heated under reflux for 16 hours.

The resulting orange precipitate was isolated *via* cannula filtration, washed with Et_2O (3 x 10 mL) and dried under vacuum to give an orange solid. (0.163 g, 0.09 mmol, 62%)

^{1}H NMR (400 MHz, $CDCl_3$) δ: 2.20 (s, 36H, *p-tolyl*), 3.97 (bs, 12H, *CH₂*), 6.62-6.66 (m, 12H, Ph), 6.72-6.76 (m, 12H, Ph) ppm $^{31}P\{^1H\}$ NMR (400 MHz, $CDCl_3$) δ: 33.8 (s) ppm High Res ESI-MS m/z 1699.3152 $[M-Cl]^+$

Synthesis of 3.8 $[Ru_2Cl_3(L8)_2]$ Cl (Section 3.2.3)

L8 (0.40 g, 0.5 mmol) and $[RuCl_2(DMSO)_4]$ (0.24 g, 0.5 mmol) were added to a Schlenk flask and toluene (10 mL) was added to give a yellow suspension. The mixture was heated under reflux for 16 hours. The resulting orange precipitate was isolated *via* cannula filtration, washed with Et_2O (3 x 10 mL) and dried under vacuum to give an orange solid. (0.352 g, 0.18 mmol, 73%)

^{1}H NMR (400 MHz, $CDCl_3$) δ: 3.69 (s, 18H, OMe), 3.93 (bs, 12H, C*H₂*), 6.40 (d, 12H, Ph), 7.28-7.21 (m, 12H, Ph), ppm $^{31}P\{^1H\}$ NMR (400 MHz, $CDCl_3$) δ: 16.7 (s) ppm High Res ESI-MS m/z 1891.2542 $[M-Cl]^+$

Synthesis of L12 (Section 3.2.4)

Divinylphenylphosphine (0.66 mL, 4 mmol) was dissolved in diethyl ether (20 mL) and Diethylphosphine (1.002 g, 11.1 mmol) was dissolved in THF (20 mL). These two solutions were combined to give a yellow solution. LDA solution (1 M, 30 mL, 30 mmol) was added slowly over 1 hour giving a dark red solution. The solvent was removed under vacuum to give a brown residue which was re-dissolved in hexane (30 mL). Degassed water (10 mL) was added slowly giving two layers as well as a brown solid. The orange, organic layer was collected, dried over $MgSO_4$ and the volatiles removed under vacuum to give a dark orange oil. (1.012 g, 3.22 mmol, 80%)

^{1}H NMR (400MHz, $CDCl_3$) δ: 0.85 (m, 12H, EtC*H₃*), 1.11 (m, 8H, EtC*H₂*), 1.26-1.46 (m, 4H, -C*H₂*PEt_2), 1.96-1.81 (m, 4H, -C*H₂*PPh), 7.02-7.11 (m, 3H, *p*-Ph + *m*-Ph), 7.38-7.47 (m, 2H, *o*-Ph) ppm $^{13}C\{^1H\}$NMR (400 MHz, $CDCl_3$) δ: 9.6 (EtC*H₃*), 18.6 (EtC*H₂*), 22.3 (-*CH₂*PEt_2), 24.4 (-*C*H_2PPh), 128.5 (*p*-Ph), 132.6 (*m*-

Ph), 138.7 (*o*-Ph) ppm $^{31}P\{^{1}H\}$NMR (400 MHz, $CDCl_3$) δ: -18.6 ppm (d, $^{3}J_{PP}$ 22 Hz, *P*-Et), -16.7 ppm (t, $^{3}J_{PP}$ 22 Hz, *P*-Ph) ppm

Synthesis of 3.11 $[Ru_2Cl_3(L12)_2]Cl$ (Section 3.2.4)

$[RuCl_2(DMSO)_4]$ (0.484 g, 1 mmol) was weighed into a Schlenk flask and toluene (10 mL) was added to give a yellow suspension. **L12** (0.340 g, 1 mmol) was weighed into a separate Schlenk flask and dissolved in toluene (5 mL) to give a dark red solution. The ruthenium solution was heated to reflux and the ligand solution was added dropwise through a septum over 5 minutes. The resulting orange solution was left at reflux for 66 hours. The orange precipitate formed was isolated *via* cannula filtration and dissolved in EtOH (10 mL). The solution was filtered through a small plug of Celite and the resulting orange solution was concentrated to roughly 2 mL under vacuum. Et_2O (15 mL) was added causing a pale yellow solid to precipitate. This was washed with Et_2O and dried to give a pale yellow solid. (0.025 g, 0.024 mmol, 48%)

^{1}H NMR (400 MHz, $CDCl_3$) δ: 0.86 (m, 24H, EtCH_3), 1.15 (m, 16H, EtCH_2), 2.35 (m, 8H, -CH_2PEt$_2$), 2.61 (m, 8H, -CH_2PPh), 7.39-7.46 (m, 6H, *p*-Ph + *m*-Ph), 7.85 (t, $^{3}J_{HH}$ 9Hz, 4H, *o*-Ph) ppm $^{31}P\{^{1}H\}$ NMR (400 MHz, $CDCl_3$) δ: 19.9 (m, *P*-Et), 75.5 (m, *P*-Ph) ppm High Res ESI-MS 993.0738 $[M-Cl]^+$

Synthesis of 3.13 $[RuCl_2(L14)]$ (Section 3.2.5)

L14 (0.513 g, 0.75 mmol) and $[RuCl_2(DMSO)_4]$ (0.380 g, 0.79 mmol) were weighed out into a Schlenk flask and toluene (12 mL) was added to give a yellow suspension. This was heated under reflux for 16 hours forming an orange solution. The resulting yellow solid was isolated *via* cannula filtration, washed with Et_2O (3 x 10 mL) and dried under vacuum to give an orange powder. (0.532g, 0.64 mmol, 86%)

^{1}H NMR (400 MHz, $CDCl_3$) δ: 2.48 (m, 6H, -CH_2PPh$_2$), 2.94 (m, 6H, NCH_2-), 6.68-6.92 (m, Ph), 7.10-7.34 (m, Ph) ppm $^{31}P\{^{1}H\}$ NMR (400 MHz, $CDCl_3$) δ: 27.0 (d, 29 Hz, 2P), 47.5 (t, 29 Hz, 1P) ppm

Synthesis of 3.23 [Mn(L3)CO]Br (Section 3.2.6)

L3 (0.611 g, 1.00 mmol) and [$BrMn(CO)_5$] (0.275 g, 1.00 mmol) were weighed into a Schlenk flask. Toluene (20 mL) was added and the mixture heated to reflux giving an orange solution. This solution was left for 30 hours at reflux. The solvent was then removed under vacuum to give an orange residue. This was washed with Et_2O (3 x 5 mL) and dried under vacuum to give a yellow solid. (125 mg, 0.16 mmol, 16%)

^{1}H NMR (400 MHz, $CDCl_3$) δ: 3.92 (bm, 6H, *CH_2*), 7.04 (t, $^3J_{HH}$ 8 Hz, 6H *p*-Ph), 7.32 (m, 12H, *o*-Ph), 7.39 (m, 12H, *m*-Ph) ppm $^{31}P\{^1H\}$ NMR (400 MHz, $CDCl_3$) δ: 25.7 (s) ppm

General Procedure for Oxalate Hydrogenation

C2 Substrate (5 mmol) and ruthenium catalyst dimer (0.0125 mmol, 0.25 mol%) were weighed out into a PTFE sleeve with stirrer bar. The sleeve was loaded into a Parr 300 mL stainless steel autoclave which was then sealed. The autoclave was placed under vacuum and flushed with N_2. This was repeated for a total of three times before dry, degassed methanol (10 mL) was added against a flow of N_2. The autoclave was pressurised with H_2 and placed into a pre-heated aluminium mantle and left stirring at 700 rpm. After the desired reaction time the autoclave was placed into an ice/water bath and cooled to room temperature. Any residual gas was vented, the autoclave was opened and the liquid products analysed by GC (100 µL of sample, 25 µL of *n*-pentanol standard, 1 mL MeOH).

Analysis performed by GC-FID DB-Wax capillary column 30 m x 0.32 mm, I.D. 0.25 µm. Method: starting oven temp 35 °C, hold at 35 °C for 5 min, heat to 250 °C at 50 °C min^{-1} , hold at 250 °C for 5 min.

General Procedure for Oxalate Hydrogenation in Flow (Section 3.7)

Conducted at the BP Research Labs, Centre of Expertise for Applied Chemistry and Physics, Saltend HRTC, Hull under the supervision of industrial supervisor Prof. Glenn Sunley and Dr Greg Price.

A ThalesNano H-Cube was connected to a ThalesNano Phoenix flow reactor fitted with an 8 mL stainless steel coil. A solution of DMO (2.450 g, 20.7 mmol) and ruthenium dimer (0.625 mmol) in MeOH (200 mL) was prepared and flowed through the reaction apparatus at 1 mL/min to check for faults or leaks. The flowrate was then decreased to 0.1 mL/min and the Phoenix temperature increased to 180 °C. 80 bar H_2 was generated in the H-Cube and the reaction mixture was flowed through the system for the desired residence time (90 mins). After this time a sample of the output reaction mixture was collected for analysis. The reaction temperature was increased to 200 °C and the reaction left again for the residence time. This was repeated once more at 220 °C. The reaction mixtures was analysed neat by GC-MS.

Chapter 4

Glycerol carbonate[25] and glycerol carboxylic acid[26] were synthesised following literature preparations.

Transesterification of Ethylene Carbonate (Section 4.4)

EC (0.440 g, 5 mmol) was weighed into a PTFE sleeve with magnetic stirrer bar which was loaded into a Parr 300 mL stainless steel autoclave. The autoclave was then sealed, placed under vacuum and filled with N_2. This was repeated for a total of 3 cycles. Dry and degassed MeOH (10 ml) was then added against a flow of N_2. The autoclave was pressurised with 20 bar H_2 or Ar and placed into a pre-heated aluminium mantle (180 °C). The autoclave was left for the desired reaction time with stirring at 700 rpm. The autoclave was then placed in an ice/water bath and cooled to room temperature. After cooling, any residual gas was vented and autoclave contents were collected and analysed by GC (100 µL reaction mixture, 10 µL *n*-pentanol standard, 1.7 mL MeOH) and ^{1}H NMR.

Analysis performed by GC-FID HP-1 silica capillary column 25 m x 0.32 mm, I.D. 0.17 µm. Method: starting oven temp 70 °C, hold at 70 °C for 3 min, heat to 300 °C at 50 °C min^{-1} , hold at 300 °C for 5 min.

Chapter 5

General Procedure for Methanol and Ethanol Heterocoupling (Section 5.2.2)

Inside an argon glovebox, NaOMe (34.3 mmol, 1.851 g, 200 mol%) and ruthenium catalyst (0.017 mmol, 0.1 mol%) were weighed into separate vials then transferred to a PTFE sleeve with a magnetic stirrer bar. This sleeve was then loaded into a Parr 100 mL stainless steel autoclave which was sealed and then placed under an inert N_2 atmosphere. Against a flow of N_2, EtOH (1 mL, 17.1 mmol, 100 mol%) and MeOH (10 mL, xs) were added. The autoclave was then placed into a pre-heated aluminium mantle and left to stir at 500 rpm for the desired reaction time. After this time the autoclave was placed in an ice/water bath and left to cool to room temperature. Any residual gas was vented, and the autoclave contents were collected and analysed by GC (100 µL reaction mixture, 10 µL hexadecane standard, 1.7 mL Et_2O) and ^{1}H NMR.

Analysis performed by GC-FID Carbowax capillary column 30 m x 0.32 mm, I.D. 0.25 µm. Method: starting oven temp 60 °C, hold at 70 °C for 5 min, heat to 220 °C at 40 °C min^{-1}, hold at 220 °C for 5 min.

Methanol and Ethanol Heterocoupling Solid Analysis (Section 5.2.3)

The solid from the reaction mixture with **3.1** was isolated by Büchner filtration and washed with toluene (3 x 5 mL). The solid was then dried under vacuum at 40 °C for 1 hour to remove any remaining volatiles. The total solid was weighed (0.781 g) and a 10 mg sample taken for ^{1}H and ^{13}C (300 MHz) NMR analysis. This sample was dissolved in 0.7 mL D_2O with DMSO (0.1 mmol, 7 µL) added as a standard.

Open Vessel Catalyst Base Test (Section 5.2.4)

3.1 (100 mg, 0.06 mmol) and NaOMe (1.02 g, 18.5 mmol) were weighed into a Schlenk flask in the glovebox. Dry and degassed MeOH (10 mL) was added to give an orange solution which was heated to reflux under a flow of N_2 and left to stir overnight. After cooling to room temperature, the solid was

collected *via* filter cannula, washed with MeOH (3 x 5 mL) and dried under vacuum. Yellow solid (24 mg)

^{1}H NMR (400 MHz, $CDCl_3$) δ: 1.52 (br s, 3H, -C*H*$_3$), 2.30-2.55 (m, 6H, -C*H*$_2$-), 7.11-7.21 (m, 18H, *m*-Ph+*p*-Ph), 7.33-7.42 (m, 12H, *o*-Ph) ppm ^{31}P{^{1}H} NMR (400 MHz, $CDCl_3$) δ: 27.7 (d, 41 Hz $^{2}J_{PP}$, 2P), -8.3 (t, 40 Hz $^{2}J_{PP}$, 1P) ppm ESI-MS: 817.1 $[M]^+$, 789.1 $[M\text{-}CO]^+$, 761.1 $[M\text{-}2CO]^+$ m/z

Closed Vessel Catalyst Base Test (Section 5.2.4)

3.1 (100 mg, 0.06 mmol) and NaOMe (1.02 g, 18.5 mmol) were weighed into separate vials then transferred to a PTFE sleeve with a magnetic stirrer bar. This sleeve was then loaded into a Parr 100 mL autoclave which was sealed and then evacuated under vacuum before being refilled with N_2. This was repeated for a total of 3 cycles. Against a flow of N_2, dry and degassed MeOH (10 mL, xs) was added. The autoclave then then placed into a pre-heated aluminium block (180 °C) and left to stir at 500 rpm for 20 hours. The autoclave was then placed in an ice/water bath and left to cool to room temperature. Any residual gas was vented, and the autoclave contents were collected. The yellow solid produced was collected *via* Büchner filtration, washed with MeOH (3 x 5 mL) and dried under vacuum. Yellow solid (27 mg).

^{1}H NMR (400 MHz, $CDCl_3$) δ: -7.42 (dd, 19 Hz $^{2}J_{HP}$, 1H, Ru-*H*), 1.47 (br s, 3H, -C*H*$_3$), 2.05-2.25 (m, 6H, -C*H*$_2$-), 6.92-7.10 (m, 18H, *m*-PH+*p*-Ph), 7.63 (m, 12H, *o*-Ph) ^{31}P{^{1}H} NMR (400 MHz, $CDCl_3$) δ: 26.6 (d, 31.6 Hz $^{2}J_{PP}$, 2P), 34.2 (t, 31.6 Hz $^{2}J_{PP}$, 1P) ESI-MS: 881.0 $[M]^+$, 853.0 $[M\text{-}CO]^+$, 755.1 $[(L1)RuCO]^+$ m/z

General Procedure for Dimethyl Malonate Hydrogenation (Section 5.4)

Dimethyl malonate (0.57 mL, 5 mmol) and ruthenium catalyst dimer (0.0125 mmol, 0.25 mol%) were weighed out into a PTFE sleeve with stirrer bar. The sleeve was loaded into a Parr 300 mL stainless steel autoclave which was then sealed. The autoclave was placed under vacuum and filled with N_2. This was repeated for a total of three times before dry, degassed MeOH (10 mL) was added against a flow of N_2. The autoclave was pressurised with H_2 (30 bar) and placed into a pre-heated aluminium

mantle (180 °C) and left stirring at 700 rpm. After the desired reaction time, the autoclave was placed into an ice/water bath and cooled to room temperature. Any residual gas was vented, the autoclave opened, and the liquid products analysed using GC (100 µL reaction mixture, 10 µL *n*-pentanol standard, 1.7 mL MeOH).

Analysis performed by GC-FID HP-1 silica capillary column 25 m x 0.32 mm, I.D. 0.17 µm. Method: starting oven temp 70 °C, hold at 70 °C for 3 min, heat to 300 °C at 50 °C min^{-1} , hold at 300 °C for 5 min.

General Procedure for Amide Hydrogenation (Section 5.5)

Amide (5 mmol) and ruthenium catalyst dimer (0.0125 mmol, 0.25 mol%) were weighed out into a PTFE sleeve with stirrer bar. The sleeve was loaded into a Parr 300 mL stainless steel autoclave which was then sealed. The autoclave was placed under vacuum and filled with N_2. This was repeated for a total of three times before dry, degassed MeOH (10 mL) was added against a flow of N_2. The autoclave was pressurised with H_2 (30 bar) and placed into a pre-heated aluminium mantle (180 °C) and left stirring at 700 rpm. After the desired reaction time, the autoclave was placed into an ice/water bath and cooled to room temperature. Any residual gas was vented, the autoclave opened, and the liquid products analysed using ^1H NMR. The total volume of reaction solution was measured with a 100 µL aliquot taken and dissolved in $CDCl_3$ (0.7 mL). Mesitylene (0.1 mmol, 14 µL) was added as a standard.

General Procedure for Transfer Hydrogenation (Section 5.6)

Conducted at the BP Research Labs, Centre of Expertise for Applied Chemistry and Physics, Saltend HRTC, Hull under the supervision of industrial supervisor Prof. Glenn Sunley and Dr Greg Price.

2-ethylhexanal (1.21 mL, 7.80 mmol), ruthenium dimer (0.078 mmol, 1 mol%), NH_4HCO_2 (9.84 g, 156 mmol, 20 eq) and MeOH (10 mL) were weighed into a round bottom flask with reflux condenser attached. The yellow solution was heated to reflux (85 °C) and left overnight. After cooling to room temperature the volatiles were removed under vacuum and the yellow residue dissolved in heptane

(10 mL). This was washed with water (3 x 5 mL) and the organic fraction collected and analysed by GC-MS.

6.3 – References

1. Y. Moglie, M. J. González-Soria, I. Martín-García, G. Radivoy, and F. Alonso, *Green Chem.*, 2016, **18**, 4896–4907.

2. J. Wöltinger, J.-E. Bäckvall, and Á. Zsigmond, *Chem. Eur. J.*, 1999, **5**, 1460–1467.

3. Y. D. Y. L. Getzler, V. Mahadevan, E. B. Lobkovsky, and G. W. Coates, *J. Am. Chem. Soc.*, 2002, **124**, 1174–1175.

4. D. J. Harrison, A. L. Daniels, I. Korobkov, and R. T. Baker, *Organometallics*, 2015, **34**, 4598–4604.

5. C. H. Wei, T. M. Bockman, and J. K. Kochi, *J. Organomet. Chem.*, 1992, **428**, 85–97.

6. J. W. Kramer, D. Y. Joh, and G. W. Coates, *Org. Lett.*, 2007, **9**, 5581–5583.

7. D. Brodbeck, F. Broghammer, J. Meisner, J. Klepp, D. Garnier, W. Frey, J. Kästner, and R. Peters, *Angew. Chem. Int. Ed.*, 2017, **56**, 4056–4060.

8. C. B. Caputo, L. J. Hounjet, R. Dobrovetsky, and D. W. Stephan, *Science.*, 2013, **341**, 1374–1377.

9. E. Dulière, M. Devillers, and J. Marchand-Brynaert, *Organometallics*, 2003, **22**, 804–811.

10. E. Iengo, E. Zangrando, E. Baiutti, F. Munini, and E. Alessio, *Eur. J. Inorg. Chem.*, 2005, **2005**, 1019–1031.

11. W. Hewertson and H. R. Watson, *J. Chem. Soc.*, 1962, **0**, 1490.

12. A. Phanopoulos, N. Long, and P. Miller, *J. Vis. Exp.*, 2015, e52689.

13. M. J. Hanton, S. Tin, B. J. Boardman, and P. Miller, *J. Mol. Catal. A Chem.*, 2011, **346**, 70–78.

14. R. Gilbert-Wilson, L. D. Field, and M. M. Bhadbhade, *Inorg. Chem.*, 2012, **51**, 3239–3246.

15. W. Wu and C.-J. Li, *Chem. Commun.*, 2003, **0**, 1668.

16. M. I. García-Seijo, A. Habtemariam, P. del Socorro Murdoch, R. O. Gould, and M. E. García-Fernández, *Inorg. Chim. Acta*, 2002, **335**, 52–60.

17. H. Doucet, T. Ohkuma, K. Murata, T. Yokozawa, M. Kozawa, E. Katayama, A. F. England, T. Ikariya, and R. Noyori, *Angew. Chem. Int. Ed.*, 1998, **37**, 1703–1707.

18. M. Kawatsura and J. F. Hartwig, *Organometallics*, 2001, **20**, 1960–1964.

19. W. Schirmer, U. Flörke, and H. -J Haupt, *ZAAC - J. Inorg. Gen. Chem.*, 1987, **545**, 83–97.

20. B. Gnanaprakasam, J. Zhang, and D. Milstein, *Angew. Chem. Int. Ed.*, 2010, **49**, 1468–1471.

21. D. Benito-Garagorri, E. Becker, J. Wiedermann, W. Lackner, M. Pollak, K. Mereiter, J. Kisala, and K. Kirchner, *Organometallics*, 2006, **25**, 1900–1913.

22. T. K. Mukhopadhyay, M. Flores, R. K. Feller, B. L. Scott, R. D. Taylor, M. Paz-Pasternak, N. J. Henson, F. N. Rein, N. C. Smythe, R. J. Trovitch, and J. C. Gordon, *Organometallics*, 2014, **33**, 7101–7112.

23. C. P. Richers, J. A. Bertke, and T. B. Rauchfuss, *Dalton Trans.*, 2017, **46**, 8756–8762.

24. A. M. Bond, R. Colton, A. Van den Bergen, and J. N. Walter, *Inorg. Chem.*, 2000, **39**, 4696–4703.

25. S. H. Pyo and R. Hatti-Kaul, *Adv. Synth. Catal.*, 2016, **358**, 834–839.

26. H. Woelfle, B. Walther, M. Kohler, and S. Putzien, 2013, WO2013092011A1.